Monitoring and Managing River Corridors in the Midst of Growing Water Demand

Tyler A. Keys

Dissertation submitted to the faculty of the Virginia Polytechnic Institute and State University in partial fulfillment of the requirements for the degree of

Doctor of Philosophy
In
Biological Systems Engineering

Durelle T. Scott, Chair

David J. Sample

Erich T. Hester

Robert W. Burgholzer

March 22, 2018
Blacksburg, VA

Keywords: River corridors, river-floodplain connectivity, stream restoration, ecohydrology, ecological engineering

Copyright © 2018 Tyler A. Keys

Monitoring and Managing River Corridors in the Midst of Growing Water Demand

Tyler A. Keys

ABSTRACT

Rivers and their surrounding riparian and subsurface ecosystems, known as river corridors, are important landscape features that provide a myriad of ecological and societal benefits. While the importance of riverine flooding has been widely acknowledged and extensively studied, very little research has been conducted on the interactions between river channels and their adjacent floodplains. The importance of this hydrologic connectivity between rivers and floodplains has been emphasized in recent decades and now ecological engineering techniques such as stream restoration are often utilized to restore connectivity between streams and their riparian ecosystems. Despite its ubiquity in practice, there are still many basic components of river-floodplain connectivity that are not well understood. Furthermore, a lack of cost-effective monitoring techniques makes sustainable management of river corridors quite challenging. Thus, the overall goals of my dissertation were: 1) develop user-friendly river corridor monitoring techniques utilizing cost-effective approaches such as time-lapse digital imagery and satellite remote sensing and 2) identify the effects of anthropogenic activities on river corridor hydrologic and biogeochemical processes that occur at varying spatial and temporal scales during flood events. These goals were addressed through five independent studies that span spatiotemporal scales. The five studies utilized a combination of novel remote sensing, hydrologic/hydraulic modeling, and high frequency spatial sampling techniques to analyze river corridor dynamics. Results highlight that digital imagery and satellite remote sensing can be effective tools for monitoring river corridors in data scare regions. Additionally, impounding streams and river corridors alters floodplain connectivity and biogeochemical processing of reactive solutes such as nitrogen and phosphorus. Findings from this work highlight the important role that spatial and temporal scale plays in river corridor dynamics. Overall, this research provides new analytical techniques and findings that can be used to effectively monitor and manage river corridors.

Monitoring and Managing River Corridors in the Midst of Growing Water Demand

Tyler A. Keys

GENERAL AUDIENCE ABSTRACT

Rivers are important landscape features that provide basic societal needs such as drinking water, water for agricultural irrigation, and hydroelectric energy. Engineers have traditionally sought to manage rivers for these purposes while also minimizing flooding. However, flooding actually provides a number of environmental benefits such as increased aquatic biodiversity and removal of excess sediment and pollutants from rivers. This notion of environmentally friendly flooding is a relatively new concept and much is still unknown about how these processes differ at varying scales. Additionally, there is currently a lack of techniques for monitoring such processes primarily due to the cost required for equipment and labor. Therefore, the goals of this dissertation were twofold: 1) develop cost-effective and user-friendly monitoring techniques that can be used to study river flooding dynamics and 2) examine the impacts of river flooding dynamics at three different spatial scales ranging from a small stream to a large watershed. This was accomplished through five separate case studies that examine rivers and watersheds of varying sizes at varying time scales. The studies utilized several emerging technologies that required a combination of field monitoring, computer simulations of flood dynamics, and satellite imagery to gain a better understanding of river flood hydrology and water quality. A key finding was the important role that scale plays in both spatial and temporal domains. Utilizing varying spatial and temporal scales allowed for identification of different processes that occur across a range of river and watershed sizes. Overall, this work can be used to better inform future river management and restoration decisions.

ACKNOWLEDGMENTS

My graduate experience at Virginia Tech has been a memorable and exciting one. I am grateful for all of the relationships and collaborations I have made over the last four years within the BSE department and across the Virginia Tech community. Specifically, I would like to start by thanking my advisor, Durelle "Scotty" Scott for his mentorship and support over the past four years. I am grateful for all of the time he has invested in me and for encouraging me to participate in various projects and activities. I am also extremely appreciative of the support and feedback I have received from my committee members, Erich Hester, David Sample, and Rob Burgholzer. Their wisdom, advice, and encouragement has helped me grow substantially as a scholar. Additional thanks to Cully Hession, Heather Govenor, and Joey Kleiner for their collaboration and co-authorship on research projects that are included in this dissertation.

Additionally, I would like to thank all of the BSE staff who have spent countless hours helping me with various projects over the years. Specific thanks to Laura Lehmann and Dumitru Branisteanu for their help with fieldwork, instrumentation, and all-around problem solving. Also, thanks to Kelly Peeler for providing guidance on water quality analyses, helping with laboratory analyses, and for tolerating our outrageously messy lab bench. None of this work would have been possible without the help of these individuals.

I would also like to thank my fellow lab group members from the past four years: Nate Jones, Breanne Ensor, Dylan Cooper, Tyler Weiglein, Maddie Ryan, Mohammad Yazdi, and Connor Brogan. Your camaraderie, constructive feedback, and unsolicited advice helped make my graduate experience so enjoyable. I have enjoyed getting to know all of you and will forever be a "Team Scotty" member.

Finally, I would like to thank all of my friends and family who have supported me over the last four years. Specifically, thanks to my parents for encouraging me to pursue my passion and my brother and sister for their encouragement, albeit sarcastic at times. To all of my other friends at Virginia Tech, thank you for hanging out with me and driving me around town. I have thoroughly enjoyed my time at Virginia Tech and it has been an experience that I will never forget.

TABLE OF CONTENTS

LIST OF TABLES

LIST OF FIGURES

LIST OF ABBREVIATIONS

7Q10	Lowest 7-day average flow occurring once every 10 years
30Q2	Lowest 30-day average flow occurring once every 2 years
A	Surface area
ADV	Acoustic Doppler velocimeter
ALF	August low flows
BDA	Beaver dam analog
BMP	Best management practice
DO	Dissolved oxygen
DOC	Dissolved organic carbon
DOM	Dissolved organic matter
DNRA	Dissimilatory nitrate reduction to ammonium
GCP	Ground control point
GLWD	Global Lakes and Wetlands database
GRACE	Gravity Recovery and Climate Experiment
GRLM	Global Reservoir and Lake Monitor
HEC-RAS	Hydrologic Engineering Center River Analysis System
L	Water level
Lidar	Light detection and ranging
LW	Large wood
MNDWI	Modified normalized difference water index
MODIS	Moderate Resolution Imaging Spectroradiometer
N	Nitrogen
n	Manning's roughness coefficient
NASA	National Aeronautics and Space Administration
NDRGI	Normalized difference red green index
NDVI	Normalized difference vegetation index
NH_4^+	Ammonium
NO_3^-	Nitrate
NRMSE	Normalized root mean square error
NSE	Nash-Sutcliffe efficiency
P	Phosphorus
PO_4^{3-}	Phosphate
PT	Pressure transducer
Q	Discharge
Q_{FP}	Floodplain discharge
Q_{FP}/Q_{tot}	Floodplain discharge as percentage of total discharge
ROI	Region of interest
S:A	Surface area to shoreline ratio
TDN	Total dissolved nitrogen
USGS	United States Geological Survey
ΔV	Change in water volume
W:D	Width to depth ratio

AUTHOR'S PREFACE

This dissertation is composed of five separate research manuscripts (Chapters 2 through 6) that span the field of river corridor science. All five chapters have been published or will be submitted for publication in peer-reviewed journals. The author of this dissertation was the lead and corresponding author on all five manuscripts. Chapters 2 and 3 focus on developing cost-effective river corridor monitoring techniques for varying spatial and temporal scales. Chapters 4-6 focus on identifying hydrologic and biogeochemical processes that occur in river corridors and the degree to which anthropogenic activities can affect theses process. Specific goals and key findings of each chapter are outlined below.

Chapter 2 provides a new methodology for examining river-floodplain connectivity through the use of time lapse digital imagery. For this work, a digital network camera was set up to take hourly images of a third order stream and floodplain. Images were then processed to evaluate and characterize floodplain inundation dynamics. As a proof-of-concept, inundation estimates were validated with a LiDAR derived inundation model. Overall, this work successfully demonstrated the use of time-lapse digital imagery as a cost-effective form of river corridor monitoring. This chapter was peer-reviewed and published in the journal *Limnology and Oceanography: Methods* in June, 2016 (Keys, T.A., Jones, C.N., Scott, D.T., and Chuquin, D. 2016. A cost-effective image processing approach for analyzing the ecohydrology of river corridors. *Limnology and Oceanography: Methods*. 14(6): 359-369. doi: 10.1002/lom3.10095).

Chapter 3 demonstrates a new method for estimating storage variations in lakes and reservoirs with high temporal resolution. The goal of this work was to utilize freely available satellite imagery and altimetry to develop near-continuous estimates of lake and reservoir storage. We chose to focus specifically on the tropics as these regions generally have limited environmental data. Results demonstrate that the methodology works well for most water bodies but not for lakes and reservoirs with long shoreline to surface area ratios due to limited spatial resolution of satellite imagery. This chapter was peer-reviewed and published in the journal *Lake and Reservoir Management* (Keys, T.A. and Scott, D.T. 2017. Monitoring volumetric fluctuations in tropical lakes and reservoirs using satellite remote sensing. doi: 10.1080/10402381.2017.1402226).

Chapter 4 examines the effects of large wood on river-floodplain connectivity in a headwater stream. The overall goal of this project was to quantify the impacts of large wood on floodplain hydrodynamics during flood events. To test this, two experimental floods were conducted on a 50 meter reach of a first order stream. Field survey data and measurements were used to parameterize a 2-dimensional hydrodynamic model (HEC-RAS). The calibrated model was then used to analyze the effects of varying placement strategies and flow regimes on floodplain hydrodynamics. Overall, results illustrate that instream large wood increased river-floodplain connectivity and provide a potential best management practice for headwater streams. This chapter will be submitted to the journal *Ecological Engineering* in March, 2018 and is currently under review for publication (Keys, T.A., Govenor, H., Jones, C.N., Hession, W.C., Hester, E.T., and Scott, D.T. Effects of Large Wood on Floodplain Connectivity in a Headwater Mid-Atlantic Stream).

Chapter 5 examines the impact of a run-of-the-river hydroelectric dam on nitrogen cycling during a storm event. To do this, we collected samples at baseflow conditions in September, 2017 and

then collected samples at 1 day intervals across a storm hydrograph in October, 2017. Grab samples were measured at 5 locations along the river-reservoir-river gradient while in situ measurements were made on 3 of the days using high frequency spatial sampling. Results illustrate that the impoundment served as a net sink of nitrogen flux during the storm event but served as a significant source of ammonium downstream of the dam. Longitudinal profiles illustrate significant differences of water nitrate across the river-reservoir transition. However, low dissolved oxygen in the reservoir suggests that a lack of nitrification may be the cause of increased ammonium export and decreased nitrate concentrations. This chapter is currently in preparation for submission to *River Research and Applications* in April, 2018 (Keys, T.A., Ryan, M.F., and Scott, D.T. Storm effects on nitrogen flux and longitudinal variability in a river-reservoir system).

Chapter 6 examines the cumulative impact that small impoundments have on river-floodplain connectivity. Previous research found that there are more than 73,000 impoundments in the state of Virginia, and over 2.5 million in the United States. The effects of these impoundments on downstream hydrology are poorly understood. We explored these impacts by modeling an urban watershed in Northern Virginia that contains 39 impoundments. The watershed was modeled using the HSPF-based Chesapeake Bay Program Phase 5 watershed model and VAHydro, a web-based modeling framework run by the Virginia Department of Environmental Quality. Findings from this work highlight that small impoundments cumulatively increase low flows but decrease downstream discharge and floodplain inundation during periods of high flow. This chapter is currently in preparation for submission to *Journal of Hydrologic Engineering* in May, 2018 (Keys, T.A., Brogan, C.O., Burgholzer, R., Kleiner, J., and Scott, D.T.. Modeling the cumulative effects of small impoundments on downstream floodplain connectivity).

CHAPTER 1. INTRODUCTION

1.1 Water-Food-Energy Nexus

The global population is projected to increase by an estimated 2 to 5 billion people over the next century prior to stabilizing (United Nations, 2013; Gerland et al., 2014). Water demand will likely increase over the coming decades to meet the needs of a growing population (Ercin and Hoekstra, 2014). While multiple water sources can be used to meet such water demand, the majority of water withdrawals come from freshwater sources (Kenny et al., 2009). However, freshwater only makes up ~2.5% of the earth's total volume of water and the majority of this water is stored within glaciers and the polar icecaps (Gleick, 1993). As a result, portions of the world are already facing water scarcity (Rijsberman, 2006) and we are currently in the midst of a complex global challenge known as the water-food-energy nexus. This nexus revolves around providing the global population with food and water security while simultaneously producing energy (Bazilian et al., 2011; Siddiqi and Andadon, 2011) and will likely become increasingly more difficult to address in coming decades as anthropogenic climate change will exacerbate extreme events such as droughts and flooding (Vörösmarty et al., 2000).

The water-food-energy nexus is particularly challenging to address because it involves competing demands from different sectors and requires meeting the needs of current generations without compromising resources of future generations. While numerous studies have emphasized the importance of this idea of sustainability for the future of our planet (e.g., Foley et al., 2011), coming up with a feasible way to do so is a considerable challenge. Previous work has suggested that holistic management using an integrated systems approach is necessary for taking into account the needs of all competing sectors in the water-food-energy nexus, which often use different units of scales to measure sustainability (Hester and Little, 2013; Little et al., 2016). This will likely require the use of novel approaches that merge multiple perspectives and disciplines. Future decision makers will need to utilize a variety of tools and innovative approaches to reduce water consumption through water efficiency.

Sustainable management of riverine ecosystems is at the forefront of solving this complex global challenge. River networks play an integral role in the water-food-energy nexus as they provide a variety of benefits including municipal drinking water, agricultural irrigation, and hydroelectric power generation. While these are undoubtedly important societal needs, harnessing rivers for such benefits comes at several environmental costs. First, water withdrawals for municipal water supply and agriculture have led to severe water shortages in arid regions such as the western United States. For example, the average annual flow in the Colorado River has decreased by nearly 25,000 m^3/s over the past century due to water withdrawals from seven states and Mexico (Gleick, 2003). Second, anthropogenic activities such as the impoundment of rivers creates a discontinuity in both lateral and longitudinal flow of water (Ward and Stanford, 1995). This disruption of the natural flow regime can have negative consequences for aquatic wildlife, riparian ecosystems, sediment transport and deposition, and solute fate and transport (Poff et al., 1997). This is an increasingly important issue as there are an estimated 2.5 impoundments covering a surface area of 2.1 million hectares in the United States alone (Smith et al., 2002). The cumulative impacts of such vast

infrastructure within river networks is still largely unknown, but studies have suggested that assessment of these effects are critical for environmental sustainability (Therivel and Ross, 2007). Additionally, river networks have been largely studied at the reach scale with little attention given to watershed and regional scale effects. Therefore, it is suggested that the current paradigm be shifted from the current site-specific approach to a more holistic river management approach.

1.2 River Corridor Science: A New Perspective for Sustainable River Management

Rivers have been extensively studied over the years due to the economic importance and hazards of urban flooding (Jha et al., 2012). Historically, engineers have utilized rivers as a means of conveyance to remove water from a given system as quickly as possible to minimize the hazards of flooding. Thus, research efforts have focused primarily on the wetted river channel itself with very little consideration given to adjacent regions. While groundwater systems have also been given considerable attention due to their relevance in pollutant conveyance (Dagan, 1987), research has only recently begun to examine surface water and groundwater interactions (Sophocleous, 2002). Additionally, the role of floodplains and their connection to rivers and groundwater systems has been largely neglected until recent decades. A new perspective, known as river corridor science, emphasizes the importance of the interconnection between river channels and their adjacent surface and subsurface ecosystems (National Research Council, 2002; Harvey and Gooseff, 2015). River corridor science diverges from traditional river science in that it treats rivers as dynamic ecosystems with interactions among the main channel, floodplains, and hyporheic zones. This new perspective also challenges the notion that treating rivers as a pipe to remove water from a given system is the most effective method for minimize flooding. On the contrary, increasing hydrologic connectivity between rivers and floodplains can not only minimize urban flooding, but it also has the potential to provide a number of additional ecological benefits.

River-floodplain connectivity, defined as the exchange of water and materials between rivers and their adjacent floodplains (Covino, 2017), has emerged as one of the key principals in river corridor science. The importance of river-floodplain connectivity has become increasingly recognized over the past several decades as studies have highlighted the importance of floodplains (Junk, 1989; Mertes, 1997; Tockner et al., 2000). Floodplains are a particularly vital component of the river corridor as they provide a variety of ecosystem services ranging from flood attenuation (Woltemade et al., 1994), sediment deposition (Bridge, 2009), biogeochemical processing of reactive solutes (Tockner and Stanford, 2002), and habitat for aquatic wildlife (Ward et al., 1999). Due to the importance of floodplains, the reconnection of streams with their floodplains has become a staple in the field of stream restoration (Palmer et al., 2005). Stream restoration has developed into a multi-billion-dollar per year industry (Bernhardt et al., 2005), and yet much is still unknown about stream restoration projects due to a lack of post-restoration monitoring programs (Kondolf and Micheli, 1995; Bash and Ryan, 2002). Additionally, most stream restoration projects are conducted along individual stream reaches without incorporating scale. However, studies have suggested that scale is critical to the success of any stream restoration project (Lake et al., 2007). The field of stream restoration would greatly benefit from a new perspective and more well-defined long-term objectives. River corridor science provides such a framework for effectively managing and restoring riverine ecosystems for ecological and societal benefits.

1.3 Objectives

The current state of literature on river corridor science is lacking in several key areas that need to be further addressed. First, there are few cost-effective and user-friendly monitoring techniques for analyzing river corridors. Understanding floodplain hydrodynamics currently involves a steep learning curve and often requires significant amounts of money, time, and labor. Monitoring river corridors can be challenging for river engineers and managers, particularly in regions of the world with a lack of monitoring equipment. Second, there is a great need for understanding the effects of impounding river corridors on water quality and quantity across different spatial and temporal scales. **Therefore, the overall goal of this research was to develop and apply new monitoring techniques to identify hydrologic and biogeochemical river corridor processes across spatiotemporal gradients**. This was accomplished through five independent studies that span spatial and temporal scales. The goal of the first two chapters was to develop novel monitoring techniques for better understanding surface water dynamics in river networks. The goal of the next three chapters was to identify river corridor processes across scales through separate case studies. Overall, this work provides useful tools and information that can be utilized by a variety of end users to sustainably manage river networks.

1.4 References

Bash, J. S., and Ryan, C. M. (2002). Stream restoration and enhancement projects: is anyone monitoring?. *Environmental management*, *29*(6), 877-885.

Bazilian, M., Rogner, H., Howells, M., Hermann, S., Arent, D., Gielen, D., ... and Yumkella, K. K. (2011). Considering the energy, water and food nexus: Towards an integrated modelling approach. *Energy Policy*, *39*(12), 7896-7906.

Bernhardt, E. S., Palmer, M. A., Allan, J. D., Alexander, G., Barnas, K., Brooks, S., ... and Galat, D. (2005). Synthesizing US river restoration efforts. *Science*, *308*(5722), 636-637.

Covino, T. (2017). Hydrologic connectivity as a framework for understanding biogeochemical flux through watersheds and along fluvial networks. *Geomorphology*, *277*, 133-144.

Bridge, J. S. (2009). *Rivers and floodplains: forms, processes, and sedimentary record*. John Wiley & Sons.

Dagan, G. (1987). Theory of solute transport by groundwater. *Annual review of fluid mechanics*, *19*(1), 183-213.

Ercin, A. E., and Hoekstra, A. Y. (2014). Water footprint scenarios for 2050: A global analysis. *Environment international*, *64*, 71-82.

Foley, J. A., Ramankutty, N., Brauman, K. A., Cassidy, E. S., Gerber, J. S., Johnston, M., ... and Balzer, C. (2011). Solutions for a cultivated planet. *Nature*, *478*(7369), 337-342.

Gerland, P., Raftery, A. E., Ševčíková, H., Li, N., Gu, D., Spoorenberg, T., ... & Bay, G. (2014). World population stabilization unlikely this century. *Science*, *346*(6206), 234-237.

Gleick, P. H. (1993). Water in crisis: a guide to the worlds fresh water resources.

Gleick, P. H. (2003). Global freshwater resources: soft-path solutions for the 21st century. *Science*, *302*(5650), 1524-1528.

Harvey, J., and Gooseff, M. (2015). River corridor science: Hydrologic exchange and ecological consequences from bedforms to basins. *Water Resources Research*, *51*(9), 6893-6922.

Hester, E. T., and Little, J. C. (2013). Measuring environmental sustainability of water in watersheds. *Environmental Science and Technology*, *47*, 8083-8090.

Jha, A. K., Bloch, R., & Lamond, J. (2012). *Cities and flooding: a guide to integrated urban flood risk management for the 21st century*. World Bank Publications.

Junk, W.J., Bayley, P. B., and Sparks, R. E. (1989). The flood pulse concept in river-floodplain systems. In *Proceedings of the International Large River Symposium. Dodge, DP (Ed). Can. Spec. Publ. Fish. Aquat. Sci* (Vol. 106, pp. 110-127).

Kenny, J. F., Barber, N. L., Hutson, S. S., Linsey, K. S., Lovelace, J. K., and Maupin, M. A. (2009). *Estimated use of water in the United States in 2005* (No. 1344). US Geological Survey.

Kondolf, G. M., and Micheli, E. R. (1995). Evaluating stream restoration projects. *Environmental Management*, *19*(1), 1-15.

Lake, P. S., Bond, N., and Reich, P. (2007). Linking ecological theory with stream restoration. *Freshwater biology*, *52*(4), 597-615.

Little, J. C., Hester, E. T., and Carey, C. C. (2016). Assessing and enhancing environmental sustainability: a conceptual review. *Environmental science & technology*, *50*(13), 6830-6845.

McClain, M. E., Boyer, E. W., Dent, C. L., Gergel, S. E., Grimm, N. B., Groffman, P. M., ... & McDowell, W. H. (2003). Biogeochemical hot spots and hot moments at the interface of terrestrial and aquatic ecosystems. *Ecosystems*, *6*(4), 301-312.

Mertes, L. A. (1997). Documentation and significance of the perirheic zone on inundated floodplains. *Water Resources Research*, *33*(7), 1749-1762.

Mitsch, W. J. (2012). What is ecological engineering?. *Ecological Engineering*, *45*, 5-12.

National Research Council. (2002). *Riparian areas: functions and strategies for management*. National Academies Press.

Palmer, M. A., Bernhardt, E. S., Allan, J. D., Lake, P. S., Alexander, G., Brooks, S., ... and Galat, D. L. (2005). Standards for ecologically successful river restoration. *Journal of applied ecology*, *42*(2), 208-217.

Poff, N. L., Allan, J. D., Bain, M. B., Karr, J. R., Prestegaard, K. L., Richter, B. D., ... and Stromberg, J. C. (1997). The natural flow regime. *BioScience*, *47*(11), 769-784.

Rijsberman, F. R. (2006). Water scarcity: fact or fiction?. *Agricultural water management*, *80*(1-3), 5-22.

Siddiqi, A., and Anadon, L. D. (2011). The water–energy nexus in Middle East and North Africa. *Energy policy*, *39*(8), 4529-4540.

Smith, S. V., Renwick, W. H., Bartley, J. D., and Buddemeier, R. W. (2002). Distribution and significance of small, artificial water bodies across the United States landscape. *Science of the Total Environment*, *299*(1-3), 21-36.

Sophocleous, M. (2002). Interactions between groundwater and surface water: the state of the science. *Hydrogeology journal*, *10*(1), 52-67.

Therivel, R., & Ross, B. (2007). Cumulative effects assessment: Does scale matter?. *Environmental impact assessment review*, *27*(5), 365-385.

Tockner, K., and Stanford, J. A. (2002). Riverine flood plains: present state and future trends. *Environmental conservation*, *29*(3), 308-330.

Tockner, K., Malard, F., and Ward, J. V. (2000). An extension of the flood pulse concept. *Hydrological processes*, *14*(16-17), 2861-2883.

United Nations (2013). *World population prospects: the 2012 revision*. Population division of the department of economic and social affairs of the United Nations Secretariat, New York.

Vannote, R. L., Minshall, G. W., Cummins, K. W., Sedell, J. R., and Cushing, C. E. (1980). The river continuum concept. *Canadian journal of fisheries and aquatic sciences*, *37*(1), 130-137.

Vörösmarty, C. J., Green, P., Salisbury, J., & Lammers, R. B. (2000). Global water resources: vulnerability from climate change and population growth. *science*, *289*(5477), 284-288.

Ward, J. V., and Stanford, J. A. (1995). The serial discontinuity concept: extending the model to floodplain rivers. *River Research and Applications*, *10*(2-4), 159-168.

Ward, J. V., Tockner, K., and Schiemer, F. (1999). Biodiversity of floodplain river ecosystems: ecotones and connectivity. *Regulated rivers: research & management*, *15*(1), 125-139.

Woltemade, C. J., and Potter, K. W. (1994). A watershed modeling analysis of fluvial geomorphologic influences on flood peak attenuation. *Water Resources Research*, *30*(6), 1933-1942.

CHAPTER 2. A COST-EFFECTIVE IMAGE PROCESSING APPROACH FOR ANALYZING THE ECOHYDROLOGY OF RIVER CORRIDORS

Tyler A. Keys, C. Nathan Jones, Durelle T. Scott, Daniel Chuquin

Submitted: November 2015
To: *Limnology and Oceanography: Methods*
Status: Published February 2016. DOI: 10.1002/lom3.10095

Abstract

There is currently a need for robust, high-resolution monitoring techniques to assess and quantify ecosystem dynamics within surface water bodies and their riparian ecosystems. This study presents a cost effective, user-friendly technique for examining the ecohydrology of stream and river corridors through the use of digital imagery. Using a simple digital camera, we captured hourly images of a small portion of a headwater Appalachian stream and adjacent floodplain. Then, we utilized pixel classification techniques to evaluate ecohydrologic parameters (e.g., inundation surface area, floodplain wetness, and vegetation dynamics) in each image. Results highlight the episodic nature of river floodplain connectivity, variation in surface wetness across the gradient from river to upland ecosystems, and the seasonal variability of vegetation density and health. To validate the accuracy of image-based measurements, we then compared inundation area estimates to an existing inundation model and found a high level of agreement (R^2 = 0.94; NRMSE = 7.96%). Our study highlights the use of time-lapse imagery as a robust, cost-effective method to capture the dynamics of river corridors and associated ecosystem services.

2.1 Introduction

The study of interactions between water resources and their surrounding ecosystems, known as ecohydrology, is a critical component of evaluating and conserving ecosystem services (Braumen et al., 2007; Grygoruk and Acreman, 2015; Rodriguez-Iturbe, 2000). Of particular interest, riparian and floodplain ecosystems provide many critical ecosystem services, ranging from increased biodiversity (Harding et al., 1998; Naiman et al., 1993), flood peak attenuation (Sheaffer et al., 2002), and biogeochemical processing of reactive solutes (Boudell et al. 2015; Scott et al., 2014). While riparian zones and floodplains have been studied extensively (e.g., Tockner and Stanford, 2002), much of our understanding is based on coarse resolution observations in both spatial and temporal domains (Kirchner et al., 2004).

Because of the economic impact and ecological importance of flooding, a great deal of effort has been invested in mapping inundation extent in floodplains. Methods range from hydrodynamic modeling (e.g., Hunter et al., 2007), remote sensing (e.g., Vanderhoof et al., 2015), and even tree ring record analysis (e.g., Ballesteros et al, 2011). While these methods can produce fairly reliable

estimates of inundation, they often lack proper validation techniques because of the lack of high resolution data and the episodic nature of flooding. For example, the U. S. Army Corps of Engineers' River Analysis System (HEC-RAS) model is often used to estimate inundation extent. However, because there is a great deal of uncertainty typically associated with the model inputs (e.g., channel bathymetry, stream flow, hydraulic roughness coefficients) and because validation data is typically not available, there is often considerable error associated with the modeled inundation extent (Merwade et al., 2008). Several remote sensing products such as Light Detection and Ranging (LiDAR) and multispectral imagery have been employed to characterize inundation extent and other relevant hydrogeomorphic parameters. Traditionally, LiDAR has been used to measure high resolution topographic data (Cook and Merwade, 2009; Bates, 2012; Saksena et al, 2015). However, other relevant uses of LiDAR include the assessment of geomorphic stability (Resop et al., 2010), measurement of habitat structure and diversity (Resop et al., 2012; Milan et al., 2010), and quantification of vegetative roughness (Straatsma and Baptist, 2008; Abu-Aly et al. 2014). Recent advancements in LiDAR data have also allowed for the detection of inundated areas (Lang and McCarty, 2009; Milan and Heritage, 2012) and even the measurement of channel bathymetry (Hilldale and Raff, 2008; Skinner, 2011). Multispectral imagery has also been employed in a wide variety of fluvial studies for mapping stream features (e.g., Leckie et al., 2005) and monitoring stream morphology (e.g., Wright et al., 2000). While these methods can delineate stream inundation with high accuracy, data collection remains relatively expensive and time consuming, and thus, there is a need to develop low-cost alternatives.

Identification of "wet areas" across the landscape is also of interest for both our mechanistic understanding of ecosystem processes and from a regulatory perspective. Specifically, saturated soils drive many redox processes that lead to biogeochemical transformations including denitrification (e.g., Anderson et al., 2015), carbon sequestration (e.g., Davidson and Janssens, 2006), and greenhouse gas production (e.g., Batson et al, 2015). Because of the spatial and temporal heterogeneity of both surface and subsurface flowpaths in floodplains and riparian zones, redox conditions and associated biogeochemical processes are often intermittent and difficult to measure and generalize (Vidon et al., 2015). Currently, soil moisture is characterized through point measurements and/or remote sensing (Dobriyal et al., 2012). However, point measurements are often misleading because the heterogeneity associated with riparian soils and remote sensing often restricts the ability to capture temporal variations. This often complicates regulatory decisions associated with wetland delineation, where wetland hydrologic conditions must be proven through a series of visual indicators and/or shallow well installations (Fennessy et al., 2004). Therefore, both the research and regulatory communities would benefit from the development of a new, low cost technique that robustly identifies "wet areas" with both high spatial and temporal resolutions.

Seasonal vegetation dynamics are also crucial to understand when investigating riparian ecosystem processes. Vegetation phenology can be used as a measure of ecosystem productivity (Field et al., 1995) as well as an indicator of overall ecosystem health (Baird and Wilby, 1999). Moreover, vegetation metrics can be used as auxiliary information to aid in data interpretation from other sensors. At a broad scale, multispectral vegetation indices can be used as a remotely sensed metric to assess both terrestrial and aquatic vegetation dynamics. Most commonly used is the normalized difference vegetation index (NDVI), which calculates the difference between the near infrared and red spectral bands. The NDVI has been widely used in the field of remote sensing as a measure of

vegetative greenness and overall ecosystem health (e.g. DeFries and Townshend, 1994; Pettorelli et al., 2005). However when raster data are only comprised of 3 spectral bands, as is the case for Red Green Blue (RGB) digital imagery, multispectral vegetation indices such as the NDVI cannot be used. This becomes problematic when investigating riparian ecosystems as freely available satellite remote sensing does not have the spatial or temporal resolution necessary to accurately analyze riparian ecosystems. Similar to landscape moisture metrics, there is currently a need for high resolution spatiotemporal measurements of riparian and floodplain vegetation dynamics.

Here, we outline an approach to measure ecohydrologic parameters within riparian zones and floodplains through the use of time-lapse imagery. We demonstrate the measurement of three critical parameters within the context of ecohydrology, an emerging field with a dearth of research focusing on monitoring and assessment techniques. While the complex coupling of disciplines within ecohydrology has hindered high resolution ecohydrologic monitoring thus far (Krause et al., 2015), there is a great need for innovative techniques that can overcome the challenges associated with measuring temporally and spatially heterogeneous processes. The methodology described in this paper fills such a gap with a straight forward, inexpensive, and robust monitoring system. A comprehensive workflow of our methodology is provided within the following sections to ensure that this methodology can be easily replicated and improved upon.

2.2 Methods

2.2.1 Site description

We utilized the Virginia Tech *Stream Restoration, Education, and Management Lab* (StREAM Lab) to conduct this study. The StREAM Lab is located along Stroubles Creek, a recently restored third order stream in the Ridge and Valley physiographic province in southwestern Virginia, USA (Figure 2-1). Until the restoration in 2009, the riparian area was used for hay production and grazing. Since then, successional riparian vegetation has been established and depressional floodplain wetlands have emerged. The Stroubles Creek watershed has an area of approximately 15 km^2 and is comprised of 84% urban/residential landcover, 13% agriculture, and 3% forest (Jin et al., 2013). Stroubles Creek reaches bankfull conditions (~2 m^3/s) approximately three times per year, resulting in minor inundation of adjacent floodplain wetlands. Further, depressional wetlands experience inundation periodically from the surficial aquifer and upslope water flowpaths. However, evapotranspiration limits soil saturation and inundation of depressional wetlands during the growing season. Stroubles Creek is an ideal location for this study because it contains multiple stream gages and is a third order stream, making it unidentifiable in satellite imagery.

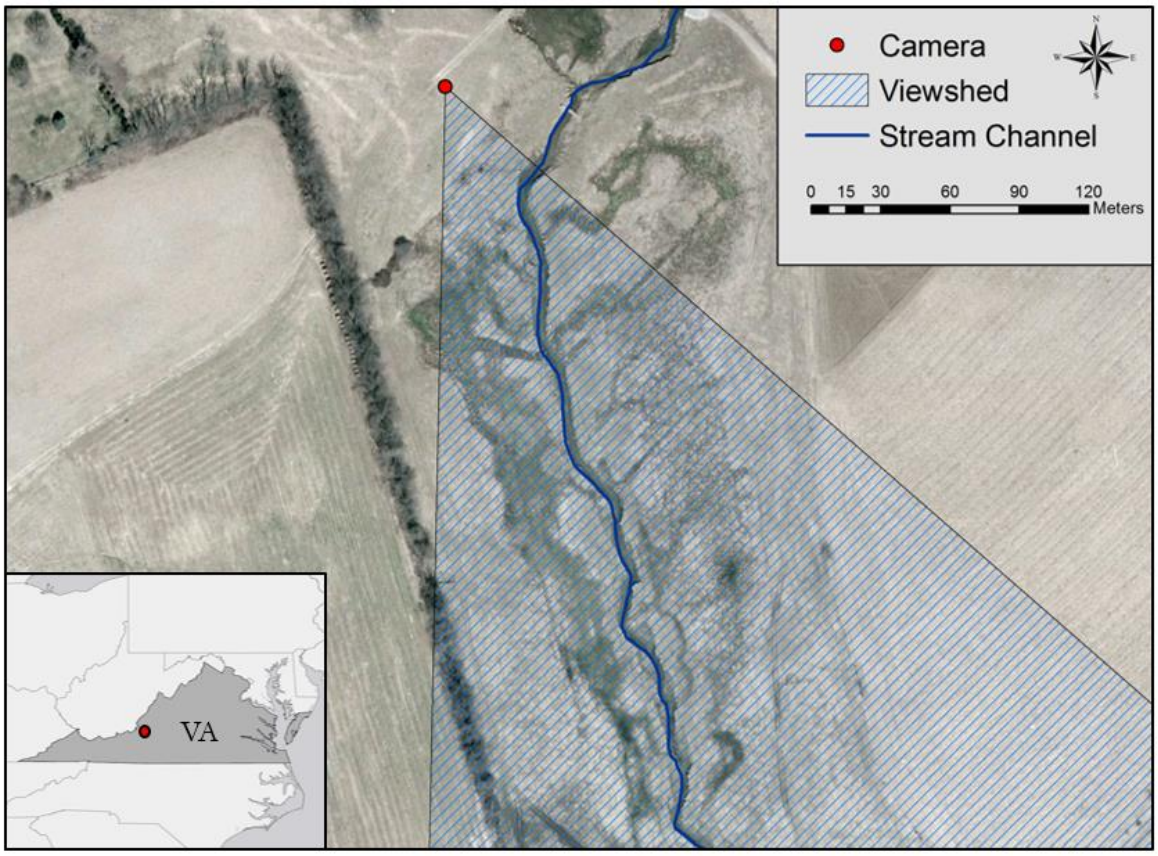

Figure 2-1. Site map illustrating the location of the camera, its viewshed, and the stream channel.

Hourly images of the southern portion of Stroubles Creek (Figure 2-1) were obtained from a NetCam XL network camera (Figure 2-2a). The camera was placed on top of a field tower at a height of 10 meters and positioned with an angle of 30º from the horizontal (Figure 2-2b). To minimize light reflection from the sun, the camera was pointed southerly. The camera and a Campbell CR1000 datalogger were powered using a deep cycle marine battery (group size 27) augmented with solar power from a BP 65-Watt solar panel. Images were taken every hour on the hour, stored on the datalogger, and transmitted to a server via a spread spectrum radio network. Real time imagery, stream flow, and meteorological parameters can be seen in real time at streamlab.bse.vt.edu.

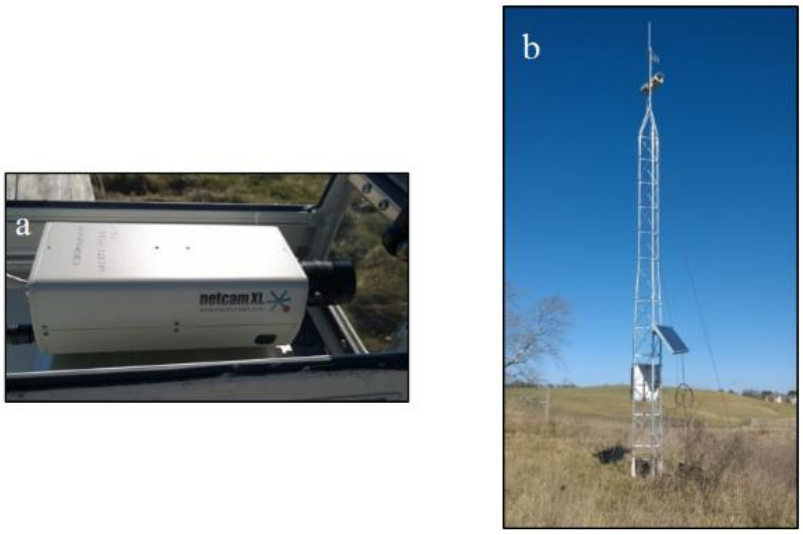

Figure 2-2. a) Close up view of the NetCam XL network digital camera, b) site setup illustrating the tower and camera setup.

2.2.2 Image processing

Once compiled within the database, digital images were processed by a MATLAB script which can be found in the supplementary material. Similar to Royem et al. 2012, which used digital image processing to determine stream stage at a single location, our MATLAB script was developed to incorporate a variety of spatial metrics including flow characteristics, floodplain saturation, and vegetation dynamics. The MATLAB routine consists of 3 primary steps: (1) image rectification, (2) region of interest (ROI) selection, and (3) image analysis. In the first step, image rectification converts the pixels within an image to correspond to the ground footprint. Four known ground control points (GCPs) are identified by the user within the image in order to adjust to the selected scale. The GCPs correspond to surveyed points on the ground that form a rectangle. Input distances based on this known geometry are required to adjust the image such that the rest of the image is converted to the same scale. Knowing and defining the exact location of GCPs is the most critical component of the analysis. If GPCs are not correctly identified, the image will not be correctly adjusted, resulting in inaccurate quantitative measurements. After GCP selection, the image is orthorectified to remove image distortion caused by the oblique camera angle. During step 2, a graphical user interface is used to select the appropriate ROI within the orthorectified image. In step 3, image classification is performed to delineate wet versus dry pixels. The user identifies wet pixels within the image and water bodies are identified by the MATLAB script based on the user's selection of wet pixels.

2.2.3 Image wetness analysis

The purpose of selecting classification points is to identify pixels within the ROI that can reasonably be considered "wet" areas. Based on the user identified points, a supervised classification is performed so that all pixels within the image that have reflectance values similar to the selected pixels will be classified into different spectral classes. The entire image is then converted to a binary matrix, where each pixel in the image is assigned a value of zero (dry) or

one (wet). Pixels classified as wet are automatically summed up and displayed in the output text file. To convert the pixel area to actual area, the output pixel area must multiplied by the spatial resolution of each image. Spatial resolution can be determined by measuring the actual area of the ROI and dividing by the number of pixels corresponding to that area. An illustration of the entire water segmentation process can be seen in Figure 2-3.

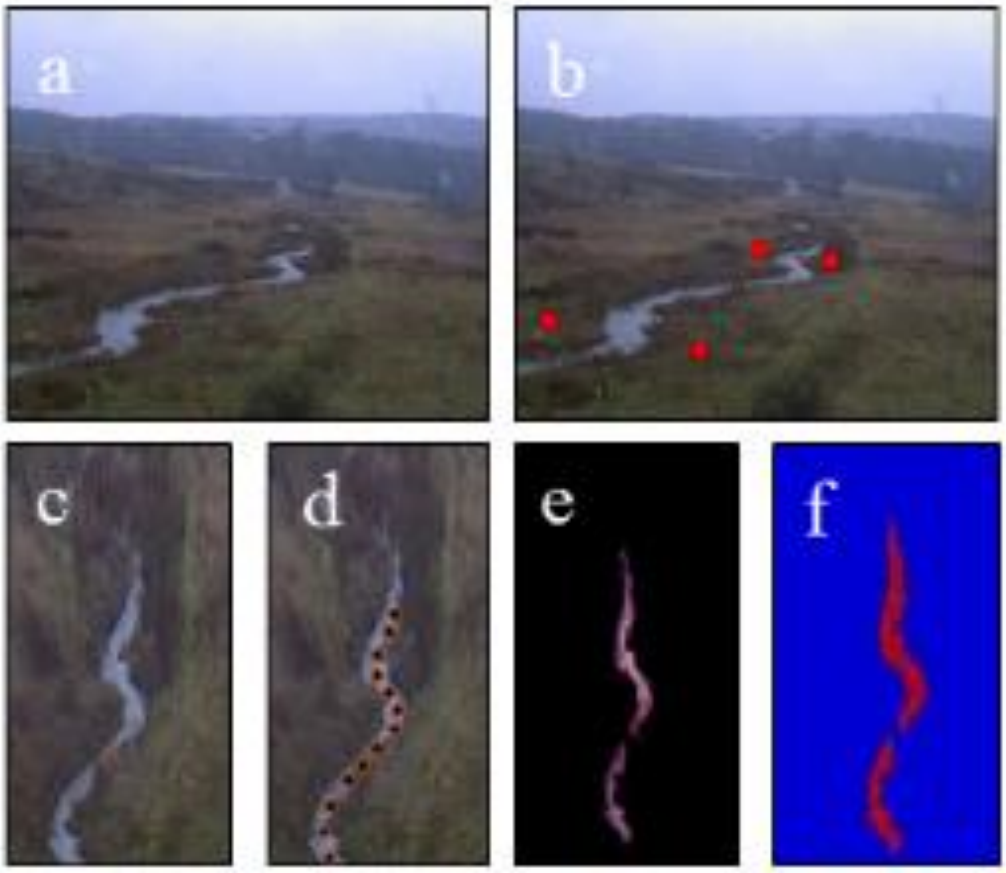

Figure 2-3. a) Plain image selected by user, b) image with identified ground control points, c) orthorectified ROI, d) classification points within ROI, e) enhanced image mask and f) final processed image with binary mask.

To further analyze flooding dynamics, our code locates wet areas on the floodplain as well as their degree of wetness. After the binary mask has separated wet pixels from dry pixels, degree of wetness is determined by creating a pixel-based color map. All wet pixels on the image are assigned a value based on their similarity to the user's selected classification pixels, where wet pixels are assigned a greater value than dry pixels. For example, the stream is given the highest value as it has the closest values to the classification points in every image. Values for large floodplain "hotspots" are assigned values that are less than the main channel but are still greater than dry pixels. This clearly separates the stream channel from dry land while still being able to identify floodplain hotspots. As illustrated in Figure 2-4, the stream channel and wet areas on the floodplain are not only identified, but also separated based on their degree of wetness.

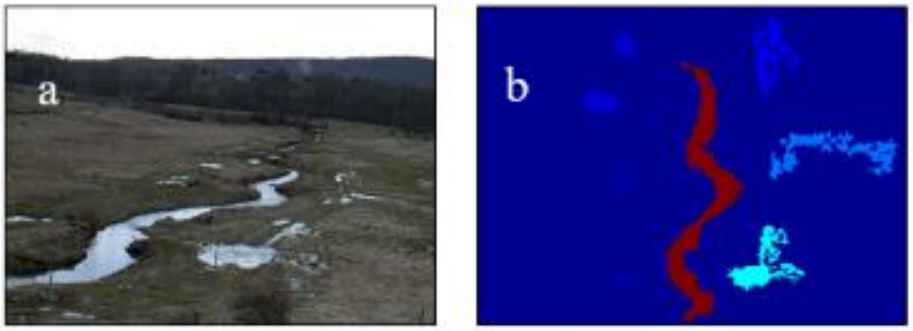

Figure 2-4. a) Image of Stroubles Creek and areas of wetness on the floodplain, b) classified image showing the degree of inundation across the image. The gradient in pixel color represents the degree of similarity between the given pixels and the user selected classification pixels, where dark red signifies a high degree of similarity and dark blue signifies no similarity.

2.2.4 Vegetation Analysis

The final metric measured by our algorithm is floodplain vegetation dynamics. To overcome the challenge of analyzing vegetation dynamics without multispectral vegetation indices, the Normalized Difference Red Green Index (NDRGI) as calculated below (Equation 1) was applied to all images.

$$\mathrm{NDRGI} = \frac{\rho_{\mathrm{Red}} - \rho_{\mathrm{Green}}}{\rho_{\mathrm{Red}} + \rho_{\mathrm{Green}}} \quad (1)$$

The NDRGI measures vegetative greenness based on difference between the reflectance values of the red (ρ_{Red}) and green (ρ_{Green}) spectral bands on a scale from 0 to 1 with a value of 0 corresponding to entirely green vegetation and a value of 1 corresponding to completely dormant vegetation (Yang et al., 2008; Stott et al., 2010). The index is highly transferable as it can be derived from any camera which produces images in RGB color space. This includes almost all forms of digital imagery, including satellite imagery. However, adjusting a camera's color space settings could constrain or inhibit the calculation of the index. Unlike wetness indices, calculation of NDRGI only depends on step 1 and step 2 in the MATLAB script: image rectification and ROI selection. Image classification has no impact on the calculated value of NDRGI because the calculations are based on stored reflectance values from the pixels in the image. For this study, weekly NDRGI values for an entire calendar year were plotted to examine the seasonal variation in floodplain vegetation dynamics (Figure 5). The plot shows that NDRGI values are highest during the winter months when vegetation is dormant and lowest during summer months when vegetation is photosynthetically active. Corresponding images of the floodplain during the different seasons are displayed as a form of visual verification.

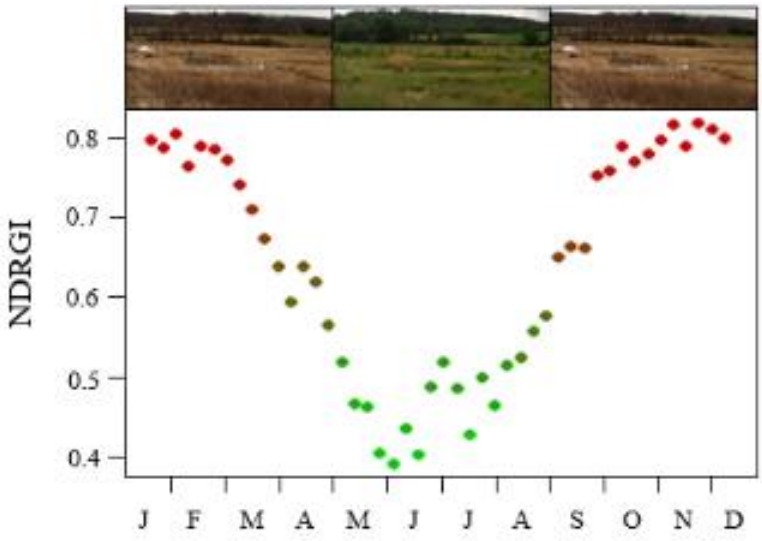

Figure 2-5. Values of NDRGI for weekly images over the course of the 2012 calendar year. Representative images of floodplain vegetation are shown above the corresponding growing seasons.

2.3 Results

2.3.1 Proof-of-concept

To validate the ability of our code to evaluate inundated surface area, we compared inundation area measured in camera imagery with inundation estimates from a previously developed inundation model. Described in Jones et al. (2015), the inundation model utilizes a digital terrain model of the floodplain and stage data measured at the site. The terrain model was derived from a combination of high resolution LiDAR and measured channel bathymetry, and developed using methods outlined by Merwade et al. (2008b). LiDAR data was provided by the City of Blacksburg. Data was collected in November of 2011, groundtruthed with a root mean square error of 1 m horizontally and 18 cm vertically, and point spacing of 1.4 m. Channel bathymetry data was measured using a real-time kinematic geographic positioning system (RTK-GPS, Topcon GR-3). The resulting digital elevation model has a 1 m by 1 m grid. Then, inundation was estimated utilizing conditional raster analysis similar to the method presented in Jones et al., 2008. The stage-surface area relationship from the model is shown in Figure 2-6.

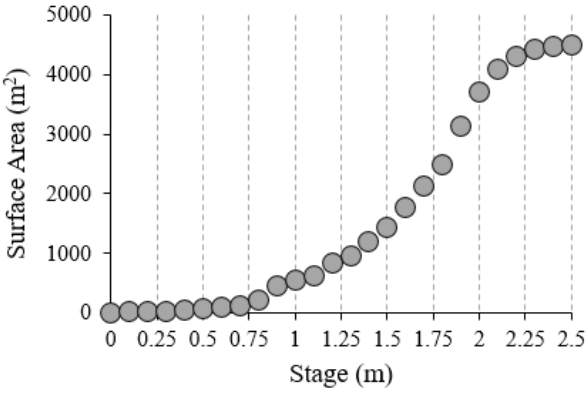

Figure 2-6. Relationship between stream stage and surface area resulting from the inundation model. Circles represent the modeled surface area at incremental stream stage values.

For validation, individual images from 20 independent 2012 storm events were selected and analyzed. Image based surface area estimations were matched with stream stage values measured at the same exact time via a pressure transducer in the thalweg of the stream. Corresponding modeled surface area estimates were determined based on the stage-surface area relationship. Results between methods were then compared using a simple regression analysis. The coefficient of determination (R^2), slope, and normalized root-mean-square error (Equation 2) were then calculated to determine goodness of fit of the data.

$$\text{NRMSE} = \frac{\sqrt{\frac{\sum_{i=1}^{n} (\hat{y} - y)^2}{n}}}{y_{max} - y_{min}} \qquad (2)$$

The NRMSE as shown above is a measure of residual variance, where $\hat{y}$ is the image based surface area estimations, y is modeled surface area estimations, and $y_{max} - y_{min}$ is the range of the modeled surface area values. The regression analysis between estimates from the two methodologies (Figure 2-7) resulted in a fairly linear relationship with a regression coefficient of determination (R^2) value of 0.94, a slope of 1.08, and a normalized root-mean-square error (NRMSE) of 7.96%, suggesting a strong correlation between the results. It should be noted that while there is a strong correlation between the modeled and image based estimations, modeled surface area predictions produced slightly higher values than image based estimations. This can be seen in Figure 2-7 where the regression line is slightly greater than the 1:1 ratio line, with a slope of 1.0792. These results are likely due to the visual obstruction of water created by the riparian vegetation and stream banks.

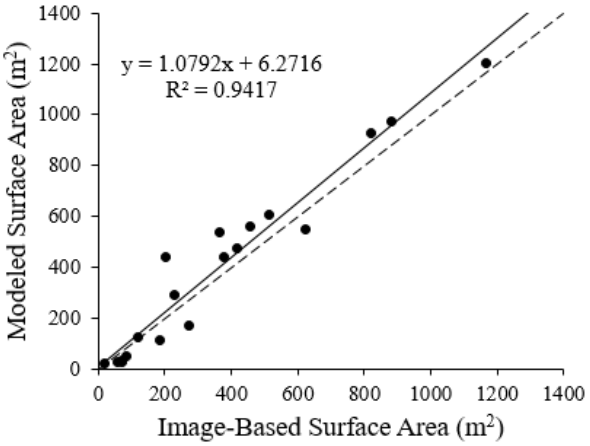

Figure 2-7. Comparison between modeled surface area and image-based estimations of surface area for 20 independent storm events. The dotted line represents the 1 : 1 ratio while the solid line represents the linear least squares regression line.

2.3.2 Limitations

While this new methodology can be easily implemented in a variety of environments, it should be noted that several limitations on applicability exist. First, stream visibility is limited during periods of low flow and high vegetation. The result of this error can be seen in the larger amount of variation associated with estimated inundation surface areas during periods of low flow in comparison with the relatively accurate estimations during periods of high flow. In the field of ecohydrology, high flows can be of greater interest than low flows as higher flows signify periods of time in which stream channels are hydrologically connected with their adjacent floodplains.

Second, water droplets on the camera lens can greatly distort or obstruct the camera's view during rain events or early in the morning due to the accumulation of dew. During storm events, water droplets can descend down the camera lens, distorting the image if on the lens at the instant when the image is taken. While this was generally not an issue in the majority of our images, instances of heavy precipitation did result in image distortion. During winter months, water on the camera can freeze, resulting in ice on the camera lens. This phenomenon generally occurs early in the morning when frost from the night before has accumulated on the surface of the camera lens. However by midday, none of the images were affected by ice on the camera lens.

Third, our system can only analyze images acquired during the day due to the limited spectral range of the imagery. The absence of nighttime data does not affect the ability to analyze vegetation dynamics, which do not change overnight but rather throughout seasons. However, flood events can occur entirely during the course of a single night due to the stochastic nature of flooding. Without nighttime data, it can be challenging to fully understand the ecohydrology of a system without other continuous variables (e.g., stream stage). Data could be retrieved in the dark by using a thermal or infrared camera. For example, infrared cameras have been used for analyzing hillslope and riparian saturation dynamics (Pfister et al., 2010) as well as wildlife habits (Claridge et al., 2005).

The fourth and final notable limitation with our code is that it relies on user selection of GCPs, ROIs, and classification points. As mentioned above, precise identification of GCPs is the most crucial aspect of the analysis. Error associated with ROI selection should be relatively low as this step is simply the selection of the analysis area in question. Classification point selection plays an important role in water identification and quantification. While this does not affect vegetation characteristic estimations which are calculated solely based on RGB reflectance values, water separability is greatly influenced by the selection of classification points. Thus the degree of accuracy in water based calculations has the potential for both random and systematic error based on the user. For example, user error could be the result of accidentally picking a dry area as a classification point or selecting a dry area that appears to be a wet. Despite its limitations and potential for error, the methodology provides a relatively simple and accurate process for monitoring surface water bodies.

2.4 Discussion

A great deal of research has been conducted on ecohydrologic dynamics of large surface water bodies and global ecohydrology (Jackson et al., 2009); nonetheless, very little research has focused on the ecohydrology of local water bodies (Janauer, 2000), which play a vital role in the overall context of ecohydrology. Furthermore, previous studies have expressed the importance of analyzing ecohydrology across scales with particular emphasis on the combination of large scale remote sensing and modeling with small scale monitoring (Janauer, 2000; Asbjornsen et al., 2013). The methodology described in this paper presents a useful new approach for monitoring and analysis of ecohydrology at multiple scales. Additionally, the presented applications illustrate just several of the many potential usages of our new methodology.

Digital imagery can be used for analyzing a variety of environmental parameters and water bodies while allowing for spatial monitoring and scaling of these variables. One such example is forested water bodies such as streams and wetlands. Forested streams and wetlands are extremely important ecosystems which provide services such as water quality improvement, flood control, and wildlife habitat (Walbridge, 1993). However, monitoring of forested systems is a major challenge as canopy cover limits the ability of freely available remote sensing to identify forested water bodies (Ozesmi and Bauer, 2002) and placing monitoring equipment in remote areas can be problematic. Innovative monitoring techniques such as our image processing approach allow for spatial and temporal studies in isolated regions without logistical issues such as transporting expensive instruments to remote locations and the dangers of consistent fieldwork in unsafe areas.

Urban streams would also benefit from this low cost monitoring system as urban systems are constantly changing and often unmonitored (Hughes and Yeakley, 2014). Moreover, urban stream management is generally focused on flood prevention as opposed to maintaining natural flow regimes (Zalewski and Wagner, 2005). The sharp contrast between low flows and sudden high flows generated from urban storm runoff can have considerable effects on stream channel-floodplain interactions and overall ecosystem health. Challenges in urban systems such as water quality degradation, habitat fragmentation, and bank erosion are difficult to address due to a lack of monitoring and public involvement (Hughes et al., 2014). Adding to these issues, storm events are often unsafe to monitor firsthand and do not get thoroughly analyzed as a result. Furthermore,

large floods can be difficult to monitor when fixed gauging stations are destroyed by high flows. These issues will be intensified by rapid urbanization and increased flooding, and thus, there is a great need for innovative monitoring techniques to overcome these obstacles. Imagery can provide valuable information (e.g., flood extent and discharge) during extreme events without being destroyed by the events themselves. Digital imagery approaches such as ours provide a new manner of addressing these challenges presented by urbanization.

The field of stream restoration has rapidly developed over the previous 20 years (Palmer et al., 2014) with a myriad of projects being undertaken across the U.S. (Bernhardt et al., 2005) and in Europe (Ormerod, 2004). However, a lack of monitoring frameworks and post project monitoring funding has limited the ability to address the successfulness of restoration projects (Buchanan et al., 2014; Morandi et al., 2014). Our methodology presents a new approach for monitoring stream restoration for long periods of time following project completion. Through digital imagery, one could observe a variety of parameters such as changes in stream channel geomorphology, successional vegetation, and success of planted trees. This idea diverges from the belief that large amounts of money and resources are necessary to monitor long term effects of stream restoration.

2.4.1 Crowdsourcing

The developed MATLAB code is robust enough that minimal alterations of the code allow for it to be implemented in a wide variety of environments. Furthermore, the code can be easily transfered to other programming languages or converted into an executable, so that users do not need a MATLAB license to utilize the script. Our code was developed this way because one of the key concepts of this study is to advance the idea of crowdsourcing and citizen science. Crowdsourcing can be defined as the participation of the general public in compiling data via the internet to be used for the greater good of society (Estellés-Arolas and González-Ladrón-de-Guevara, 2012). Citizen science has become prominent in environmental fields such as hydrology and ecology as environmental protection requires active participation from the general public (Buytaert et al., 2014). Despite its simplicity and voluntary nature, crowdsourcing has been a highly effective source of innovation in various environmental disciplines (Brabham, 2013). The monitoring methodology described in this paper lends itself well to innovative forms of crowdsourcing in multiple environmental fields. While our study utilizes a field camera, contemporary cellular phone cameras can be almost equally as effective in acquiring relatively high resolution digital images. With the advancement of smartphones, geographically referenced or geotagged images can be obtained via a smartphone camera and sent to a database. This allows for a crowdsourced monitoring approach which can be implemented in practically any location across the globe.

2.5 Conclusion

The following guidelines are provided as a basis for future studies or deployment. If performing a time-lapse analysis such as the one in our study, it is essential that the camera to be used can withstand environmental conditions such as precipitation and extreme temperatures. Depending on the length and scope of the project, a variety of camera options can be utilized. While our study used a high-tech camera, field cameras such as a trail and game cameras are readily available and relatively inexpensive (~ $100). Similar to camera selection, camera placement should aid in

optimizing the image analysis for specific questions. For example, placing the camera near the stream at a low elevation will provide coverage across all flow regimes, whereas higher placement (e.g. a tower) will provide greater spatial coverage. If at all possible, the camera should be directed due North or due South to avoid light interference from the sun's East to West movement. Positioning the camera in an area which is exposed to sunlight is necessary in colder regions where ice could accumulate on the camera lens. On the contrary, the camera should be placed in a shaded area if the local climate is warm and excess sun could potentially overheat the camera.

To utilize the methodology as a form of crowdsourcing, a variety of image acquisition approaches can be employed. For example, images from cell phones could be taken from a specified location or within a given region and sent to a database. Alternatively, designated areas could be set up so that images are taken at a precise monitoring location. This would be ideal in areas with large numbers of tourists visiting. For example, supraglacial streams in subarctic regions such as Alaska receive a great number of annual tourists and are also at the center of ecohydrology research due to drastically changing hydrology and nutrient fluxes (Hood and Scott, 2008; Blaen et al., 2014). Another example of potential applicability exists in developing countries where cameras are in abundance yet environmental data is scarce. For example, Frommberger and Schmid, 2013 implemented a disaster reporting system based on crowdsourcing from smartphones in Laos, a developing nation with very little publicly available environmental information. As the world continues to develop and environmental issues become greater, the incorporation of crowdsourcing into the field of ecohydrology will become increasingly more important.

The future of research in ecohydrology depends largely on a paradigm shift from the complex, discipline specific approach taken in research to a simplified yet holistic ecosystem approach. Thus far, an interdisciplinary manner has only been applied at a broad scale while neglecting local scale ecohydrology. The methodology described in this paper presents a breakthrough that bridges the gap between scales in the field of ecohydrology. While not without limitations, our new method provides a low-cost, user friendly, and widely applicable ecohydrologic monitoring system. Ideally, future studies will be able to improve upon the methodology by reducing its limitations and using it as a means of crowdsourcing.

2.6 Acknowledgements

The authors would like to thank Dan Lluch for his help in developing and revising our MATLAB code. We would also like to thank the Virginia Water Resources Research Center for their support with data collection.

2.7 References

Abu-Aly, T. R., G. B. Pasternack, J. R. Wyrick, R. Barker, D. Massa, and T. Johnson. 2014. Effects of LiDAR-derived, spatially distributed vegetation roughness on two-dimensional hydraulics in a gravel-cobble river at flows of 0.2 to 20 times bankfull. Geomorphology 206: 468-482, doi: 10.1016/j.geomorph.2013.10.017

Anderson, T. R., P.M. Groffman, and M. T. Walter. 2015. Using a soil topographic index to distribute denitrification fluxes across a northeastern headwater catchment. J. Hydrol. 522: 123-134, doi: 10.1016/j.jhydrol.2014.12.043

Asbjornsen, H., G.R. Goldsmith, M. S. Alvarado-Barrientos, and others. 2011. Ecohydrological advances and applications in plant–water relations research: a review. J Plant Ecol. 4: 3-22, doi: 10.1093/jpe/rtr026

Baird, A. J., and R. L. Wilby. 1999. Eco-hydrology: plants and water in terrestrial and aquatic environments. New York: Routledge Press.

Ballesteros, J. A., J. M. Bodoque, A. Díez-Herrero, M. Sanchez-Silva, and M. Stoffel. 2011. Calibration of floodplain roughness and estimation of flood discharge based on tree-ring evidence and hydraulic modelling. J. Hydrol. 403: 103-115, doi: 10.1016/j.jhydrol.2011.03.045

Bates, P. D. 2012. Integrating remote sensing data with flood inundation models: how far have we got? Hydrol. Process. 26: 2515-2521, doi: 10.1002/hyp.9374

Batson, J., G. B. Noe, C. R. Hupp, K. W. Krauss, N. B. Rybicki, E. R. and Schenk. 2015. Soil greenhouse gas emissions and carbon budgeting in a short-hydroperiod floodplain wetland. J. Geophys. Res.-Biogeo. 120: 77-95, doi: 10.1002/2014JG002817

Bernhardt, E. S., M. Palmer, J. D. Allan, and others. 2005. Synthesizing U. S. river restoration efforts. Science. 308: 636-637, doi: 10.1126/science.1109769

Blaen, P. J., A. M. Milner, D. M. Hannah, J. E. Brittain, and L. E. Brown. 2014. Impact of changing hydrology on nutrient uptake in high arctic rivers. River Res. Appl. 30: 1073-1083, doi: 10.1002/rra.2706

Boudell, J. A., M.D. Dixon, S. B. Rood, and J. C. Stromberg. 2015. Restoring functional riparian ecosystems: concepts and applications. Ecohydrology. 8: 747-752, doi: 10.1002/eco.1664

Brabham, D. C. 2013. Crowdsourcing. MIT Press.

Brauman, K. A., G. C. Daily, T. K. E. Duarte, and H. A. Mooney. 2007. The nature and value of ecosystem services: an overview highlighting hydrologic services. Annu. Rev. Env. Resour. 32: 67-98, doi: 10.1146/annurev.energy.32.031306.102758

Buchanan, B. P., G.N. Nagle, and M. T. Walter. 2014. Long-term monitoring and assessment of a stream restoration project in central new york. River Res. Appl. 30: 245-258, doi: 10.1002/rra.2639

Buytaert, W., Z. Zulkafli, S. Grainger, and others. 2014. Citizen science in hydrology and water resources: opportunities for knowledge generation, ecosystem service management, and sustainable development. Front. Earth Sci. 2: 1-21, doi: 10.3389/feart.2014.00026

Claridge, A. W., G. Mifsud, J. Dawson, and M. J. Saxon. 2005. Use of infrared digital cameras to investigate aspects of the social behaviour of cryptic species. Wildlife Res. 31: 645-650, doi: 10.1071/WR03072

Cook, A., and V. Merwade. 2009. Effect of topographic data, geometric configuration and modeling approach on flood inundation mapping. J. Hydrol. 377: 131-142, doi: 10.1016/j.jhydrol.2009.08.015

Davidson, E. A., and I. A. Janssens. 2006. Temperature sensitivity of soil carbon decomposition and feedbacks to climate change. Nature. 440: 165-173, doi: 10.1038/nature04514

DeFries, R. S., and J.R. G. Townshend. 1994. NDVI-derived land cover classifications at a global scale. Int. J. Remote Sens. 15: 3567-3586, doi: 10.1080/01431169408954345

Dobriyal, P., A. Qureshi, R. Badola, and S. A. Hussain. 2012. A review of the methods available for estimating soil moisture and its implications for water resource management. J. Hydrol. 458: 110-117, doi: 10.1016/j.jhydrol.2012.06.021

Estellés-Arolas, E., and F. González-Ladrón-de-Guevara. 2012. Towards an integrated crowdsourcing definition. J. Inf. Sci. 38: 189-200, doi: 10.1177/0165551512437638

Field, C. B., J. T. Randerson, and C. M. Malmström. 1995. Global net primary production: combining ecology and remote sensing. Remote Sens. Environ. 51: 74-88, doi: 10.1016/0034-4257(94)00066-V

Fennessy, M. S., A. D. Jacobs, and M. E. Kentula. 2004. Review of rapid methods for assessing wetland condition. EPA/620/R-04/009. US Environmental Protection Agency, Washington, DC.

Frommberger, L., and F. Schmid. 2013. Crowdsourced bi-directional disaster reporting and alerting on smartphones in Lao PDR. arXiv preprint arXiv:1312.6036.

Grygoruk, M., and M. Acreman. 2015. Restoration and management of riparian and riverine ecosystems: ecohydrological experiences, tools and perspectives. Ecohydrol. Hydrobiolo. 15: 109-110, doi: 10.1016/j.ecohyd.2015.07.002

Harding, J. S., E. F. Benfield, P. V. Bolstad, G. S. Helfman, and E. B. D. Jones. 1998. Stream biodiversity: the ghost of land use past. Proc. Natl. Acad. Sci. U.S.A. 95: 14843-14847, doi: 10.1073/pnas.95.25.14843

Hilldale, R. C., and D. Raff. 2008. Assessing the ability of airborne LiDAR to map river bathymetry. Earth Surf. Proc. Land. 33: 773-783, doi: 10.1002/esp.1575

Hood, E., and D. Scott. 2008. Riverine organic matter and nutrients in southeast Alaska affected by glacial coverage. Nat. Geosci. 1: 583-587, doi: 10.1038/ngeo280

Hughes, R. M., S. Dunham, K. G. Maas-Hebner, and others. 2014. A review of urban water body challenges and approaches: (1) rehabilitation and remediation. Fisheries. 39: 18-29.

Hughes, R. M., and J. A. Yeakley. 2014. Major Research and Monitoring Needs for Urban Streams and Watersheds. p. 243-252. In J. A. Yeakley, K. G. Maas-Hebner, and R. M. Hughes [eds.], Wild Salmonids in the Urbanizing Pacific Northwest. Springer New York.

Hunter, N. M., P. D. Bates, M. S. Horritt, and M. D. Wilson. 2007. Simple spatially-distributed models for predicting flood inundation: a review. Geomorphology. 90: 208-225, doi: 10.1016/j.geomorph.2006.10.021

Jackson, R. B., E. G. Jobbágy, and M. D. Nosetto. 2009. Ecohydrology in a human-dominated landscape. Ecohydrology. 2: 383-389, doi: 10.1002/eco.81

Janauer, G. A. 2000. Ecohydrology: fusing concepts and scales. Ecol. Eng. 16: 9-16, doi: 10.1016/S0925-8574(00)00072-0

Jin, S., L. Yang, P. Danielson, C. Homer, J. Fry, and G. Xian. 2013. A comprehensive change detection method for updating the National Land Cover Database to circa 2011. Remote. Sens. Environ. 132: 159-175, doi: 10.1016/j.rse.2013.01.012

Jones, C.N., D.T. Scott, C. R. Guth, E. R. Hester, and W. C. Hession. 2015. Seasonal variation in floodplain biogeochemical processing in a restored headwater stream. Env. Sci. Tech. 49: 13190-13198, doi: 10.1021/acs.est.5b02426

Jones, K., G. Poole, S. O'Daniel, L. Mertes, and J. Stanford. 2008, Surface hydrology of low-relief landscapes: Assessing surface water flow impedance using LIDAR-derived digital elevation models, Remote Sens. Environ. 112: 4148–4158. doi: 10.1016/j.rse.2008.01.024.

Kirchner, J. W., X. Feng, C. Neal, and A. J. Robson. 2004. The fine structure of water-quality dynamics: the (high-frequency) wave of the future. Hydrol. Process. 18: 1353-1359, doi: 10.1002/hyp.5537

Krause, S., J. Lewandowski, C. N. Dahm, and K. Tockner. 2015. Frontiers in real-time ecohydrology–a paradigm shift in understanding complex environmental systems. Ecohydrology. 8: 529-537. doi: 10.1002/eco.1646

Lang, M. W., and G. W. McCarty. 2009. LiDAR intensity for improved detection of inundation below the forest canopy. Wetlands. 29: 1166-1178, doi: 10.1672/08-197.1

Leckie, D. G., E. Cloney, C. Jay, and D. Paradine. 2005. Automated Mapping of Stream Features with High-Resolution Multispectral Imagery. Photogramm. Eng. Rem. S. 71: 145-155, doi: 10.14358/PERS.71.2.145

Merwade, V., F. Olivera, M. Arabi, and S. Edleman. 2008a. Uncertainty in flood inundation mapping: current issues and future directions. J. Hydrol. Eng. 13: 608-620, doi: 10.1061/(ASCE)1084-0699(2008)13:7(608)

Merwade V., A. Cook, and J. Coonrod. 2008b. GIS techniques for creating river terrain models for hydrodynamic modeling and flood inundation mapping. Environ. Model. Softw. 23: 1300-1311, doi: 10.1016/j.envsoft.2008.03.005

Milan, D. J., and G. L. Heritage. 2012. LiDAR and ADCP Use in Gravel-Bed Rivers: Advances Since GBR6. p. 286-302. In M. Church, P. M. Biron, and A. G. Roy [eds.] Gravel-Bed Rivers: Processes, Tools, Environments. John Wiley & Sons, Ltd, Chichester, UK, doi: 10.1002/97811199claridg52497.ch22

Milan, D. J., G. L. Heritage, A. R. G. Large, and N. S. Entwistle. 2010. Mapping hydraulic biotopes using terrestrial laser scan data of water surface properties. Earth Surf. Proc. Land. 35: 918-931, doi: 10.1002/esp.1948

Morandi, B., H. Piégay, N. Lamouroux, and L. Vaudor. 2014. How is success or failure in river restoration projects evaluated? Feedback from French restoration projects. J. Environ. Manage. 137: 178-188, doi: 10.1016/j.jenvman.2014.02.010

Naiman, R. J., H. Decamps, and M. Pollock. 1993. The role of riparian corridors in maintaining regional biodiversity. Ecol. Appl. 3: 209-212, doi: 10.2307/1941822

Ormerod, S. J. 2004. A golden age of river restoration science? Aquat. Conserv. Mar. Freshw. Ecosys. 14: 543-549, doi: 10.1002/aqc.663

Ozesmi, S. L., and M. E. Bauer. 2002. Satellite remote sensing of wetlands. Wetl. Ecol. Manage. 10: 381-402, doi: 10.1023/A:1020908432489

Palmer, M. A., K. L. Hondula, and B. J. Koch. 2014. Ecological restoration of streams and rivers: shifting strategies and shifting goals. Annu. Rev. Ecol. Evol. Syst. 45: 247-269, doi: 10.1146/annurev-ecolsys-120213-091935

Pettorelli, N., J. O. Vik, A. Mysterud, J. M. Gaillard, C. J. Tucker, and N. C. Stenseth. 2005. Using the satellite-derived NDVI to assess ecological responses to environmental change. Trends Ecol. Evol. 20: 503-510, doi: 10.1016/j.tree.2005.05.011

Pfister, L., J. J. McDonnell, C. Hissler, and L. Hoffmann. 2010. Ground-based thermal imagery as a simple, practical tool for mapping saturated area connectivity and dynamics. Hydrol. Process. 24: 3123-3132. doi: 10.1002/hyp.7840

Resop, J. P., and W. C. Hession. 2010. Terrestrial laser scanning for monitoring streambank retreat: Comparison with traditional surveying techniques. J. Hydraul. Eng. 136: 794-798, doi: 10.1061/(ASCE)HY.1943-7900.0000233

Resop, J. P., J. L. Kozarek, and W. C. Hession, W. C. Terrestrial laser scanning for delineating in-stream boulders and quantifying habitat complexity measures. Photogramm. Eng. Rem. S.78: 363-371, doi: 10.14358/PERS.78.4.363

Rodriguez-Iturbe, I. 2000, Ecohydrology: A hydrologic perspective of climate-soil-vegetation dynamics. Water Resour. Res. 36: 3–9. doi:10.1029/1999WR900210.

Royem, A. A., C. K. Mui, D. R. Fuka, and M. T. Walter. 2012. Technical note: proposing a low-tech, affordable, accurate stream stage monitoring system. T. ASABE. 55: 237-242, doi: 10.13031/2013.42512

Saksena, S., and V. Merwade. 2015. Incorporating the effect of DEM resolution and accuracy for improved flood inundation mapping. J. Hydrol. 530: 180-194, doi: 10.1016/j.jhydrol.2015.09.069

Scott, D. T., R. F. Keim, B. L. Edwards, C. N. Jones, and D. E. Kroes. 2014. Floodplain biogeochemical processing of floodwaters in the Atchafalaya River Basin during the Mississippi River flood of 2011. J. Geophys. Res. Biogeo. 119: 537-546, doi: 10.1002/2013JG002477

Sheaffer, J. R., J. D. Mullan, and N. B. Hinch. 2002. Encouraging wise use of floodplains with market-based incentives. Environ. Sci. Pol. Sustain. Devel. 44: 32-43, doi: 10.1080/00139150209605590

Skinner, K.D. 2011. Evaluation of LiDAR-acquired bathymetric and topographic data accuracy in various hydrogeomorphic settings in the Deadwood and South Fork Boise Rivers, West-Central Idaho, 2007: U.S. Geological Survey Scientific Investigations Report 2011–5051, 30 p.

Stott, D., D. S. Boyd, A. Beck, and A. G. Cohn. 2015. Airborne LiDAR for the detection of archaeological vegetation marks using biomass as a proxy. Remote Sens. 7: 1594-1618, doi: 10.3390/rs70201594

Straatsma, M. W., and M. J. Baptist. 2008. Floodplain roughness parameterization using airborne laser scanning and spectral remote sensing. Remote Sens. Environ. 112: 1062-1080, doi: 10.1016/j.rse.2007.07.012

Tockner, K., and J. A. Stanford. 2002. Riverine flood plains: present state and future trends. Environ. Conserv. 29: 308-330, doi: 10.1017/S037689290200022X

Vanderhoof, M. K., L. C. Alexander, and M. J. Todd. Temporal and spatial patterns of wetland extent influence variability of surface water connectivity in the Prairie Pothole Region, United States. Landsc. Ecol. 30: 1-20. doi: 10.1007/s10980-015-0290-5

Vidon, P., S. Marchese, M. Welsh, and S. McMillan. 2015. Short-term spatial and temporal variability in greenhouse gas fluxes in riparian zones. Environ. Monit. Assess. 187: 1-9, doi: 10.1007/s10661-015-4717-x

Walbridge, M. R. 1993. Functions and values of forested wetlands in the southern United States. J. For. 91: 15-19.

Wright, A., W. A. Marcus, and R. Aspinall. 2000. Evaluation of multispectral, fine scale digital imagery as a tool for mapping stream morphology. Geomorphology. 33: 107-120, doi: 10.1016/S0169-555X(99)00117-8

Yang, Z., P. Willis, and R. Mueller. 2008. Impact of band-ratio enhanced AWIFS image to crop classification accuracy. In: Proc. Pecora 17, The Future of Land Imaging Going Operational. November 18 – 20, 2008, Denver, Colorado, USA

Zalewski, M., and I. Wagner. 2005. Ecohydrology- the use of water and ecosystem processes for healthy urban environments. Ecohydrol. Hydrobiol. 5: 263-268.

CHAPTER 3. MONITORING VOLUMETRIC FLUCTUATIONS IN TROPICAL LAKES AND RESERVOIRS USING SATELLITE REMOTE SENSING

Tyler A. Keys and Durelle T. Scott

Submitted: June 2017
To: *Lake and Reservoir Management*
Status: Published December 2017. DOI: 10.1080/10402381.2017.1402226

Abstract

Sustainable management of lakes and reservoirs is currently a major challenge in regions of the world with limited hydrologic data and monitoring equipment. Specifically, temporal variability of water storage is difficult to quantify and is often neglected in lake and reservoir management. Here, we present a high temporal resolution remote sensing technique for quantifying volumetric fluctuations in surface water bodies without any field data. For this study, we utilized Moderate Resolution Imaging Spectroradiometer (MODIS) satellite imagery in conjunction with satellite radar altimetry from two altimetry databases to develop high frequency time series of storage variations in ten large tropical surface water bodies. For three of the sites, altimetry-based water level (L) estimates were validated by in situ data from monitoring stations while estimates of surface area (A) and changes in water volume (ΔV) were validated by bathymetric maps with corresponding L-A and L-ΔV polynomial relationships. Results indicate that remotely sensed ΔV estimates agree well with in situ measurements for two of the three water bodies. For the third, A and ΔV estimates were greatly underestimated due to the coarse spatial resolution of MODIS. Our findings suggest that the presented methodology works well for lakes and reservoirs with well-defined boundaries and low shoreline to surface area (S:A) ratios, in contrast to reservoirs with dendritic geometry and high S:A ratios. Overall, this method provides a free, user-friendly platform for monitoring and managing lakes and reservoirs.

3.1 Introduction

Sustainable management of lakes and reservoirs is becoming increasingly more important as global population and water demand increases. There are currently 117 million lakes and reservoirs greater than 0.002 km^2 (2,000 m^2) in the world, making up 3.7% of the Earth's land surface area (Verpoorter et al. 2014). Societal well-being depends on these surface water bodies and yet very few lakes or reservoirs are actually monitored (Alsdorf et al. 2007). Generally, hydrographic surveying of water body bathymetry is conducted via Sound Echoing and Ranging (SONAR) (Yesuf et al. 2013) or bathymetric Light Detection and Ranging (LiDAR) (Hilldale and Raff 2008, Skinner 2011). Unfortunately, these methods require a great deal of money, time, and labor (Peng et al. 2006). Furthermore, in situ monitoring of lakes and reservoirs is often problematic in

developing nations due to the hydro-political dangers of monitoring in international basins (Hossain et al. 2007).

Satellite remote sensing has great potential for monitoring surface water bodies but is often limited by temporal resolution as well as the computational time required for image processing and interpretation (Lillesand et al. 2014). Since the introduction of satellite remote sensing, studies have measured inundation dynamics through imagery from various satellite sensors such as JERS-1 Synthetic Aperture Radar (e.g., Hess et al. 2015), AVHRR (e.g., Jain et al. 2006), and SPOT (e.g., Blasco et al. 1992). However, the most ubiquitously used satellite imagery comes from the Landsat and MODIS sensors, largely due to their free availability (Wulder et al. 2012). Landsat's high spatial resolution (30 m) has proved useful for identifying fine details, but the satellite's return time of once every 16 days has limited its use in temporal studies. Additionally, Landsat images are often obscured by cloud cover, further reducing the temporal resolution from 16 days to several months. This issue was aided by the 1999 introduction of the MODIS sensor flown on NASA's Terra and Aqua satellites, both of which have return times of 1-2 days. The main caveat with MODIS is its coarse spatial resolution (250-1000 m), which is an order of magnitude lower than that of Landsat's 30 m resolution. As a result, Landsat and MODIS have been used to study markedly different questions. For example, studies have used Landsat for assessing water quality in reservoirs at a single point in time (Nellis et al. 1998, Wang et al. 2004). On the contrary, MODIS has been utilized to develop time series of flood inundation extent and variations (Ordoyne and Friedl 2008, Islam et al. 2010, Brakenridge and Anderson 2006, Wang et al. 2008, Yan et al. 2010, Feng et al. 2012).

In addition to areal inundation analysis, measuring water level fluctuations in inland water bodies became possible through the introduction of satellite altimetry. Altimeters emit radar or laser pulses and measure the distance from the satellite to the earth's surface (range) based on the amount of time it takes for the pulse to return to the sensor. Water elevation can be estimated by calculating the difference between the range and the known altitude of the altimeter above a known datum while taking into account corrections for several factors such as atmospheric, tropospheric, and ionospheric disturbances (Calmant et al. 2008). Altimetry data collection began in 1985 with the original purpose of measuring sea levels, however the global tracks also proved useful for measuring water levels in lakes and reservoirs (Birkett 1995). Satellite altimetry has been widely utilized to measure water level variations in a variety of inland water bodies including lakes (Alsdorf et al. 2001, Crétaux and Birkett 2006, Crétaux et al. 2011), wetlands (Birkett 1998, Kim et al. 2009, Lee et al. 2009), rivers (Birkett 1998, Maheu 2003), and floodplains (Alsdorf et al. 2000). In recent decades, studies have successfully utilized satellite remote sensing to quantify more complex hydrologic metrics such as river discharge (Smith and Pavelsky 2008, Muala et al. 2014, Coe and Birkett 2004), floodplain volumetric fluctuations (Alsdorf 2003, Frappart et al. 2005), and lake/reservoir volumetric fluctuations, the latter of which has primarily been conducted using a combination of remotely sensed and in situ data (Sawunyama et al. 2006, Zhang et al. 2006, Smith and Pavelsky 2009). While this approach has yielded accurate estimates, it requires either water level or bathymetry data, both of which can be difficult to obtain. More recent studies have avoided this issue by quantifying volumetric fluctuations in lakes and reservoirs entirely using remote sensing (Singh et al. 2012, Duan and Bastiaanssen 2013, Zhu et al. 2014). This approach has yielded promising results but is still a challenge due to limited numbers of days with both a high quality satellite image and altimetry measurement.

Here, we demonstrate a high temporal resolution approach for quantifying volumetric fluctuations within tropical lakes and reservoirs through the use of satellite imagery and altimetry. Our methodology utilizes altimetry data from multiple satellite altimeters and imagery from the MODIS satellite sensor. All of this data is freely available and has been produced at 8-10 day intervals consistently since 2000. Volumetric fluctuations were estimated by integrating the polynomial relationships between water level (L) and surface area (A). To validate our results, in situ water levels from gaging stations and bathymetry derived L-A and L-ΔV relationships were compared with satellite derived estimates. Results illustrate the ability of this methodology to accurately calculate volumetric fluctuations in tropical lakes and reservoirs. We found that the methodology worked well for large (surface area > 100 km^2) lakes and reservoirs. However, reservoirs with complex geometric features such as branching channels are much more difficult to assess due to the coarse spatial resolution of MODIS imagery. Thus, we present possible solutions to this problem as well as ways to incorporate these solutions into our methodology.

3.2 Methods

3.2.1 Study Sites

We studied 10 different inland water bodies of varying size and distribution across the tropics (Figure 3-1, Table 3-1). These ten sites were selected because they represent a wide range of volumes, surface elevations, and geographic locations. Furthermore, the sites are all located within rapidly developing regions of the world and are in the midst of the grand challenge of producing energy, providing food and water, and maintaining critical ecosystem services (Winemiller et al. 2016). With proposed hydropower development in the foreseeable future for all of these basins, accurate monitoring of water storage and allocation is critical. Additionally, all ten sites have freely available altimetry data that can be used for water level estimates. However, of the ten sites, only three contain freely available bathymetric data for validation. Thus, these three were further investigated to validate results for this study: Tonle Sap Lake in Cambodia, Lake Tana in Ethiopia, and Balbina Reservoir in Brazil (Figure 3-2). These validation sites were selected because they have bathymetric maps with L-A and L-V relationships as well as water level data from monitoring stations.

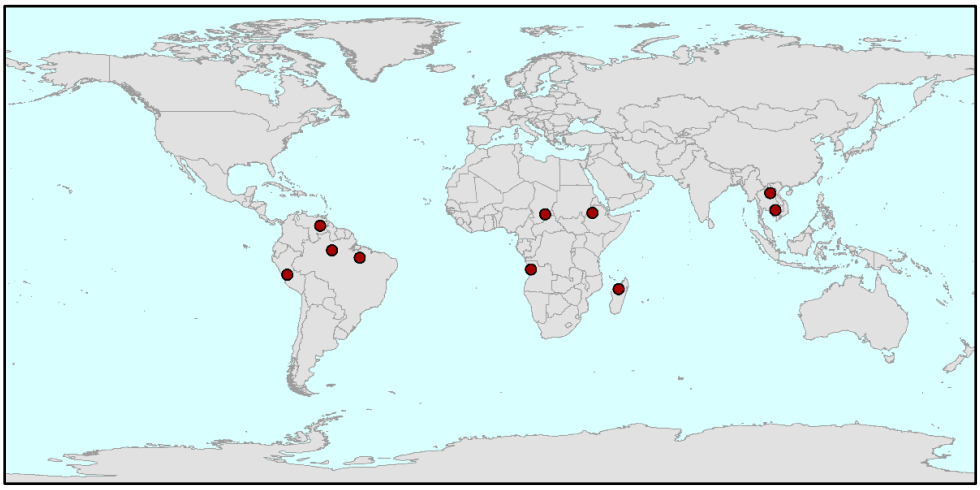

Figure 3-1. Locations of the ten water bodies across the tropics.

Table 3-1. Site characteristics compiled from a variety of sources: Kummu et al. 2014, Kebedee et al., 2006, Wale et al., 2009, Duan and Bastiaanssen, 2014, Kemenes et al., 2011, Palmeirim et al., 2014, and the GLWD.

Lake/ Reservoir	Major River Basin	Latitude	Longitude	Surface Elevation (masl)	Shoreline Length (km)	Mean Surface Area (km^2)	Shoreline : Area (km/km^2)	Primary Use
Tonle Sap	Mekong	12°53'N	104°04'E	5	22723	8640	2.63	Agriculture
Tana	Nile	12°00'N	37°15'E	1786	385	3156	0.12	Hydropower
Balbina	Amazon	1°53'S	59°28'W	47	13683	2360	5.8	Hydropower
Guri	Caroni	7°12'N	62°49'W	329	7413	3950	1.88	Hydropower
Tucurui	Tocantins	4°34'S	49°29'W	53	5500	2430	2.26	Hydropower
Iro	Bahr Salamat	10°6'N	19°25'E	361	44	120	0.37	None
Quiminha	Cuanza	8°57'S	14°0'E	51	307	120	2.55	Unknown
Junin	Mantaro	11°1'S	76°9'W	3975	95	141	0.67	None
Kinkony	Mahavavy	16°9'S	45°48'E	63	240	116	2.06	Unknown
Nam Ngum	Nam Ngum	18°37'N	102°40'E	221	1072	387	2.77	Hydropower

* Shoreline:Area ratio was calculated using average shoreline length and average surface area.

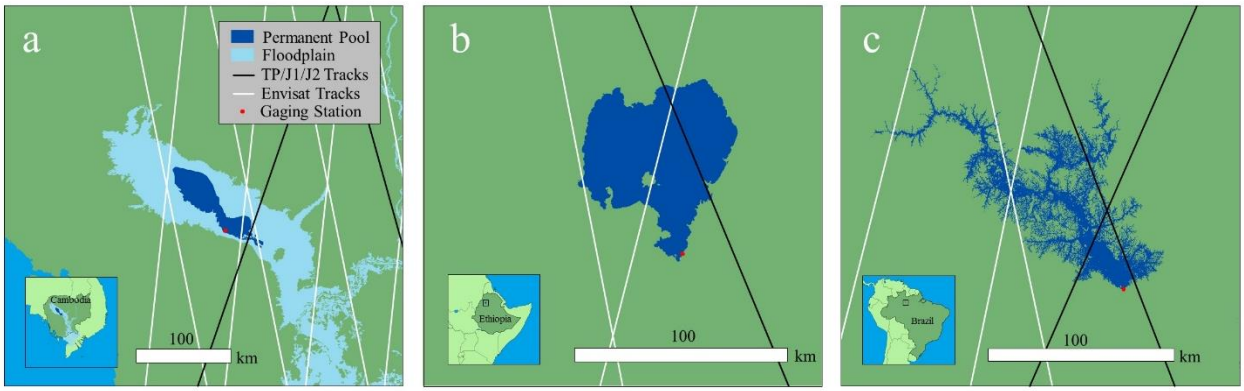

Figure 3-2. Locations of the three selected validation water bodies: a) Tonle Sap Lake located in the Mekong River Basin b) Lake Tana in the Nile River Basin and c) the Balbina Reservoir in the Amazon River Basin. Black Lines represent altimetry tracks for Topex/Poseidon (TP), Jason-1 (J1), and Jason-2 (J2) satellite altimeters while with lines represent altimetry tracks for the Envisat satellite altimeter.

Although the water bodies are all tropical, each has unique attributes that affect their hydrology. Tonle Sap Lake is a natural, unregulated lake located in the Mekong River Basin with its permanent pool spreading across the Cambodian provinces of Siem Reap, Battambang, Pursat, and

Kampong Thom and its floodplain extending into the lower portions of Vietnam. The Tonle Sap is unique in two ways: (1) its surface area fluctuates between 2,000 and 16,000 km^2 between the wet and dry seasons, and (2) the direction of flow changes between seasons with water flowing in during the wet season and out during the dry season (Kummu et al. 2008). Lake Tana is located within the Nile River Basin in the Amhara region of Ethiopia. Despite being fed by over 40 rivers, Lake Tana has only one outflow, the Blue Nile. Though it is a natural lake, the flow of Lake Tana is regulated by a water level regulation weir that was built in 1996 to aid downstream hydropower production (Kebede et al. 2006). Balbina Reservoir is located on the Uatumã River, one of the largest tributaries of the Amazon River, in the Brazilian state of Amazonas. The reservoir was created in 1987 following the construction of the Balbina Dam, the largest hydropower station in the Amazon River Basin (Fearnside 1989). The reservoir contains ~1,500 small islands separated by shallow valleys surrounding its main pool (Alsdorf et al. 2001).

3.2.2 Water Level Estimation

To estimate water levels in each of the water bodies, pre-processed satellite altimetry derived water level data was acquired from two different altimetry databases: Global Reservoir and Lake Monitor (GRLM) (http://www.pecad.fas.usda.gov/cropexplorer/global_reservoir) and Hydroweb (http://www.legos.obs-mip.fr/soa/hydrologie/hydroweb/). The GRLM database contains a combination of Topex/Poseidon, Jason-1, Jason-2, and ENVISAT satellite altimetry data for large lakes and reservoirs around the world. Water levels in the GRLM database are all referenced to the 9-year Topex/Poseidon mean level (Duan and Bastiaanssen 2013) at ten day temporal resolution. Similar to GRLM, Hydroweb contains water level data derived from the same satellites but at less frequent intervals (once every 30 days). Water levels in the Hydroweb database are all referenced to the Gravity Recovery and Climate Experiment (GRACE) GCM02C geoid datum. Both GRLM and Hydroweb contain data from 1992-present, but at different time intervals as mentioned above. Here, we used GRLM altimetry data for the nine of the sites, and Hydroweb for the Balbina Reservoir due to limited data availability. While several sites were available in both the GRLM and Hydroweb databases, we chose to use GRLM due to the higher temporal resolution of data.

3.2.3 Surface Area Estimation

For this study, we selected 500 m resolution, 8-day surface reflectance MODIS images from the MOD09A1 dataset due to its high quality and temporal resolution. While the spatial resolution of this MODIS dataset (500 m) is substantially coarser than that of Landsat (30 m), its temporal resolution of 8 days is better than that of Landsat's 16 days. Additionally, Landsat images often have low quality and cannot be used due to cloud cover, further increasing the interval of time between quality images. The MOD09A1 dataset avoids these complications by automatically selecting the highest quality image from the previous 8 days of MODIS images. While this reduces temporal resolution to 8 days, it provides higher quality images and filters out low quality images. We downloaded and processed MOD09A1 images using the newly developed MODISTools package for R Statistical computing language (Tuck et al. 2014). Image subsets were created by selecting a precise geographic location in the middle of each lake/reservoir and setting a subset radius that would capture the entire surface area of the lake/reservoir without capturing other bodies of water within the MODIS tile (e.g., 100 km for a lake with a 98 km radius). Additionally,

the MODISTools package has a unique quality control feature that removes poor quality images (primarily due to cloud cover) from the downloaded dataset. The R script that we used to download and process imagery is provided in the supplementary materials section.

We used the Modified Normalized Difference Water Index (MNDWI) to delineate water bodies within the MODIS images due to its robust and simplistic nature. The MNDWI, developed by Xu (2006), uses the ratio of the difference between the reflectance values of the Green and Middle Infrared (MIR) spectral bands to the sum of the Green and MIR bands (Equation 1):

$$\text{MNDWI} = \frac{\text{Green - MIR}}{\text{Green + MIR}} \quad (1)$$

where MNDWI is the calculated value ranging between -1 and 1, Green is the reflectance value of the Green band (MODIS band 4) and MIR is the Middle Infrared band (MODIS band 7). All pixels within MODIS subset images were classified via the MNDWI. Then, water and land pixels were delineated using a simple threshold value of 0, where a pixel with an MNDWI value less than 0 was classified as land and a pixel with an MNDWI value greater than 0 was classified as water (Figure 3-3). For each water body, we examined the classified images in ArcGIS to ensure that the threshold value of 0 worked well. Water pixels were then summed up in each image and multiplied by the spatial resolution of the image (500 m x 500 m in this case) to determine the total surface area (A) of each lake/reservoir.

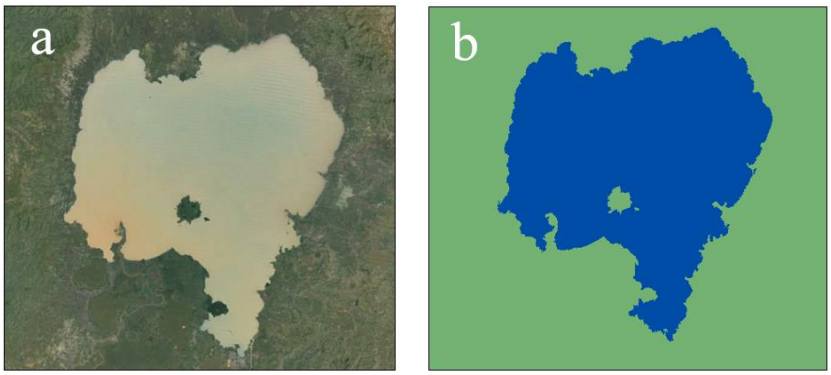

Figure 3-3. Aerial images of Lake Tana demonstrating a) an unclassified image and b) a classified raster image with land and water pixels delineated using the MNDWI.

3.2.4 Volumetric Estimation

To quantify volumetric fluctuations, we created a L-A relationship (Equation 2) using altimetry water level estimates and corresponding imagery derived surface area estimates and integrated the relationship (Equation 3). However, because we wanted to calculate volumetric fluctuations, the water level above the lowest recorded water level was used in the L-A relationship.

$$A(L) = aL^2 + bL + c \quad (2)$$

$$\int A(L) = \frac{aL^3}{3} + \frac{bL^2}{2} + cL + d \quad (3)$$

$$\Delta V(L) = \frac{aL^3}{3} + \frac{bL^2}{2} + cL \quad (4)$$

where A is the surface area as a function of water level, L is the water level above the lowest recorded level, a, b, and c are polynomial coefficients, and d is the constant of integration. Because L and ΔV are both 0 at the lowest recorded level, d is also 0 (Equation 4). Changes in volume were then calculated by substituting values of the corresponding water level above the lowest value into the newly generated L-ΔV relationship (Equation 4). This approach has been used in previous studies (e.g., Duan and Bastiaanssen 2013, Muala et al. 2014) and was determined to be most reliable at estimating volumetric fluctuations. Furthermore, this method avoids the error generated by estimating lake/reservoir bathymetry, particularly in water bodies with highly irregular bathymetry.

3.2.5 Validation

To validate our satellite derived water level estimates, we used in situ water level data for each of the three validation sites. For validation of surface area and volumetric fluctuations, we used bathymetry derived L-A and L-ΔV polynomial relationships from previous studies. For the Tonle Sap, we utilized relationships from Kummu et al. (2014) based on a bathymetry map of the Tonle Sap and its floodplain. Lake Tana relationships were inversely derived from Wale et al. (2009) as performed by Duan and Bastiaanssen (2013), which developed polynomial relationships as a function of volume instead of water level. For the Balbina Reservoir, we used a quadratic regression model created from a bathymetric map of the Reservoir (Kemenes et al. 2011). Error was assessed for each variable (L, A, and ΔV) using the Normalized Root Mean Square Error (NRMSE), a common metric for determining residual variance at different scales (Equation 5):

$$NRMSE = \frac{\sqrt{\sum_{i=1}^{i=n} \frac{(Est_i - Obs_i)^2}{n}}}{\Delta Obs} \quad (5)$$

where Est_i represents remotely sensed estimates, Obs_i represents in situ observed values, n represents the total number of paired samples, and ΔObs represents the range of the observed data.

3.3 Results

Results for each variable (L, A, and ΔV) were primarily limited by the availability of altimetry and in situ water level data. For the ten sites, the number of ΔV estimates that were made over the selected time period ranged from 60 to 266. Results highlight the seasonal variability for each of the ten sites as well as periods of time with available data (Figure 3-4). Of the ten sites, Lake Junin, Lake Kinkony, and Tonle Sap Lake had the greatest number of ΔV estimates and also showed the greatest seasonal variability. In contrast, the Guri Reservoir, the Tucurui Reservoir, Lake Iro, the Nam Ngum Reservoir, and the Balbina Reservoir had the fewest number of ΔV estimates due to limited altimetry data. Lake Quiminha and the Balbina Reservoir were the only two of the ten sites that did not show seasonal variability. For the three validation sites, the total number of estimates that could be made over the same time period were 203, 126, and 60 for Tonle Sap Lake, Lake

Tana, and the Balbina Reservoir, respectively. Of these three sites, Tonle Sap Lake had the greatest number of estimates due to continuous datasets of both altimetry data and in situ water level data. Lake Tana was constrained by a limited, five year period of available in situ water level data. Estimates for Balbina Reservoir were further limited due to minimal altimetry data. Because the GRLM database did not contain the Balbina Reservoir, a fewer number of L (60) estimates were available. Daily water level data from 2000-2009 was available for the Tonle Sap, 2000-2005 for Lake Tana, and 2000-2009 for the Balbina Reservoir.

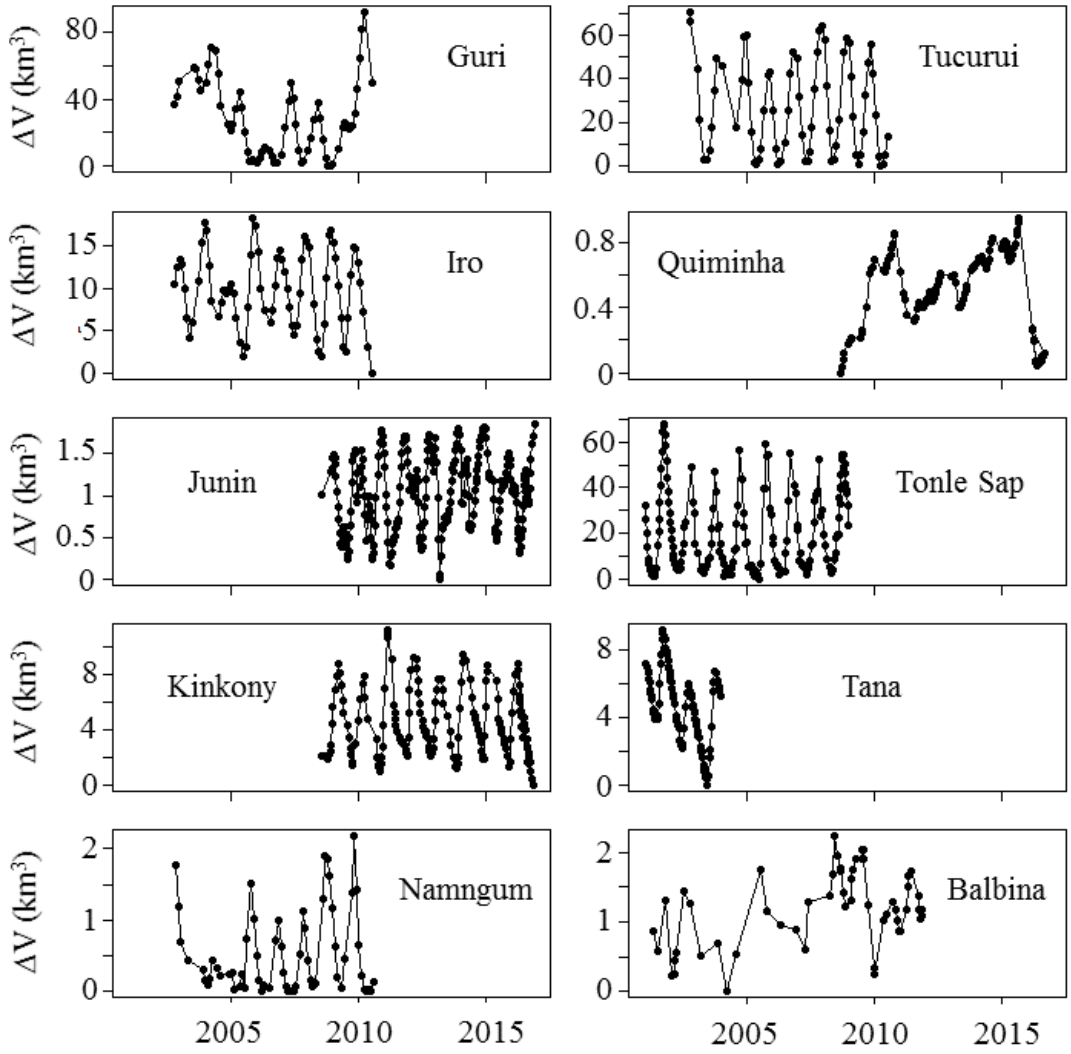

Figure 3-4. Storage variation time series for the ten study sites from 2000 to 2015. Lake Quiminha, Lake Junin, Lake Kinkony, Tonle Sap Lake, and Lake Tana were all estimated at 10-15 day time steps while the Guri Reservoir, Tucurui Reservoir, Lake Iro, Nam Ngum Reservoir, and Balbina Reservoir were all estimated at 30 day time steps. Continuous estimates of 5-10 years were made for all of the sites, but none of the sites could be estimated for the entire 15 year period due to limited data availability.

Overall, water level estimates were very accurate for all three validation water bodies (Table 3-2). Estimated and observed water levels for the Tonle Sap resulted in an R^2 of 0.96 and a NRMSE of 6.3%. The Tonle Sap's water levels exhibited a range of 9 m with an average of 4 m above the lowest level. Comparisons between estimated and measured water levels for Lake Tana produced an R^2 of 0.97 and a NRMSE of 4.5%. Lake Tana's water levels exhibited a range of 3 m with an average of 1.7 m above the lowest level. For the Balbina Reservoir, data acquired from both altimeters and gauges were highly variable and do not demonstrate the relatively uniform patterns exhibited by the other two lakes. Despite the non-uniform patterns, a comparison between altimetry and in situ water levels produced an R^2 of 0.89 and a NRMSE of 8.9%. Results from water level estimates are shown in the top row of Figure 3-5.

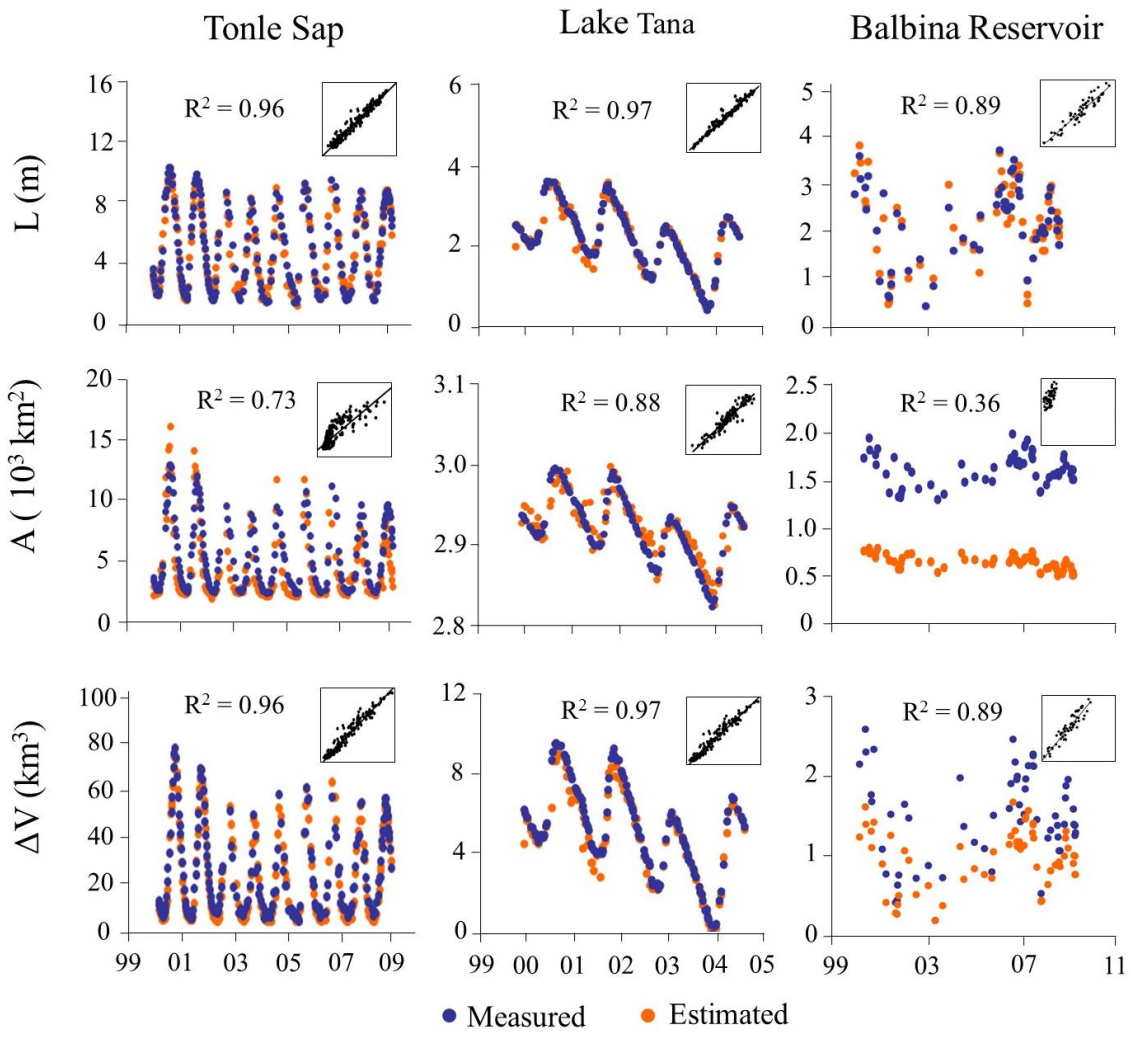

Figure 3-5. Time series of measured and estimated water levels above the lowest level (L), surface areas (A), and volumetric fluctuations (ΔV) for each of the three sites. Values on the x-axis represent calendar year starting from the year 1999. Blue circles represent measured values

while orange circles represent values estimated from remote sensing. Regression plots comparing measured and estimated results are shown in the upper right corner of each graph.

Table 3-2. Summary table of water level estimation results with number of samples (*n*), R^2, NRMSE values, and slope of the regression line

Lake/Reservoir	*n*	R^2	NRMSE (%)	Regression Slope
Tonle Sap	203	0.96	6.26	1.05
Lake Tana	126	0.97	4.48	0.99
Balbina Resevoir	60	0.89	8.90	0.59

Surface area estimates had a relatively high level of agreement with measured surface areas for Lake Tana, reasonably high with the Tonle Sap, and very poorly with those from the Balbina Reservoir (Table 3-3). Values for Tonle Sap Lake ranged from 1,880 to 16,000 km^2 with an average of 4,500 km^2, while yielding an R^2 of 0.73 and a NRMSE of 17.9%. Lake Tana had estimated surface areas ranging from 2786 to 3043 km^2, averaging 2935 km^2, and producing an R^2 of 0.88 and a NRMSE of 8.9% when compared to measured values. In contrast, estimated and measured surface area values for the Balbina Reservoir had a lower R^2 of 0.36 and higher NRMSE of 142.9%. Surface area results for the three water bodies are illustrated in the middle row of Figure 3-5.

Table 3-3. Summary table of surface area estimation results with number of samples (*n*), R^2, NRMSE values, and slope of the regression line

Lake/Reservoir	*n*	R^2	NRMSE (%)	Regression Slope
Tonle Sap	203	0.73	17.89	0.82
Lake Tana	126	0.88	8.87	1.10
Balbina Resevoir	60	0.36	142.91	1.31

Volumetric fluctuations were consistent with water level estimates (Table 3-4). For the Tonle Sap, estimated ΔV values exhibited a range of 74 km^3 with an average value of 21.5 km^3, while estimated and observed ΔV values produced an R^2 of 0.96 and a NRMSE of 5.8%. Similarly, Lake Tana's ΔV values yielded an R^2 of 0.97 and a NRMSE of 5.4% with estimates averaging 5 km^3 above the lowest level and an overall range of 9 km^3. Values for the Balbina Reservoir produced a similar R^2 of 0.89, but a high NRMSE of 38.0%. Overall results of ΔV estimates for each of the three water bodies are shown in the bottom row of Figure 3-5.

Table 3-4. Summary table of water volume variation estimation results with number of samples (*n*), R^2, NRMSE values, and slope of the regression line

Lake/Reservoir	*n*	R^2	NRMSE (%)	Regression Slope
Tonle Sap	203	0.96	5.82	1.05
Lake Tana	126	0.97	5.41	1.03
Balbina Resevoir	60	0.89	37.95	1.51

3.4 Discussion

3.4.1 Implications for Remotely Sensed Water Management

As illustrated by the results, our methodology worked very well for two of the three validation lakes. All three parameters (L, A, and ΔV) were estimated with a high level of accuracy and agreed well with previous estimates for the Tonle Sap (Kummu et al. 2014) and Lake Tana (Duan and Bastiaanssen 2013). However, estimates of A for the Tonle Sap exhibited more error than those for Lake Tana likely due the sheer size of the Tonle Sap and pixel misclassification along the perimeter of the Tonle Sap floodplain, particularly during the rainy season. Remotely sensed values of A and ΔV were both greatly underestimated for the Balbina Reservoir. This error was likely due to the reservoir's geometry and the coarse spatial resolution of MODIS imagery. To verify this error, a visual inspection of pixel classification was performed for MODIS and Landsat images of the Balbina Reservoir (Figure 3-6). Approximately 50% of the surface area corresponding to water in the MODIS image was incorrectly classified as land. This phenomenon was observed by Gao et al. (2012), which suggested that water bodies with large ratios of shoreline to surface area (S:A) are more likely to have a greater error. This is highlighted here by the Balbina Reservoir with an S:A ratio of 5.80 compared to values of 0.12 and 0.20 for Lake Tana and Tonle Sap, respectively. Such a large S:A ratio results in pixel mixing at the borders of water bodies, thereby making it difficult to precisely identify water outside the main channel.

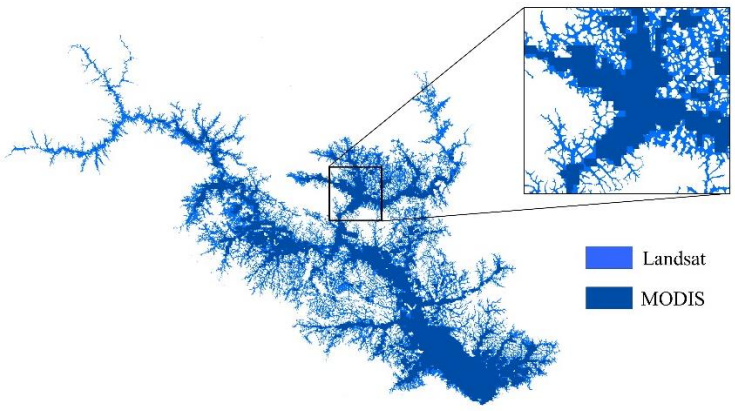

Figure 3-6. Comparison of water body delineation of the Balbina Reservoir using Landsat and MODIS imagery. The light blue area corresponds to Landsat pixels that were classified by the MNDWI as water while dark blue pixels correspond to MODIS pixels classified as water.

The three different end members here illustrate the effectiveness of this methodology for water bodies with varying S:A ratios. Intuitively, the technique works best for lakes with bowl shaped bathymetry where water moves primarily in the vertical direction. The methodology still works well for certain water bodies that are characterized by lateral water movement across a floodplain. However, water bodies with complex bathymetry and branching channels cannot be fully analyzed using this technique and require different image processing approaches. This remote sensing technique can be a useful tool for managing water bodies by providing precise estimates of water storage as well as seasonal variations in water availability.

3.4.2 Seasonal Variability

A unique aspect of our remote sensing approach is that it allows for analysis of seasonal variability, a crucial component of water resources management in tropical regions. In this study, eight of the ten sites illustrated seasonal trends while the Balbina Reservoir and Lake Quiminha did not have any seasonal (or temporal) pattern (Figure 3-4). However, the seasonal variability of the Balbina Reservoir could not be completely analyzed due to the limited amount of water level data and difficulties in estimating A and ΔV. Despite the data being coarser than that of the other sites, visual inspection of Landsat images containing the Balbina Reservoir indicate that it does follow a seasonal inundation pattern. This makes sense as the Amazon River Basin, similar to most tropical regions, has both a rainy season and dry season. This temporal pattern has been highlighted by a number of studies within the Amazon River Basin (e.g. de Oliveira Campos et al. 2001, Liebmann and Marengo 2001), and thus the Balbina Reservoir needs to be further evaluated to elucidate temporal patterns.

Water levels in Lake Tana were highly variable with an average annual amplitude of 0.8 m about the mean annual water level. This can largely be attributed to its altitude and unusually small catchment area to lake area ratio (Kebede et al. 2006). Unlike both the Tonle Sap and Balbina Reservoir, Lake Tana is located at a very high elevation (~1786 masl) and is surrounded by very steep terrain. Due to its tropical climate, Lake Tana experiences a rainy season (June-September) with precipitation reaching levels of 13 mm/day during the rainy season (Abdo et al. 2009). Water levels are consistently higher during the rainy season but rarely more than 0.5 m above the mean annual water level. Furthermore, the water level of Lake Tana is regulated such that excess flow from the rainy season can be stored to augment low flows during the dry season (Kebede et al. 2006). The coupling of these factors control the seasonal variability of Lake Tana which can be seen in the range of its L, A, and ΔV values (Figure 3-5).

Of the three selected water bodies, the Tonle Sap had the most seasonal variability in all three of the measured parameters with an average yearly amplitude of 3.7 m about the mean annual water level. This phenomenon can be explained by two factors. First, the Tonle Sap's permanently flooded pool is surrounded by a vast area with very flat topography, meaning that small increases in water level result in considerable increases in surface area. Second, the Tonle Sap receives a substantial flood pulse from the Mekong River as a result of the annual monsoon cycle. During this time (May-October), the direction of flow in the Tonle Sap River reverses such that water from the Mekong River flows into the Tonle Sap, functioning as an endorheic water body. The result of this seasonal flood pulse is illustrated by the substantial seasonal variability of the Tonle Sap's L, A, and ΔV values (Figure 3-5). A unique aspect of our remote sensing technique, as highlighted by the Tonle Sap, is its ability to capture accurate snapshots of inundation and water storage dynamics at sub-monthly intervals through time. This knowledge is invaluable for people who depend on surface water bodies for critical natural resources, particularly in regions where data is scarce or not freely available.

3.4.3 Monitoring Surface Water in Data Scarce Regions

The research presented here is intended to aid in monitoring and assessment of water bodies in regions with limited environmental data. Developing nations, most of which are located in the

tropics, could benefit from high temporal resolution monitoring of water resources. Previous studies have illustrated how remote sensing can be a useful tool for monitoring water resources in data scarce regions (e.g., Keys et al. 2016). In particular, societies which depend on large water bodies for basic societal needs could benefit from high frequency hydrologic monitoring techniques. One example presented here is the Mekong River Basin, where the Tonle Sap provides critical natural resources within the basin. With more than a 1.2 million people living within its floodplain alone (Sokhem and Sunada 2006), there is clearly a great need for day-to-day monitoring of the Tonle Sap's hydrodynamics and variability. Nonetheless, there is currently a considerable shortage of hydrologic monitoring in the Tonle Sap Basin (Bonheur and Lane 2002) as well as other developing regions of the world. This presents a major problem in developing regions due to competition for water across food, energy, and environmental sectors as well as across international boundaries. Simple, high-resolution remote sensing techniques such as ours can be very useful tools for monitoring water resources in developing regions without access to expensive monitoring equipment. Additionally, these approaches provide an opportunity for fair water allocation in areas with strong competition for water resources. Several nonprofit organizations such as the International Water Management Institute (IWMI) have started using such techniques in conjunction with extension programs to assist governments of developing nations with sustainable water management. This provides water managers who may not have the necessary computational resources with valuable information regarding their decision making, forecasting, and water allocation.

3.4.4 Future Research

There are two key issues with our technique that can be improved with further research. First is the inability to accurately approximate the surface area of water bodies with high S:A ratios. For our sites, S:A ratios vary from 0.12 to 5.8 with a an average value of 2.1 (Table 3-1). To evaluate S:A at a larger scale, we conducted a geospatial analysis on large lakes and reservoirs across the entire globe. We utilized data from the Global Lakes and Wetland Database (GLWD) and performed a spatial interpolation using inverse distance weighting in ArcGIS. There appears to be no regional patterns across the world (Figure 3-7), suggesting that S:A ratios depend largely upon local variables such as topography. While the methodology presented here works well for lakes and reservoirs with well-defined boundaries (i.e. water bodies with low to medium S:A ratios), future studies should modify this high temporal resolution approach such that it works for lakes and reservoirs with complex geometry. This can be accomplished by taking images from a sensor with high spatial resolution (e.g., Landsat) and interpolating between images with images from a high temporal resolution sensor (e.g., MODIS) using a data fusion algorithm such as the Spatial and Temporal Adaptive Reflectance Fusion Model (STARFM) (Gao et al. 2006) or the Spatial and Temporal Reflectance Unmixing Model (STRUM) (Gevaert and García-Haro 2015). Alternatively, the recent development of freely available multispectral images from the European Space Agency's SENTINEL-2 mission provides another approach for high resolution monitoring of water bodies (Drusch et al., 2012). However, similar to the provided methodology, data from the SENTINEL-2 mission provides a tradeoff between spatial and temporal resolution.

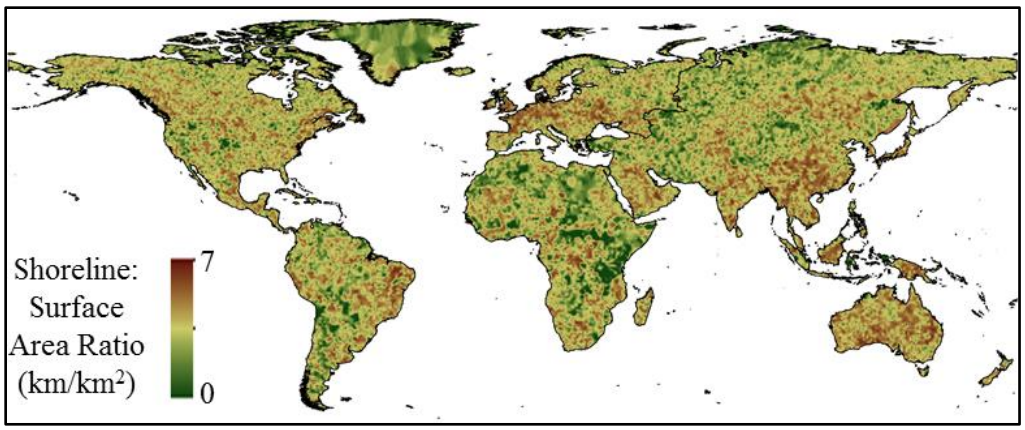

Figure 3-7. S:A ratios for lakes and reservoirs across the world. Areas of red correspond to lakes/reservoirs with a high S:A ratio while areas of green correspond to lakes/reservoirs with low S:A ratios.

The second disadvantage of our approach is that a limited number of water bodies can be analyzed by satellite altimetry. Currently, radar altimetry can only be used to study large water bodies (greater than 100 km^2) due to a variety of factors including narrow swaths, large footprints, and interferences (Gao et al. 2012). Similar to the MODIS images used for surface area estimation, the radar altimeters used in this study are also low in resolution. Additionally, both the imagery and altimetry used in this study can be greatly impacted by meteorology and atmospheric disturbances, leading to increased error in estimates. Thus, there is a great need for both higher quality and higher resolution satellite imagery and altimetry. The Surface Water Ocean Topography (SWOT) mission which is planned for launch in 2020 will provide near global imagery and altimetry and will thus be revolutionary in quantifying inland water body storage through time (Lee et al. 2010). SWOT will be able to identify volumetric fluctuations in 50 to 65% of surface water bodies as compared to 15% currently (Biancamaria et al. 2010). Despite the potential of the future SWOT mission, there is still a great need to understand current and past trends of surface water bodies. With almost four decades of quality remote sensing data freely available to the public and a myriad of analytical techniques, there is ample opportunity for comprehensive analyses of current data to help aid future research.

3.5 Conclusions

In this study, we quantified volumetric fluctuations in ten tropical surface water bodies at frequent intervals using entirely remote sensing. Through close examination of the three validation sites, we found that the high temporal resolution approach worked well for Tonle Sap Lake and Lake Tana, but did not work well for the Balbina Reservoir. This discrepancy was attributed to the large shoreline to surface area ratio of the Balbina Reservoir in comparison to those of Tonle Sap Lake and Lake Tana. Overall, results from the study demonstrate the capability of this methodology for accurately estimating volumetric fluctuations in lakes and reservoirs at near continuous time steps. While our study focused on lakes and reservoirs in the tropics, this methodology can be used in any region of the world and is highly transferrable.

Global monitoring of lakes and reservoirs would benefit from a high temporal resolution monitoring framework. This is particularly true in developing regions of the world which often lack the necessary resources required for surface water monitoring. Thus far, volumetric fluctuations in surface water bodies have largely been quantified via in situ data and remote sensing. Studies have successfully measured volumetric variations of lakes and reservoirs using entirely remote sensing but have only been able to do so at low temporal resolution. The methodology presented here takes the first step quantifying surface water storage variations at near continuous intervals through the use of satellite remote sensing. As highlighted by the Tonle Sap, this approach can be particularly beneficial for monitoring surface water bodies that experience seasonal variability. By improving the spatial resolution of this technique, the future of lake and reservoir monitoring can be greatly improved.

3.6 Acknowledgments

We would like to thank the Mekong River Commission for Tonle Sap water level data, Brazil's National Water Agency for open access to water level data for the Balbina Reservoir, and Lisa-Maria Rebelo for providing water level data for Lake Tana. Additional thanks to the authors of Kummu et al. 2014, Kemenes et al., 2011, and Wale et al., 2009, for publishing bathymetry derived relationships for Tonle Sap Lake, the Balbina Reservoir, and Lake Tana, respectively. Additionally, we would like to thank three anonymous reviewers whose comments improved the quality of this manuscript.

3.7 References

Alsdorf DE. 2003. Water storage of the central Amazon floodplain measured with GIS and remote sensing imagery. Ann. Assoc. Am. Geogr. 93:55-66.

Alsdorf D, Birkett C, Dunne T, Melack J, Hess L. 2001. Water level changes in a large Amazon lake measured with spaceborne radar interferometry and altimetry. Geophys. Res. Lett. 28:2671-2674.

Alsdorf DE, Melack JM, Dunne T, Mertes LA, Hess LL, Smith LC. 2000. Interferometric radar measurements of water level changes on the Amazon flood plain. Nature. 404:174-177.

Alsdorf DE, Rodríguez E, Lettenmaier DP. 2007. Measuring surface water from space. Rev. Geophys. 45.

Biancamaria S, Andreadis KM, Durand M, Clark EA, Rodriguez E, Mognard NM, ... and Oudin Y. 2010. Preliminary characterization of SWOT hydrology error budget and global capabilities. IEEE J. Sel. Top. Appl. *3*:6-19.

Birkett CM. 1995. The contribution of TOPEX/POSEIDON to the global monitoring of climatically sensitive lakes. J. Geophys. Res. Oceans. 100:25179-25204.

Birkett CM. 1998. Contribution of the TOPEX NASA radar altimeter to the global monitoring of large rivers and wetlands. Water Resour. Res. 34:1223-1239.

Blasco F, Bellan MF, Chaudhury MU. 1992. Estimating the extent of floods in Bangladesh using SPOT data. Remote Sens. Environ. 39:167-178.

Bonheur N, Lane BD. 2002. Natural resources management for human security in Cambodia's Tonle Sap Biosphere Reserve. Environ. Sci. Policy. 5:33-41.

Brakenridge R, Anderson E. 2006. MODIS-based flood detection, mapping and measurement: The potential for operational hydrological applications, in Transboundary floods: reducing risks through flood management, pp. 1-12, Springer, Netherlands.
Calmant S, Seyler F, Cretaux JF. 2008. Monitoring continental surface waters by satellite altimetry. Surv. Geophys. 29:247-269.
Coe MT, Birkett CM. 2004. Calculation of river discharge and prediction of lake height from satellite radar altimetry: Example for the Lake Chad basin. Water Resour. Res. 40.
Crétaux JF, Birkett C. 2006. Lake studies from satellite radar altimetry. C. R. Geosci. 338:1098-1112.
Crétaux JF, Jelinski W, Calmant S, Kouraev A, Vuglinski V, Bergé-Nguyen M, ... Maisongrande P. 2011. SOLS: A lake database to monitor in the Near Real Time water level and storage variations from remote sensing data. Adv. Space Res. 47:1497-1507.
Drusch M, Del Bello U, Carlier S, Colin O, Fernandez V, Gascon F, ... Meygret A. 2012. Sentinel-2: ESA's optical high-resolution mission for GMES operational services. Remote Sens. Environ. 120:25-36.
Duan Z, Bastiaanssen WGM. 2013. Estimating water volume variations in lakes and reservoirs from four operational satellite altimetry databases and satellite imagery data. Remote Sens. Environ. 134:403-416.
Duan Z, Bastiaanssen WGM, Muala E. 2013. Icesat-derived water level variations of roseires reservoir (Sudan) in the Nile basin, paper presented at 2013 IEEE International Geoscience and Remote Sensing Symposium, Inst. Electr. Electron. Eng., Melbourne, Australia.
Fearnside PM. 1989. Brazil's Balbina Dam: Environment versus the legacy of the pharaohs in Amazonia. Environ. Manage. 13:401-423.
Feng L, Hu C, Chen X, Cai X, Tian L, Gan W .2012. Assessment of inundation changes of Poyang Lake using MODIS observations between 2000 and 2010. Remote Sens. Environ. 121:80-92.
Frappart F, Seyler F, Martinez JM, Leon JG, Cazenave A. 2005. Floodplain water storage in the Negro River basin estimated from microwave remote sensing of inundation area and water levels. Remote Sens. Environ. 99:387-399.
Gao F, Masek J, Schwaller M, Hall F. 2006. On the blending of the Landsat and MODIS surface reflectance: Predicting daily Landsat surface reflectance. IEEE T. Geosci. Remote. 44:2207-2218.
Gao H, Birkett C, Lettenmaier DP. 2012. Global monitoring of large reservoir storage from satellite remote sensing. Water Resour. Res. 48.
Gevaert CM, García-Haro FJ. 2015. A comparison of STARFM and an unmixing-based algorithm for Landsat and MODIS data fusion. Remote Sens. Environ. 156:34-44.
Hess LL, Melack JM, Affonso AG, Barbosa C, Gastil-Buhl M, Novo EM. 2015. Wetlands of the lowland Amazon basin: Extent, vegetative cover, and dual-season inundated area as mapped with JERS-1 Synthetic Aperture Radar. Wetlands. 35:745-756.
Hilldale RC, Raff D. 2008. Assessing the ability of airborne LiDAR to map river bathymetry. Earth Surf. Proc. Land. 33:773.
Hossain F, Katiyar N, Hong Y, Wolf A. 2007. The emerging role of satellite rainfall data in improving the hydro-political situation of flood monitoring in the under-developed regions of the world. Nat. Hazards. 43:199-210.

Islam AS, Bala SK, Haque MA. 2010. Flood inundation map of Bangladesh using MODIS time-series images. J. Flood Risk Manag. 3:210-222.
Kebede S, Travi Y, Alemayehu T, Marc V. 2006. Water balance of Lake Tana and its sensitivity to fluctuations in rainfall, Blue Nile basin. Ethiopia. J. Hydrol. 316: 233-247.
Kemenes A, Forsberg BR, Melack JM. 2011. CO2 emissions from a tropical hydroelectric reservoir (Balbina, Brazil). J. Geophys. Res. Biogeosci. 116.
Keys TA, Jones CN, Scott DT, Chuquin D. 2016. A cost-effective image processing approach for analyzing the ecohydrology of river corridors. Limnol. Oceanogr. Meth. 14:359-369.
Kim JW, Lu Z, Lee H, Shum CK, Swarzenski CM, Doyle TW, Baek SH. 2009. Integrated analysis of PALSAR/Radarsat-1 InSAR and ENVISAT altimeter data for mapping of absolute water level changes in Louisiana wetlands. Remote Sens. Environ. 113:2356-2365.
Kummu M, Penny D, Sarkkula J, Koponen J. 2008. Sediment: curse or blessing for Tonle Sap Lake? AMBIO. 37:158-163.
Kummu M, Tes S, Yin S, Adamson P, Józsa J, Koponen J, Richey J, Sarkkula J. 2014. Water balance analysis for the Tonle Sap Lake–floodplain system. Hydrol. Process. 28:1722-1733.
Lee H, Durand M, Jung HC, Alsdorf D, Shum CK, Sheng Y. 2010. Characterization of surface water storage changes in Arctic lakes using simulated SWOT measurements. Int. J. Remote Sens. 31:3931-3953.
Lee H, Shum CK, Yi Y, Ibaraki M, Kim JW, Braun A... Lu Z. 2009. Louisiana wetland water level monitoring using retracked TOPEX/POSEIDON altimetry. Mar. Geod. 32:284-302.
Lillesand T, Kiefer RW, Chipman J. 2014. Remote sensing and image interpretation. John Wiley, Hoboken, N. J.
Maheu C, Cazenave A, Mechoso CR. 2003. Water level fluctuations in the Plata basin (South America) from Topex/Poseidon satellite altimetry. Geophys. Res. Lett. 30.
Muala E, Mohamed YA, Duan Z, van der Zaag P. 2014, Estimation of reservoir discharges from Lake Nasser and Roseires Reservoir in the Nile Basin using satellite altimetry and imagery data. Remote Sens. 6:7522-7545.
Nellis MD, Harrington JA, Wu J. 1998. Remote sensing of temporal and spatial variations in pool size, suspended sediment, turbidity, and Secchi depth in Tuttle Creek Reservoir, Kansas: 1993. Geomorphology. 21:281-293.
Ordoyne C, Friedl MA. 2008. Using MODIS data to characterize seasonal inundation patterns in the Florida Everglades. Remote Sens. Environ. 112:4107-4119.
Palmeirim AF, Peres CA, Rosas FC. 2014. Giant otter population responses to habitat expansion and degradation induced by a mega hydroelectric dam. Biol. Conserv. 174:30-38.
Peng D, Guo S, Liu P, Liu T. 2006. Reservoir storage curve estimation based on remote sensing data. J. Hydrol. Eng. 11:165-172.
Sawunyama T, Senzanje A, Mhizha A. 2006. Estimation of small reservoir storage capacities in Limpopo River Basin using geographical information systems (GIS) and remotely sensed surface areas: Case of Mzingwane catchment. Phys. Chem. Earth. 31:935-943.

Singh A, Seitz F, Schwatke C. 2012. Inter-annual water storage changes in the Aral Sea from multi-mission satellite altimetry, optical remote sensing, and GRACE satellite gravimetry. Remote Sens. Environ. 123:187-195.

Skinner KD. 2011. Evaluation of LiDAR-acquired bathymetric and topographic data accuracy in various hydrogeomorphic settings in the Deadwood and South Fork Boise Rivers, West-Central Idaho, 2007: U.S. Geological Survey Scientific Investigations Report 2011–5051, 30 p.

Smith LC, Pavelsky TM. 2008. Estimation of river discharge, propagation speed, and hydraulic geometry from space: Lena River, Siberia. Water Resour. Res. 44.

Smith LC, Pavelsky TM. 2009. Remote sensing of volumetric storage changes in lakes. Earth Surf. Proc. Land. 34:1353-1358.

Sokhem P, Sunada K. 2006. The governance of the Tonle Sap Lake, Cambodia: integration of local, national and international levels. Int. J. Water Resources Development, 22:399-416.

Tuck SL, Phillips HR, Hintzen RE, Scharlemann JP, Purvis A, Hudson LN. 2014. MODISTools–downloading and processing MODIS remotely sensed data in R. Ecol. Evol. 4:4658-4668.

Verpoorter C, Kutser T, Seekell DA, Tranvik LJ. 2014. A global inventory of lakes based on high-resolution satellite imagery. Geophys. Res. Lett. 41:6396-6402.

Wale A, Rientjes THM, Gieske ASM, Getachew HA. 2009. Ungauged catchment contributions to Lake Tana's water balance. Hydrol. Process. 23:3682-3693.

Wang Y, Sun G, Liao M, Gong J. 2008. Using MODIS images to examine the surface extents and variations derived from the DEM and laser altimeter data in the Danjiangkou Reservoir, China. Int. J. Remote Sens. 29:293-311.

Wang Y, Xia H, Fu J, Sheng G. 2004. Water quality change in reservoirs of Shenzhen, China: detection using LANDSAT/TM data. Sci. Total Environ. 328:195-206.

Winemiller KO, McIntyre PB, Castello L, Fluet-Chouinard E, Giarrizzo T, Nam S, ... Stiassny MLJ. 2016. Balancing hydropower and biodiversity in the Amazon, Congo, and Mekong. Science. 351:128-129.

Wulder MA, Masek JG, Cohen WB, Loveland TR, Woodcock CE. 2012. Opening the archive: How free data has enabled the science and monitoring promise of Landsat. Remote Sens. Environ. 122:2-10.

Xu H. 2006. Modification of normalised difference water index (NDWI) to enhance open water features in remotely sensed imagery. Int. J. Remote Sens. 27:3025-3033.

Yan YE, Ouyang ZT, Guo HQ, Jin SS, Zhao B. 2010. Detecting the spatiotemporal changes of tidal flood in the estuarine wetland by using MODIS time series data. J. Hydrol. 384:156-163.

Yesuf HM, Alamirew T, Melesse AM, Assen M. 2013. Bathymetric study of Lake Hayq, Ethiopia. Lakes Reserv. Res. Manag. 18:155-165.

Zhang J, Xu K, Yang Y, Qi L, Hayashi S, Watanabe M. 2006. Measuring water storage fluctuations in Lake Dongting, China, by Topex/Poseidon satellite altimetry. Environ. Monit. Assess. 115:23-37.

Zhu W, Jia S, Lv A. 2014. Monitoring the Fluctuation of Lake Qinghai Using Multi-Source Remote Sensing Data. Remote Sens. 6:10457-10.

CHAPTER 4. EFFECTS OF LARGE WOOD ON FLOODPLAIN CONNECTIVITY IN A HEADWATER MID-ATLANTIC STREAM

Tyler A. Keys, Heather Govenor, C. Nathan Jones, W. Cully Hession, Erich T. Hester, and Durelle T. Scott

Submitted: March 2018
To: *Ecological Engineering*
Status: In Review

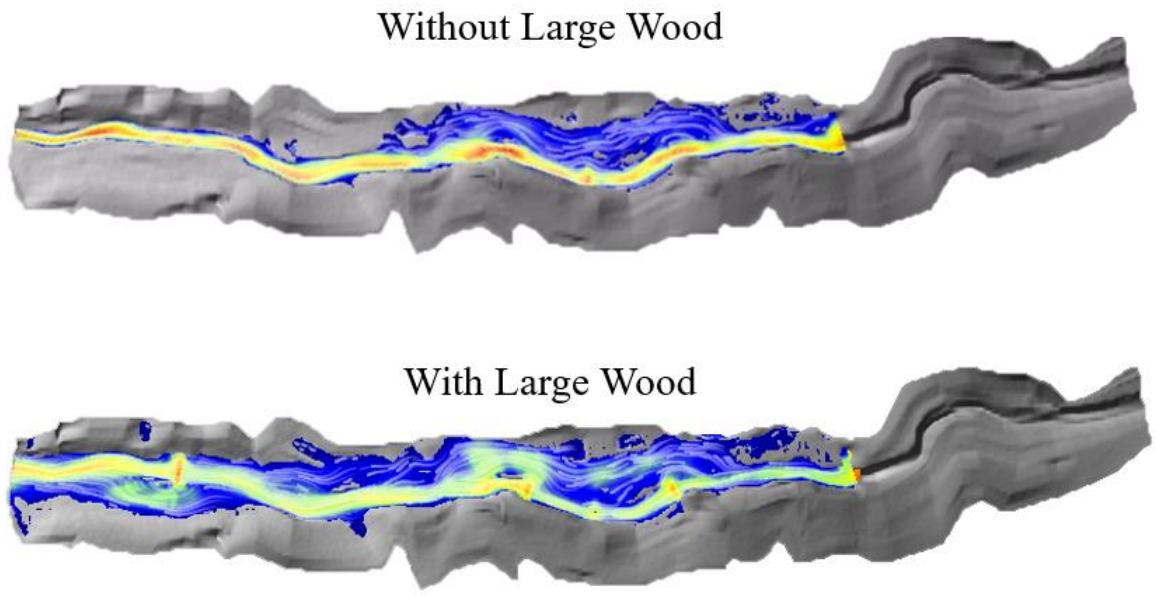

Abstract

Large wood (LW) plays an essential role in aquatic ecosystem health and function. Traditionally, LW has been removed from streams to minimize localized flooding and increase conveyance efficiency. More recently, LW is often added to streams as a component of stream and river restoration activities. While much research has focused on the role of LW in habitat provisioning, geomorphic stability, and hydraulics at low to medium flows, we know little about the role of LW during storm events. To address this question, we investigated the role of LW on floodplain connectivity along a headwater stream in the Mid-Atlantic region of the United States. Specifically, we conducted two artificial floods, one with and one without LW, and then utilized field measurements in conjunction with hydrodynamic modeling to quantify floodplain connectivity during the experimental floods and to characterize potential management variables for optimized restoration activities. Experimental observations show that the addition of LW increased maximum floodplain inundation extent by 34%, increased floodplain inundation depth by 33%, and decreased maximum thalweg velocity by 10%. Model results demonstrated that different placement of LW along the reach has the potential to increase floodplain flow by up to 40%, with highest flooding potential at cross sections with high longitudinal velocity and shallow depth. Additionally, model simulations show that the effects of LW on floodplain discharge decrease as storm recurrence interval increases, with no measurable impact at a recurrence interval of more than 25 years.

4.1 Introduction

Large wood (LW) plays an important, yet undervalued role in river ecosystems. One of the most important functions of LW is its ability to increase floodplain connectivity, the lateral exchange of water and material between rivers or streams and their adjacent floodplains (Harvey & Gooseff, 2015; Covino, 2017). LW plays a crucial role in floodplain connectivity as it decreases longitudinal stream flow velocity (Davidson & Eaton, 2013), increases floodplain inundation (Collins & Montgomery, 2002), and increases transient storage (Mueller Price et al., 2016; Rana et al., 2017). This in turn can provide a variety of ecosystem services such as promoting geomorphic stability/instability (Montgomery et al., 2003), influencing the transport and storage of sediment (Parker et al., 2017), providing habitat for aquatic wildlife (Dolloff & Warren, 2003; Johnson et al., 2003), and enhancing water quality (Krause et al., 2014). While these ecological benefits are well acknowledged, LW can also be hazardous to infrastructure and people (Wohl et al., 2016). Historically, LW has been removed from streams for the purpose of limiting flood hazards (Wilford et al., 2004), lowering water tables to comply with Federal Emergency Management Agency (FEMA) regulations (Schmocker & Weitbrecht, 2013), and limiting damage to infrastructure such as culverts, roads, and bridges (Lagasse et al., 2012). Thus, management of LW is important and often requires a balance of ensuring infrastructure stability and protection of critical ecosystem services (Ruiz-Villanueva et al., 2016).

The importance of instream LW on fluvial processes has been widely acknowledged and extensively studied over the past 30 years (Abbe & Montgomery, 1996; Jeffries et al., 2003; Sear et al., 2000; Gurnell et al., 2002). LW is useful for resotring streams as it is relatively inexpensive and serves as a natural form of stream restoration and rehabilitation (Kail et al., 2007). As such, LW has widely been used in stream restoration, a multi-billion dollar industry in the U.S. and

Europe (Bernhardt et al., 2005; Angelopoulos et al., 2017). Due to the widespread use of LW in stream restoration projects, there is a need to improve and optimize the use of LW.

There are currently several critical aspects of LW science that remain unexplored. First, the effects of LW in streams have been studied primarily at baseflow (Matheson et al., 2017). In contrast, little is known about the effects of LW during stormflow, when the majority of solute and sediment transport occurs (Ensign et al., 2006). However, directly measuring the impacts of LW during stormflow is challenging due to the stochastic nature of storm events and difficulty in capturing natural flood pulses. In addition, LW has been studied primarily in the Western U. S. (e.g., Bilby & Ward, 1991; May & Gresswell, 2003; Wohl & Goode, 2008). While these studies have provided valuable insight on LW dynamics, water resources management in this region differs greatly from that of humid regions of the world where water quality is of greater concern than water quantity (Karr & Dudley, 1981). Finally, studies have primarily focused on the transport and deposition of LW (e.g., Dixon & Sear, 2014; Ruiz-Villanueva et al., 2014), treating LW as dynamic system components as opposed to static instream structures. However, LW can also act as more permanent in-stream structures and affect critical ecological processes such as hyporheic exchange (Hester & Doyle, 2008), nitrate removal (Hester et al., 2016), and habitat provisioning (Johnson et al., 2003). Due to these limitations, the effects of LW on stream flooding dynamics have been largely neglected. The shortage of and need for experimental research on these effects was the primary motivation for our research effort.

The overall goal of this study was to assess the impacts of LW on floodplain connectivity by utilizing experimental field observations and hydraulic modeling of a headwater stream in the US Mid-Atlantic region. Here, we hypothesized that the addition of LW increases floodplain connectivity while decreasing longitudinal velocity in the main channel. Specific research objectives included: 1) quantifying the impact of LW on floodplain inundation extent, depth, and velocity; 2) assessing the impact of LW at varying locations along the reach; and 3) quantifying the influence of LW on floodplain connectivity across a gradient of flood magnitudes. We addressed these objectives by conducting a series of experimental floods along a headwater stream, and then utilized hydrodynamic modeling combined with our field-scale measurements to characterize floodplain connectivity during the experimental floods and across a synthetic flow record. These results both improve our understanding of LW flood dynamics and provide further guidance for the restoration community in the use of LW.

4.2. Methods

4.2.1 Study Site

The study site is located in Blacksburg, Virginia at the Virginia Tech Stream Research, Education, and Management (StREAM) Lab (vtstreamlab.weebly.com/) in the Valley and Ridge physiographic province. We selected this location because it is representative of headwater streams. In addition, the StREAM Lab provided an advantageous location for flood experimentation as flood dynamics have been extensively studied there and there are several continuous flow monitoring stations (Jones et al., 2015; Azinheira et al., 2014; Hester et al., 2016; Keys et al., 2016). Within the StREAM Lab, the study was conducted on a 50-m reach of Docs Branch (Figure 4-1), a first-order tributary to Stroubles Creek with an average bankfull width of

0.93 m. This specific reach contains an H-flume with discharge measurements, which was used to set upstream boundary conditions. The stream is located at an altitude of 610 m above mean sea level and has an average slope of 0.01. The contributing watershed encompasses an area of 1 km^2 and is primarily composed of agricultural land use.

4.2.2 Flooding Experiments

We conducted three experimental floods over a three-day period (e.g., one flood per day). During each flood, we dammed the stream channel upstream of the study reach by sealing two side-by-side 48" diameter concrete culverts with a wooden sluice gate and plastic tarp. The experimental floods were then initiated by pulling the sluice gate and releasing the dammed water into the study reach. Prior to releasing the dammed water, ponded depth was measured to ensure that floods were similar in total volume. The initial flood was conducted to prime the system and ensure that floodplain soil moisture conditions were similar for the subsequent experimental floods. The second and third flood events (hereafter flood without LW and flood with LW, respectively) were used to examine the effects of LW on floodplain connectivity. Specifically, the flood without LW was released under normal conditions without wood in the stream, and the flood with LW was released after installing three pieces of LW in the reach (Figure 4-1). We collected the three pieces of LW from a nearby upland and placed them horizontally in the stream with the rootwads facing upstream, based on the guidelines from previous research (Rafferty, 2013). All three pieces of LW spanned the stream channel width (Figure 4-1 b-d), as is generally the case in small streams (Gurnell et al., 2002). Floods were conducted from May 24-May 26, 2016. Using regional curves for non-urban streams in the ridge and Valley Province (Keaton et al., 2005), we found that the 1.5 year flood event for a 1 km^2 watershed would be 515 L/s. This is approximately 9 times greater than peak flows generated in both floods, indicating that the experimental floods are representative of realistic floods that would occur multiple times per year.

At the upstream boundary of the reach, discharge was measured using a 0.9 m HL-type flume (Brakensiek et al., 1979) and an Onset HOBO Pressure Transducer (PT). Flow measurements from the flume were taken every minute and uploaded to a Campbell CR-1000 data logger. At the downstream end of the reach, flow measurements were taken using a SonTek Argonaut-SW Acoustic Doppler Velocimeter (ADV). Measurements from the ADV were also taken at 1-min intervals and directly uploaded to a field computer. Additionally, three Onset HOBO PTs were placed throughout the floodplain to measure flow depth (Figure 4-1).

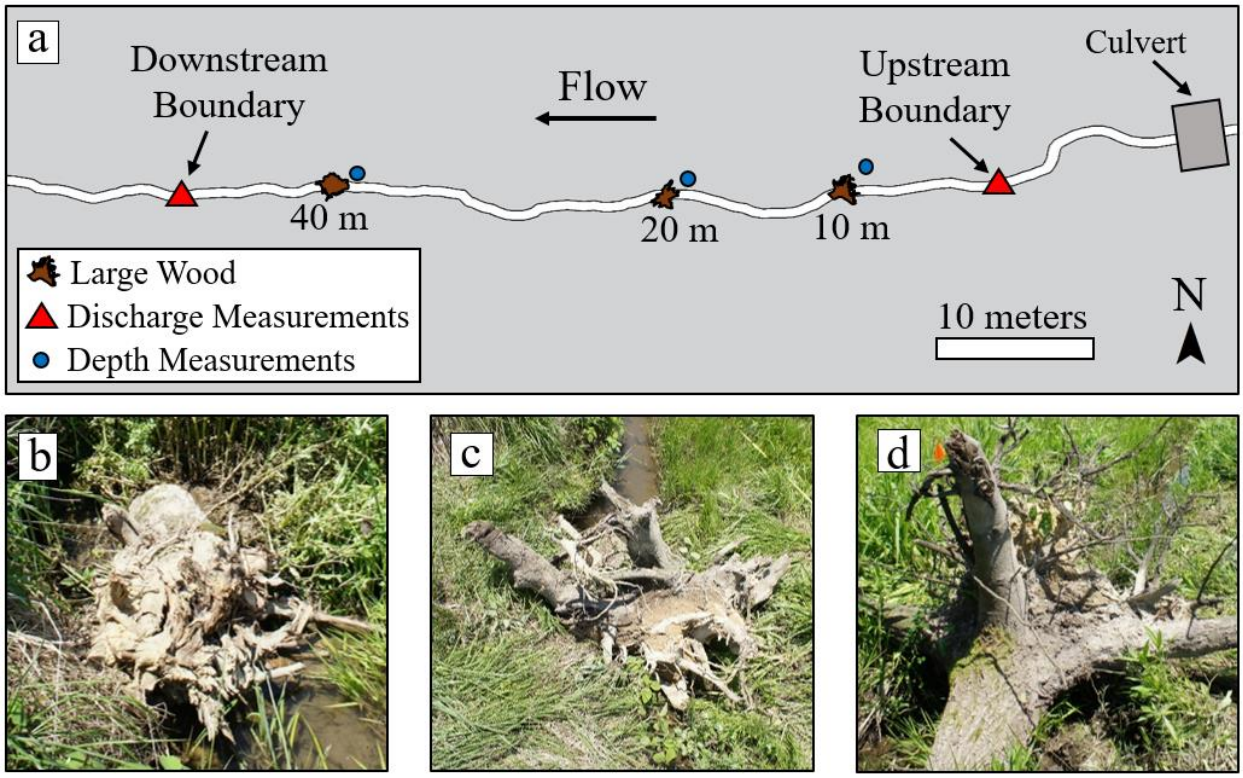

Figure 4-1. a) Map of the experimental setup and b-d) the three pieces of LW used in the study

4.2.3 Hydrodynamic Modeling

We used Hydrologic Engineering Center's River Analysis System (HEC-RAS) hydraulic modeling software to model 2-dimensional (2D) surface water hydrodynamics for the stream reach. HEC-RAS is commonly used for hydraulic modeling due to its strong computational abilities, quick processing time, and free availability through the U.S. Army Corps of Engineers. The recent addition of 2D modeling to HEC-RAS makes it an appealing option for floodplain modeling studies such as the one presented here. Specifically, HEC-RAS numerically solves the 2D Saint-Venant equations for conservation of mass (Equation 1), conservation of momentum in the x direction (Equation 2), and conservation of momentum in the y direction (Equation 3):

$$\frac{\partial \mathrm{H}}{\partial \mathrm{t}} + \frac{\partial(\mathrm{h}v_x)}{\partial \mathrm{x}} + \frac{\partial(\mathrm{h}v_y)}{\partial \mathrm{y}} = 0 \quad (1)$$

$$\frac{\partial v_x}{\partial \mathrm{t}} + v_x \frac{\partial v_x}{\partial \mathrm{x}} + \mathrm{g}\frac{\partial \mathrm{H}}{\partial \mathrm{x}} + \mathrm{g}\,(\mathrm{S_f} - \mathrm{S_0}) = 0 \quad (2)$$

$$\frac{\partial v_y}{\partial \mathrm{t}} + v_y \frac{\partial v_y}{\partial \mathrm{y}} + \mathrm{g}\frac{\partial \mathrm{H}}{\partial \mathrm{y}} + \mathrm{g}\,(\mathrm{S_f} - \mathrm{S_0}) = 0 \quad (3)$$

where H is the water surface elevation, h is hydraulic head, v_x is velocity in the downstream direction, v_y is velocity in the transverse direction, g is acceleration due to gravity, S_f is the energy

slope, and S_0 is the channel slope. The Saint Venant Equations (Equations 1-3) are numerically solved using finite volume approximations discretized with respect to time and space. HEC-RAS can solve the full Saint-Venant equations or the diffusive wave approximation of the Saint-Venant Equations. When the diffusive wave approach is selected, the first and second terms on the left side of Equations 2 and 3 are not used.

We chose to use the 2D diffusive wave routing approach due to its computational speed and model stability. The diffusive wave simplification is a common assumption used in 2D hydrodynamic modeling of rivers as it assumes that pressure and slope are an order of magnitude greater than local and convective acceleration terms and thus these terms can be ignored (Henderson, 1966). We found that the full Saint-Venant and diffusive wave approaches produced similar results, but the diffusive wave technique was approximately 20 times faster and resulted in better model stability. This observation has been noted in previous research (Horritt & Bates, 2001), and studies have successfully employed diffusive wave approximations for 2D modeling of flood events (e.g., Quiroga et al., 2016).

We utilized topography and streamflow data to parameterize the model. Reach topography and stream channel bathymetry were surveyed using a real-time kinematic geographic positioning system (RTK-GPS, Topcon GR-3). Prior to the flood events, we surveyed 1088 elevation data points within the stream channel and across the floodplain to capture channel bathymetry and micro-topography of the 50 m long reach. These elevation data points were then used to develop a triangulated irregular network and produce a seamless digital elevation model (DEM) of the stream and adjacent floodplain. We then imported the DEM of the reach into HEC-RAS for hydraulic analysis. A 2D flow area of 877 m^2 was created around the border of the DEM to ensure that the entire reach was analyzed. Grid discretization of 0.5 m by 0.5 m, similar to the density of surveyed GPS points, was used to balance model accuracy and computational time. This resulted in a computational mesh containing 3853 cells across the flow area. Bank lines were enforced within the mesh to ensure that the stream channel was properly discretized. Three cross sections were incorporated into the mesh and used to model LW locations along the stream.

Boundary conditions were established using discharge data from the flume measured at the upstream boundary and normal depth at the downstream boundary of the reach. A computational time step of 5 seconds was used to meet the Courant condition ($\Delta t > \Delta x/c$) for model stability (Pappenberger et al., 2005), where Δt is the computational time step, Δx is the space step and c is the speed of the flood wave. Alternatively, the HEC-RAS dam breach user manual (Brunner, 2014) suggests using a computations time step of $\Delta t < Tr/20$, where Tr is the time of rise of the flood hydrograph. This approach would yield a time step of 6 seconds, and therefore, 5 seconds was still an appropriate selection for the computational time step. We assumed initial Manning's n values of 0.05 and 0.1 in the channel and floodplain, respectively based on estimates from similar headwater streams (Jarrett, 1984; Marcus et al., 1992).

The flood without LW was calibrated by comparing modeled outflows with flow measurements from the ADV. To calibrate the model, the Manning's *n* values for the channel and floodplain were adjusted to minimize error and improve the overall model fit. For the model of the flood with LW, Manning's *n* values were kept at the same calibrated values and modeled LW geometry was adjusted to improve the model fit. The LW cross sections were modeled as weir embankments

with orifices randomly placed across the face of the embankment. Previous studies have utilized similar techniques for modeling LW in streams (e.g., Hafs et al., 2014), and we found that it yielded the most accurate geometric representation of instream LW. To validate the model, modeled floodplain stage values were compared to measured stage values. To evaluate error and calibrate/validate the models, we used coefficient of determination (R^2), normalized root mean square error (NRMSE), and Nash-Sutcliffe efficiency (NSE).

4.2.4 Modeling Alternative Scenarios

To assess spatial variability along the reach, floodplain discharge was modeled by simulating a single piece of LW at different locations longitudinally along the reach. Overall, 50 simulations were conducted, each with a single LW cross section located at 1 m intervals along the reach. Floodplain discharge (Q_{FP}) was calculated in HEC-RAS as the total volume of water moving laterally across the stream banks and into the floodplain per unit time. Total discharge (Q_{tot}) for each cross section was calculated as the total volume of water moving longitudinally across the given cross section per unit time. Ratios of Q_{FP} to Q_{tot} were then calculated for each cross section both with and without LW incorporated. To better understand the variability of Q_{FP}/Q_{tot} values along the reach, we also analyzed maximum velocity, water depth, channel slope, width to depth (W:D) ratio, and channel sinuosity for each cross section.

Alternative storm events were modeled to determine the impacts of LW across varying flow regimes. To simulate various storm events, we developed a 1000-year synthetic rainfall distribution by applying a Bartlett-Lewis model (Rodriguez-Iturbe et al., 1987) to over 70 years of meteorological data measured at the Virginia Tech Montgomery Executive Airport, located ~1 kilometer from the study reach. The rainfall data were disaggregated to a sub-hourly timescale with R statistical software (R Development Core Team, 2017) using the HyetosMinute package (Kossieris et al., 2016). An exceedance curve was calculated from the 1000-year synthetic rainfall dataset and used to estimate 1, 2, 3, 5, 10, 15, 25, 50, 100, 250, 500, and 1000-year storms events for the same duration. Runoff from the selected storm events was calculated using the Natural Resources Conservation Service (NRCS) curve number unit hydrograph approach (Arnold et al., 1998). Runoff hydrographs were then used as inflow hydrographs in HEC-RAS, and the reach was modeled with and without LW present. This allowed us to quantify the impact that LW would have on flooding caused by a wide range of storm events.

4.3 Results

4.3.1 Experimental Flooding

We observed relatively similar inflow (upstream boundary) hydrographs between the two experimental floods. Peak discharge values at the upstream boundary of the reach were 55.8 L/s and 54.8 L/s for the flood without LW and the flood with LW, respectively (Figure 4-2a). Outflow (downstream boundary) hydrographs showed evidence of a dampened peak discharge and delayed time to peak discharge. Downstream peak discharge for the flood without wood was 53.0 L/s occurring 3 min after the upstream peak discharge (Figure 4-2b). For the flood with wood, peak discharge at the downstream boundary was 48.7 L/s occurring 4 min after the upstream peak discharge (Figure 4-2c).

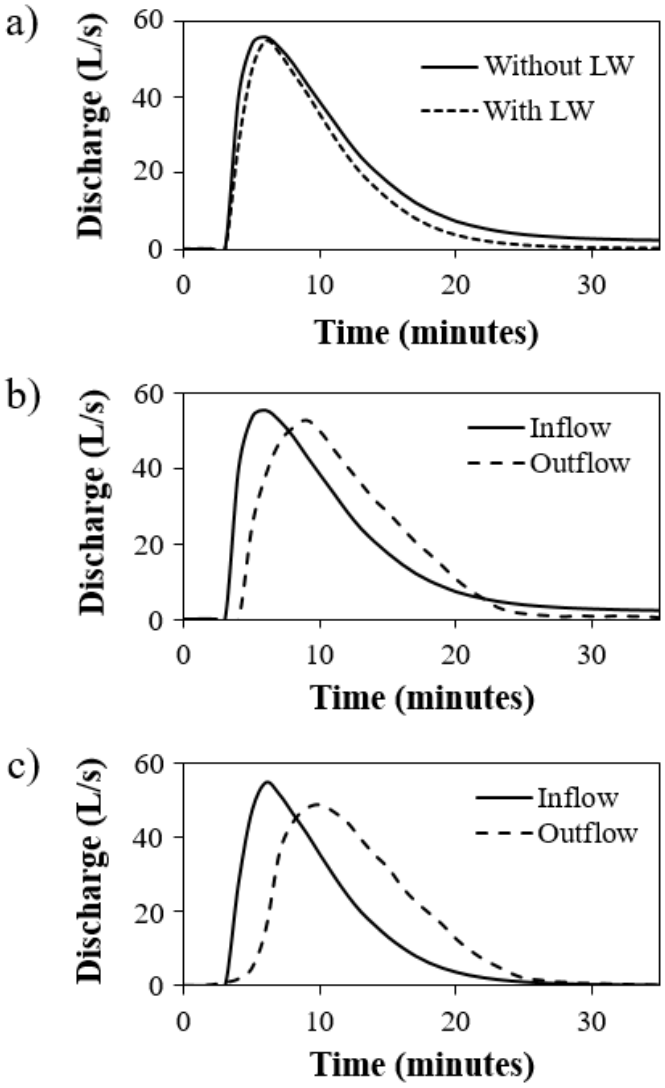

Figure 4-2. a) Hydrographs of inflow to the study reach for both floods, b) Upstream and downstream hydrographs for the first flood without LW in the channel, and c) Upstream and downstream hydrographs for the second flood with LW in the channel.

The addition of LW also increased floodplain stage and inundation duration at all three LW cross sections (Figure 4-3a; Table 4-1). Average inundation duration at the three LW cross sections was 14 minutes for the flood without LW and 18.7 minutes for the flood with LW. Average maximum water depth measured at the three LW cross sections was 8 cm for the flood without LW and 10.8 cm for the flood with LW. Additionally, stage-discharge hysteresis plots illustrate that the addition of LW increased the total area within the hysteresis loops for all three cross sections (Figure 4-3b). The greater area within the hysteresis loops indicates that there was a greater difference between the rising and falling limbs of the hydrographs, and thus LW increased the floodplain residence time at each of the three LW cross sections. Additionally, all of the hysteresis loops followed a

counter-clockwise direction, indicating that floodplain stage was greater during the falling limb of the flood hydrograph.

Table 4-1. Summary of inundation duration and maximum depth at each of the three LW cross sections

Location	Without LW		With LW	
	Inundation Duration (min)	Maximum Depth (cm)	Inundation Duration (min)	Maximum Depth (cm)
XS1 (10 m)	9	4.5	14	5.8
XS2 (20 m)	13	7.5	14	10
XS3 (40 m)	20	12	28	16.5

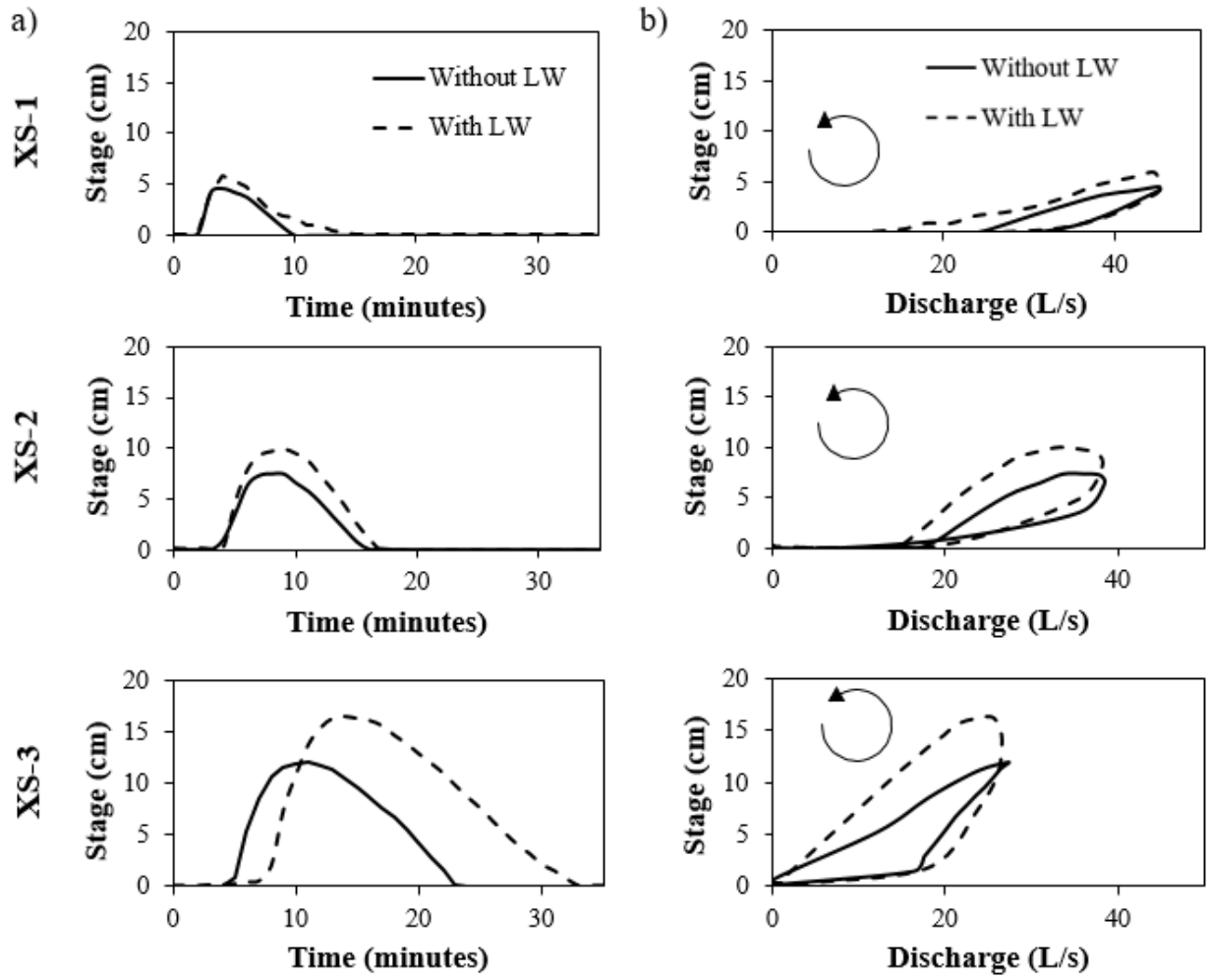

Figure 4-3. a) Stage hydrographs at each of the LW cross sections and b) Stage-Discharge hysteresis at each of the LW cross sections.

4.3.2 Model Fit

Manning's *n* values of 0.06 within the channel and 0.1 on the floodplain yielded the best fit for the flood without LW and were used for model simulations. At the downstream boundary, modeled and observed results from the flood without LW produced an R^2 of 0.88, an NRMSE of 8.9%, and a NSE of 0.91, while calibration of the flood with LW produced an R^2 of 0.89, and NRMSE of 9.4%, and an NSE of 0.92. Floodplain measurements and modeled depths produced an average R^2 of 0.83, NRMSE of 15.9%, and NSE of 0.77 for the flood without LW and an average R^2 of 0.82, NRMSE of 14.6%, and NSE of 0.8 for the flood with LW. A summary of the calibration and validation statistics for each location are shown in Table 4-2.

Table 4-2. Statistics from calibration of both floods at the downstream boundary and validation at three LW cross sections

Location	Without LW			With LW		
	R^2	NRMSE (%)	NSE	R^2	NRMSE (%)	NSE
Downstream	0.88	8.9	0.91	0.89	9.4	0.92
XS1 (10 m)	0.88	13.8	0.74	0.85	13.1	0.8
XS2 (20 m)	0.83	15.2	0.8	0.89	11.5	0.88
XS3 (40 m)	0.79	18.6	0.76	0.71	19.2	0.72

4.3.3 Simulation of Experimental Floods

Across the reach, maximum modeled inundation surface area was 265 m^2 during the flood without LW and 356 m^2 during the flood with LW (Figure 4-4). Maximum modeled water depth in the thalweg was 0.48 m during the flood without LW and 0.50 m during the flood with LW. Maximum modeled water depth in the floodplain was 0.12 m during the flood without LW and 0.16 m during the flood with LW. The addition of LW to the channel increased modeled floodplain inundation duration at all three LW cross sections.

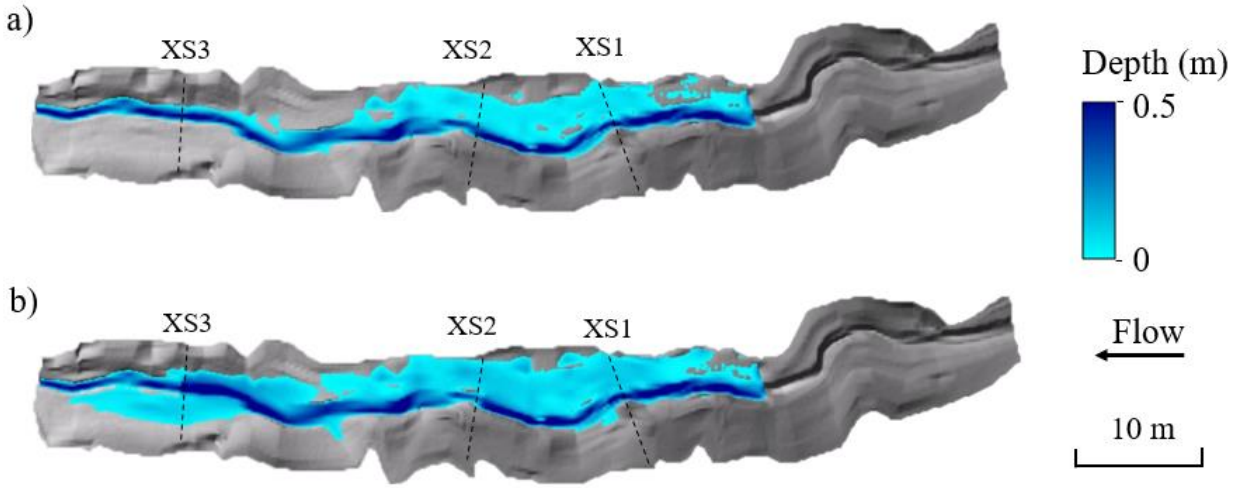

Figure 4-4. Planform view of modeled maximum floodplain inundation extent and depth along the reach for a) the flood without LW in the channel and b) the flood with LW in the channel.

Velocity dynamics for the reach also varied between the flood without LW and the flood with LW (Figure 4-5). During the flood without LW, velocity was highest in the stream channel and lowest in the floodplain. Velocity in the flood with LW was fairly uniform across the reach with the lowest values along the edge of the floodplain and highest values in the stream channel immediately downstream of the LW cross sections. Maximum water velocity in the thalweg was 0.92 m/s during the flood without LW and 0.83 m/s during the flood with LW. Maximum water velocity in the floodplain increased from 0.30 m/s during the flood without LW to 0.66 m/s during the flood with LW.

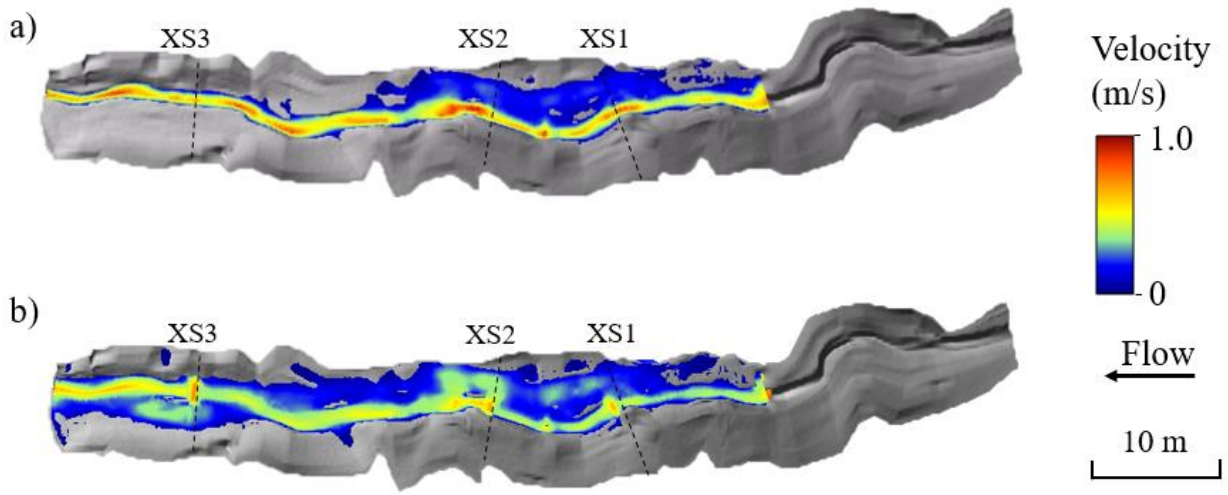

Figure 4-5. Planform view of maximum velocity along the reach for a) the flood without LW in the channel and b) the flood with LW in the channel.

4.3.4 Alternative Scenario Model Simulations

Variation in the location of LW placement along the stream affected the magnitude and spatial distribution of hydrologic exchange between the stream channel and floodplain (Figure 4-6a). The presence of LW in the channel consistently increased floodplain connectivity ($p<0.0001$), with an average cross-sectional Q_{FP}/Q_{tot} value of 16.6% for the flood without LW and 32.3% for the flood with LW. Maximum simulated Q_{FP}/Q_{tot} for the flood without LW occurred 28 m downstream of the inflow and 25 m downstream of the inflow for the flood with LW. The average difference between the two floods was 15.6% with the maximum difference occurring 18 m downstream of the upper boundary. When simulating the location of LW along the reach, geomorphic characteristics of the stream (i.e. channel slope, W:D ratio, and channel sinuosity) all had very little impact ($R^2 < 0.03$) on flooding dynamics. Modeled floodplain connectivity increased the most when LW was placed in relatively shallow portions of the reach or in places where water was moving fast. Channel velocity and water depth at each cross section without LW in the channel were correlated with $\Delta Q_{FP}/Q_{tot}$, the floodplain discharge difference between simulations with and

without LW. Specifically, thalweg velocity and water depth compared with $\Delta Q_{FP}/Q_{tot}$ produced R^2 values of 0.62 and 0.46, respectively (Figure 4-6b and 4-6c).

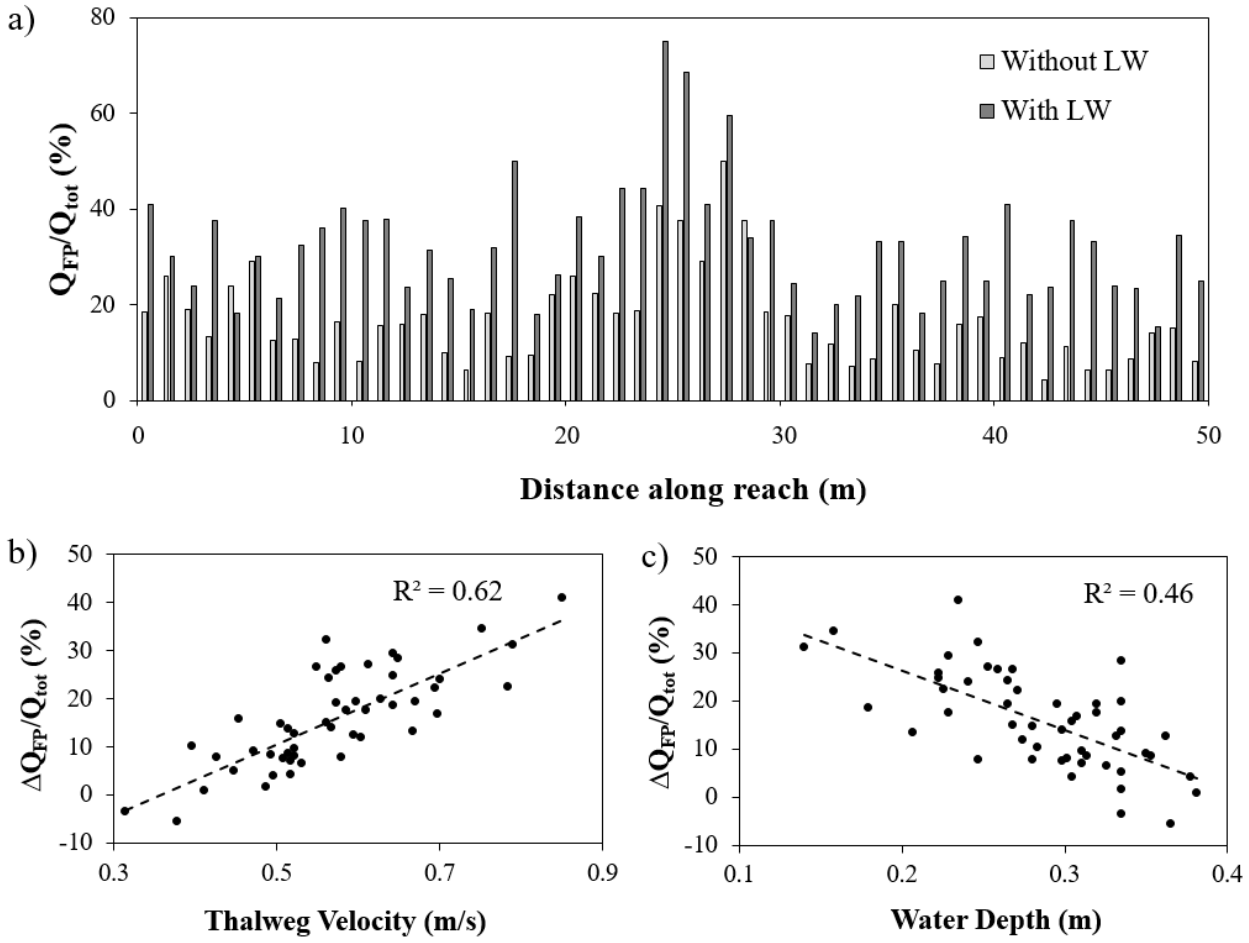

Figure 4-6. a) Q_{FP}/Q_{tot} for the 50 m reach during model simulations in which one piece of LW was placed at each cross section. Each bar representes the ratio of flows during one simulation, b) $\Delta Q_{FP}/Q_{tot}$ vs thalweg velocity for each cross section, and c) $\Delta Q_{FP}/Q_{tot}$ vs thalweg water depth for each cross section.

The addition of LW increased Q_{FP}/Q_{tot} for storm events of different magnitudes. Across the range of hypothetical storm events, values of Q_{FP}/Q_{tot} ranged from 14.8% to 88.3% without incorporating LW, while values ranged from 42.7% to 88.3% when incorporating LW. However, as the magnitude and recurrence interval of the storm event increased, the percent difference in Q_{FP}/Q_{tot} decreased, with values converging at an approximately 25-year recurrence interval (Figure 4-7). For example, the addition of LW increased Q_{FP}/Q_{tot} by 28% for a 1-year storm event, 16% for a 2-year storm event, but only 3% for a 5-year storm event.

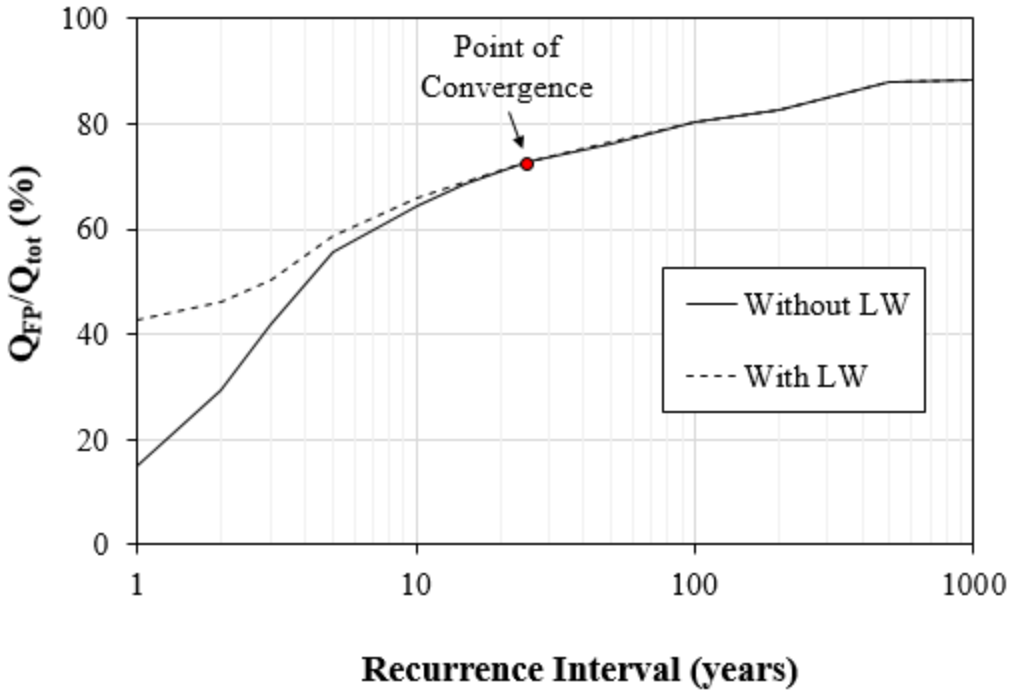

Figure 4-7. Q_{FP}/Q_{tot} vs recurrence interval for a range of modeled storm events. A convergence point was reached at a recurrence interval of 25 years.

4.4. Discussion

4.4.1 Impacts of LW on Floodplain Connectivity

As anticipated, addition of LW to the stream channel increased inundation extent, depth, duration, and floodplain discharge for the entire reach. Additionally, LW decreased longitudinal flow velocity and increased lateral flow velocity by diverting water onto the floodplain. These findings support the hypothesis that LW increases overall connectivity between the main channel and adjacent floodplain of small, headwater streams and agree with previous research on the hydraulic effects of LW in streams (e.g., Wohl, 2013). Additionally, these findings are consistent with the converse notion that removing LW from streams increases conveyance efficiency and decreases localized flooding, the rationale for removing LW from streams over the past century. Unlike previous research though, this study provides insight on LW flooding dynamics under differing placement strategies and across various flow regimes.

Model simulations indicate that varying placement strategies would affect the flooding dynamics within the floodplain at different locations along the stream. Specifically, channel velocity and water depth were found to be the most important factors controlling flooding along the reach. For example, the channel has high velocity and shallow depth at the cross section with the greatest potential for flood enhancement by LW (27 meters downstream of the upper boundary in the current study). Placement of LW at this cross section would also create the largest increase in Q_{FP}/Q_{tot} due to the diversion of fast flowing water onto the floodplain. On the contrary, cross

sections with low velocity and greater water depth have the lowest flooding potential (e.g., 5-6 m downstream of the upper boundary in the current study). These findings agree with previous studies (e.g., Curran & Wohl, 2003), which suggest that LW creates greater flood potential in steeper channels. Thus, knowing the longitudinal velocity (i.e. the velocity head) and water depth can provide a rough estimate of flooding potential along a reach. However, a number of additional characteristics such as roughness, soil hydraulic conductivity, and floodplain geometry could also affect the flooding potential at a given cross section (Darby, 1999; Bates & De Roo, 2000; Curran & Hession, 2013). Thus, the effects of LW on floodplain discharge dynamics is highly site dependent and likely depends on multiple variables.

Simulations of storm events with varying return intervals showed that the impact of LW on floodplain connectivity decreased as recurrence interval increased. At a recurrence interval of 25 years or greater, LW did not have any impact on flooding dynamics. Specifically, results showed that once floodplain flow made up ~70% of total flow (at a return interval of ~ 25 years), the effects of LW were negligible. Intuitively, the effects of LW on flooding decrease as flood magnitude increases because once a channel reaches bankfull flow, lateral flooding caused by LW is no longer the primary mechanism controlling floodplain flow. This is consistent with previous studies examining the effects of instream structures on hyporheic exchange (Hester & Doyle, 2008; Crispell and Endreny, 2009; Azinheira et al., 2014). Overall, results indicate that differing placement strategies and flow regimes can influence the degree to which LW influences floodplain connectivity.

4.4.2 Implications for Nutrient and Sediment Management

Here, we propose that the addition of LW to headwater, agricultural streams can serve as a best management practice (BMP) to improve downstream water quality. Nitrogen (N) and phosphorus (P) are of particular interest as increased loading of these nutrients to surface water bodies is the primary cause of worldwide eutrophication (e.g., Vitousek, 1997). Inputs of inorganic N come largely from agricultural areas drained by headwater streams (Mulholland et al., 2008). While much work has focused on incorporating forested riparian buffer strips into these areas, many of these watersheds still do not supply fallen timber to provide a sustainable budget for LW (Soulsby et al., 2017). In many floodplain systems, biogeochemical processing is limited by the amount of solute transported into floodplains (Forshay & Stanley 2005; Noe & Hupp 2009; Jones et al., 2014; Scott et al., 2014; Jones et al., 2015). Adding LW to streams could increase biogeochemical processing through increased floodplain connectivity of solutes like N, thus enhancing downstream water quality.

Increased floodplain connectivity created by adding LW to stream channels also has implications for both P and sediment management. Similar to N, the majority of P and sediment loading comes from excess runoff, particularly from headwater streams with limited BMPs (McFarland & Hauck, 1999). Adding LW to a stream channel can slow down the transport of sediment as well as the transport of P, which is often adsorbed to and transported by sediment (Records et al., 2016). However, as sediment settles within the channel, P can solubilize and be exported as soluble reactive P (Jones et al., 2015). Similarly, N can change forms through mineralization and nitrification depending on other factors such as the amount of available organic matter (McMillan et al., 2010). Additionally, in systems with a high sediment load, LW could enhance trapping of

sediment in the stream channel and eventually cause the LW to become buried. Thus, nutrient and sediment dynamics are often site-specific and fairly complex in nature. While LW can be a tool for nutrient and sediment management, the addition of LW to streams must be carefully considered from a holistic point of view as the removal of one pollutant can lead to unexpected and undesired side effects.

4.4.3 Future Work and Limitations

This study did not take into account the spatial variability of the longitudinal or lateral Manning's *n* value. While we were able to use different *n* values for the main channel and floodplain, this does not give an accurate representation of the spatial heterogeneity of roughness across the study reach. Even at the reach scale, roughness can vary substantially and affect connectivity (Curran & Hession, 2013). Future modeling studies should use a spatially distributed n value to get a more accurate representation of channel and floodplain roughness. This can be done using aerial LIDAR (Abu-Aly et al., 2014), structure-from-motion photogrammetry (Smith et al., 2004), or laser scanning (Straatsma & Baptist, 2008). While outside the scope of this research, inclusion of such a spatially-varying roughness coefficient would create a more accurate representation of the river corridor and improve the overall model fit.

Future work should also examine the long-term effects of LW on stream hydrogeomorphology. The effects of LW on flooding have been largely overlooked in the field of fluvial geomorphology but studies suggests that these effects are actually a critical component of stream geomorphology (Gurnell et al., 2002). A number of studies have emphasized the important role that LW plays in morphological processes (e.g., Piégay & Gurnell, 1997; Gurnell, 2012), but few studies have explicitly examined the role of LW on flooding, a key component of fluvial geomorphology (Woltemade, 1994). Additionally, long-term effects are often difficult to examine due to the monetary cost of long-term stream monitoring and small scope of most stream restoration projects. However, the availability of emerging technologies such as freely-available, high-resolution remote sensing data allows for more frequent and accurate monitoring of streams. This type of monitoring is crucial for understanding the long-term effects of LW on the geomorphology of streams and rivers.

A unique aspect of this study that could be valuable for future studies is simulating and recreating beaver dams. Beaver dams provide ecological benefits by increasing floodplain connectivity (Westbrook et al., 2006), increasing hyporheic connectivity (Briggs et al., 2013), and serving as a sink of reactive solutes during periods of high flow (Wegener et al., 2017). Once highly ubiquitous across the landscape, beaver dams have been largely removed as a result of anthropogenic activities (Pollock et al., 2014). The loss of beaver dams over the years has resulted in an increase of sediment and pollutant transport (Levine & Meyer, 2014). However, recent studies have highlighted the potential for restoring streams with recreated beaver dam analogs (BDAs) (Pollock et al., 2014; Bouwes et al., 2016), which are structures that can be designed to mimic natural beaver dams. Similar to BDAs, LW has the potential to reestablish stream ecosystem health by restoring the natural flow regime. Adding LW to streams is a simple, cost-effective technique that can provide ecological benefits that are similar to those of BDAs.

4.5 Conclusions

There is currently a need for understanding the impacts of LW on headwater stream floodplain dynamics, particularly in the mid-Atlantic region of the U.S. Our research addressed this issue by examining the impacts that LW has on floodplain connectivity in a headwater mid-Atlantic stream. Results indicate that the addition of LW to small, headwater streams increases floodplain inundation extent, depth, and discharge, and decreases longitudinal stream velocity. Additionally, we found that placement strategies and varying flow regimes could influence the role that LW plays in floodplain hydrodynamics. These findings confirm the overall hypothesis that LW plays an important role in floodplain connectivity of headwater streams. Overall, this work provides insight into the impacts of LW on flooding dynamics during storm events.

4.6 Acknowledgements

The authors would like to thank Dumitru Branisteanu and Laura Lehmann for assisting with the experimental setup as well as Daniel Frisbee, Allison Guzman, and Rachel Molloy for their assistance with surveying. This research did not receive any specific grant from funding agencies in the public, commercial, or not-for-profit sectors.

4.7 References

Abbe, T. B., & Montgomery, D. R. (1996). Large woody debris jams, channel hydraulics and habitat formation in large rivers. *Regulated Rivers Research and Management*, *12*(23), 201-221.

Abu-Aly, T. R., Pasternack, G. B., Wyrick, J. R., Barker, R., Massa, D., & Johnson, T. (2014). Effects of LiDAR-derived, spatially distributed vegetation roughness on two-dimensional hydraulics in a gravel-cobble river at flows of 0.2 to 20 times bankfull. *Geomorphology*, *206*, 468-482. https://doi.org/10.1016/j.geomorph.2013.10.017

Angelopoulos, N. V., Cowx, I. G., & Buijse, A. D. (2017). Integrated planning framework for successful river restoration projects: Upscaling lessons learnt from European case studies. *Environmental Science and Policy*, *76*, 12-22. https://doi.org/10.1016/j.envsci.2017.06.005

Arnold, J. G., Srinivasan, R., Muttiah, R. S., & Williams, J. R. (1998). Large area hydrologic modeling and assessment part I: model development. *Journal of the American Water Resources Association*, *34*(1), 73-89. https://doi.org/10.1111/j.1752-1688.1998.tb05961.x

Azinheira, D. L., Scott, D. T., Hession, W., & Hester, E. T. (2014). Comparison of effects of inset floodplains and hyporheic exchange induced by in-stream structures on solute retention. *Water Resources Research*, *50*(7), 6168-6190. https://doi.org/10.1002/2013WR014400

Bates, P. D., & De Roo, A. P. J. (2000). A simple raster-based model for flood inundation simulation. *Journal of Hydrology*, *236*(1), 54-77. https://doi.org/10.1016/S0022-1694(00)00278-X

Bernhardt, E. S., Palmer, M. A., Allan, J. D., Alexander, G., Barnas, K., Brooks, S., ... & Galat, D. (2005). Synthesizing US river restoration efforts. *Science*, *308*(5722), 636-637. https://doi.org/10.1126/science.1109769

Bilby, R. E., & Ward, J. W. (1991). Characteristics and function of large woody debris in streams draining old-growth, clear-cut, and second-growth forests in southwestern Washington. *Canadian Journal of Fisheries and Aquatic Sciences*, *48*(12), 2499-2508. https://doi.org/10.1139/f91-291

Brakensiek, D. L., Osborn, H. B., & Rawls, W. J. (1979). *Field Manual for Research in Agricultural Hydrology* (Agriculture Handbook No. 224). Washington, DC: U.S. Department of Agriculture.

Briggs, M. A., Lautz, L. K., Hare, D. K., & González-Pinzón, R. (2013). Relating hyporheic fluxes, residence times, and redox-sensitive biogeochemical processes upstream of beaver dams. *Freshwater Science, 32*(2), 622-641. https://doi.org/10.1899/12-110.1

Bouwes, N., Weber, N., Jordan, C. E., Saunders, W. C., Tattam, I. A., Volk, C., ... & Pollock, M. M. (2016). Ecosystem experiment reveals benefits of natural and simulated beaver dams to a threatened population of steelhead (Oncorhynchus mykiss). *Scientific Reports*, *6*, 28581. https://doi.org/10.1038/srep28581

Brunner, W. G. (2014). *Using HEC-RAS for Dam Break Studies* (Rep. TD-39). Davis, CA: U.S. Army Corps of Engineers Hydrologic Engineering Center (HEC).

Collins, B. D., & Montgomery, D. R. (2002). Forest development, wood jams, and restoration of floodplain rivers in the Puget Lowland, Washington. *Restoration Ecology*, *10*(2), 237-247. https://doi.org/10.1046/j.1526-100X.2002.01023.x

Covino, T. (2017). Hydrologic connectivity as a framework for understanding biogeochemical flux through watersheds and along fluvial networks. *Geomorphology*, *277*, 133-144. https://doi.org/10.1016/j.geomorph.2016.09.030

Crispell, J. K., & Endreny, T. A. (2009). Hyporheic exchange flow around constructed in-channel structures and implications for restoration design. *Hydrological Processes*, *23*(8), 1158-1168. https://doi.org/10.1002/hyp.7230

Curran, J. C., & Hession, W. C. (2013). Vegetative impacts on hydraulics and sediment processes across the fluvial system. *Journal of Hydrology*, *505*, 364-376. https://doi.org/10.1016/j.jhydrol.2013.10.013

Curran, J. H., & Wohl, E. E. (2003). Large woody debris and flow resistance in step-pool channels, Cascade Range, Washington. *Geomorphology*, *51*(1), 141-157. https://doi.org/10.1016/S0169-555X(02)00333-1

Darby, S. E. (1999). Effect of riparian vegetation on flow resistance and flood potential. *Journal of Hydraulic Engineering*, *125*(5), 443-454. https://doi.org/10.1061/(ASCE)0733-9429(1999)125:5(443)

Davidson, S. L., and Eaton, B. C. (2013). Modeling channel morphodynamic response to variations in large wood: Implications for stream rehabilitation in degraded watersheds. *Geomorphology*, *202*, 59-73. https://doi.org/10.1016/j.geomorph.2012.10.005

Dixon, S. J., & Sear, D. A. (2014). The influence of geomorphology on large wood dynamics in a low gradient headwater stream. *Water Resources Research*, *50*(12), 9194-9210. https://doi.org/10.1002/2014WR015947

Dolloff, C. A., & Warren Jr, M. L. (2003). Fish relationships with large wood in small streams. In *American Fisheries Society Symposium 37: 179-193, 2003*.

Ensign, S. H., McMillan, S. K., Thompson, S. P., & Piehler, M. F. (2006). Nitrogen and phosphorus attenuation within the stream network of a coastal, agricultural watershed. *Journal of Environmental Quality*, *35*(4), 1237-1247. https://doi.org/10.2134/jeq2005.0341

Forshay, K. J., & Stanley, E. H. (2005). Rapid nitrate loss and denitrification in a temperate river floodplain. *Biogeochemistry*, *75*(1), 43-64. https://doi.org/10.1007/s10533-004-6016-4

Gurnell, A. (2012). Fluvial Geomorphology: Wood and river landscapes. *Nature Geoscience*, *5*(2), 93. https://doi.org/10.1038/ngeo1382

Gurnell, A. M., Piegay, H., Swanson, F. J., & Gregory, S. V. (2002). Large wood and fluvial processes. *Freshwater Biology*, *47*(4), 601-619. https://doi.org/10.1046/j.1365-2427.2002.00916.x

Hafs, A. W., Harrison, L. R., Utz, R. M., & Dunne, T. (2014). Quantifying the role of woody debris in providing bioenergetically favorable habitat for juvenile salmon. *Ecological Modelling*, *285*, 30-38. https://doi.org/10.1016/j.ecolmodel.2014.04.015

Harvey, J., & Gooseff, M. (2015). River corridor science: Hydrologic exchange and ecological consequences from bedforms to basins. *Water Resources Research*, *51*(9), 6893-6922. https://doi.org/10.1002/2015WR017617

Henderson, F. M. (1966). *Open Channel Flow*. New York City, NY: Macmillan.

Hester, E. T., & Doyle, M. W. (2008). In-stream geomorphic structures as drivers of hyporheic exchange. *Water Resources Research*, *44*(3). https://doi.org/10.1029/2006WR005810

Hester, E. T., Guth, C. R., Scott, D. T., & Jones, C. N. (2016). Vertical surface water–groundwater exchange processes within a headwater floodplain induced by experimental floods. *Hydrological Processes*, *30*(21), 3770-3787. https://doi.org/10.1002/hyp.10884

Hester, E. T., Hammond, B., & Scott, D. T. (2016). Effects of inset floodplains and hyporheic exchange induced by in-stream structures on nitrate removal in a headwater stream. *Ecological Engineering*, *97*, 452-464. https://doi.org/10.1016/j.ecoleng.2016.10.036

Jeffries, R., Darby, S. E., & Sear, D. A. (2003). The influence of vegetation and organic debris on flood-plain sediment dynamics: case study of a low-order stream in the New Forest, England. *Geomorphology*, *51*(1-3), 61-80. https://doi.org/10.1016/S0169-555X(02)00325-2

Johnson, L. B., Breneman, D. H., & Richards, C. (2003). Macroinvertebrate community structure and function associated with large wood in low gradient streams. *River Research and Applications*, *19*(3), 199-218. https://doi.org/10.1002/rra.712

Jones, C. N., Scott, D. T., Edwards, B. L., & Keim, R. F. (2014). Perirheic mixing and biogeochemical processing in flow-through and backwater floodplain wetlands. *Water Resources Research*, *50*(9), 7394-7405. https://doi.org/10.1002/2014WR015647

Jones, C. N., Scott, D. T., Guth, C., Hester, E. T., & Hession, W. C. (2015). Seasonal variation in floodplain biogeochemical processing in a restored headwater stream. *Environmental Science and Technology*, *49*(22), 13190-13198. https://doi.org/10.1021/acs.est.5b02426

Kail, J., Hering, D., Muhar, S., Gerhard, M., & Preis, S. (2007). The use of large wood in stream restoration: experiences from 50 projects in Germany and Austria. *Journal of Applied Ecology*, *44*(6), 1145-1155. https://doi.org/10.1111/j.1365-2664.2007.01401.x

Karr, J. R., & Dudley, D. R. (1981). Ecological perspective on water quality goals. *Environmental Management*, *5*(1), 55-68. https://doi.org/10.1007/BF01866609

Keaton, J. N., Messinger, T., & Doheny, E. J. (2005). *Development and analysis of regional curves for streams in the non-urban valley and ridge physiographic province, Maryland, Virginia, and West Virginia*. US Department of the Interior, US Geological Survey.

Keys, T. A., Jones, C. N., Scott, D. T., & Chuquin, D. (2016). A cost-effective image processing approach for analyzing the ecohydrology of river corridors. *Limnology and Oceanography: Methods*, *14*(6), 359-369. https://doi.org/10.1002/lom3.10095

Kossieris, P., Makropoulos, C., Onof, C., & Koutsoyiannis, D. (2016). A rainfall disaggregation scheme for sub-hourly time scales: Coupling a Bartlett-Lewis based model with adjusting procedures. *Journal of Hydrology*. https://doi.org/10.1016/j.jhydrol.2016.07.015

Lagasse, P. F., Zevenbergen, L. W., Spitz, W. J., & Arneson, L. A. (2012). *Stream Stability at Highway Structures* (Rep. FHWA-HIF-12-004). Washington, DC: Federal Highway Administration.

Levine, R., & Meyer, G. A. (2014). Beaver dams and channel sediment dynamics on Odell Creek, Centennial Valley, Montana, USA. *Geomorphology*, *205*, 51-64. https://doi.org/10.1016/j.geomorph.2013.04.035

Marcus, W. A., Roberts, K., Harvey, L., & Tackman, G. (1992). An evaluation of methods for estimating Manning's n in small mountain streams. *Mountain Research and Development*, 227-239. https://doi.org/10.2307/3673667

Matheson, A., Thoms, M., & Reid, M. (2017). Does reintroducing large wood influence the hydraulic landscape of a lowland river system?. *Geomorphology*, *292*, 128-141. https://doi.org/10.1016/j.geomorph.2017.03.035

May, C. L., & Gresswell, R. E. (2003). Large wood recruitment and redistribution in headwater streams in the southern Oregon Coast Range, USA. *Canadian Journal of Forest Research*, *33*(8), 1352-1362. https://doi.org/10.1139/x03-023

McFarland, A., & Hauck, L. M. (1999). Relating agricultural land uses to in-stream stormwater quality. *Journal of Environmental Quality*, *28*(3), 836-844. https://doi.org/10.2134/jeq1999.00472425002800030014x

McMillan, S. K., Piehler, M. F., Thompson, S. P., & Paerl, H. W. (2010). Denitrification of nitrogen released from senescing algal biomass in coastal agricultural headwater streams. *Journal of Environmental Quality*, *39*(1), 274-281. https://doi.org/10.2134/jeq2008.0438

Montgomery, D. R., Collins, B. D., Buffington, J. M., & Abbe, T. B. (2003*). Geomorphic effects of wood in rivers*. Paper presented at American Fisheries Society Symposium, Bethesda, MD.

Mueller Price, J. S., Baker, D. W., & Bledsoe, B. P. (2016). Effects of passive and structural stream restoration approaches on transient storage and nitrate uptake. *River Research and Applications*, *32*(7), 1542-1554. https://doi.org/10.1002/rra.3013

Mulholland, P. J., Helton, A. M., Poole, G. C., Hall, R. O., Hamilton, S. K., Peterson, B. J., ... & Dodds, W. K. (2008). Stream denitrification across biomes and its response to anthropogenic nitrate loading. *Nature*, *452*(7184), 202. https://doi.org/10.1038/nature06686

Noe, G. B., & Hupp, C. R. (2009). Retention of riverine sediment and nutrient loads by coastal plain floodplains. *Ecosystems*, *12*(5), 728-746. https://doi.org/10.1007/s10021-009-9253-5

Pappenberger, F., Beven, K., Horritt, M., & Blazkova, S. (2005). Uncertainty in the calibration of effective roughness parameters in HEC-RAS using inundation and downstream level

observations. *Journal of Hydrology*, *302*(1), 46-69. https://doi.org/10.1016/j.jhydrol.2004.06.036
Parker, C., Henshaw, A. J., Harvey, G. L., & Sayer, C. D. (2017). Reintroduced large wood modifies fine sediment transport and storage in a lowland river channel. *Earth Surface Processes and Landforms*. https://doi.org/10.1002/esp.4123
Piégay, H., & Gurnell, A. M. (1997). Large woody debris and river geomorphological pattern: examples from SE France and S. England. *Geomorphology*, *19*(1-2), 99-116. https://doi.org/10.1016/S0169-555X(96)00045-1
Pollock, M. M., Beechie, T. J., Wheaton, J. M., Jordan, C. E., Bouwes, N., Weber, N., & Volk, C. (2014). Using beaver dams to restore incised stream ecosystems. *BioScience*, *64*(4), 279-290. https://doi.org/10.1093/biosci/biu036
Quiroga, V. M., Kure, S., Udo, K., & Mano, A. (2016). Application of 2D numerical simulation for the analysis of the February 2014 Bolivian Amazonia flood: Application of the new HEC-RAS version 5. *RIBAGUA-Revista Iberoamericana del Agua*, *3*(1), 25-33. https://doi.org/10.1016/j.riba.2015.12.001
R Development Core Team (2017) *R: A language and Envrionment for Statistical Computing*. R Foundation for Statistical Computing. Vienna, Austria.
Rafferty, M. (2013). *Development of a Computational Design Tool for Evaluating the Stability of Large Wood Structures Proposed for Stream Enhancement* (Master's Thesis). Fort Collins, Colorado: Colorado State University.
Rana, S. M., Scott, D. T., & Hester, E. T. (2017). Effects of in-stream structures and channel flow rate variation on transient storage. *Journal of Hydrology*, *548*, 157-169. https://doi.org/10.1016/j.jhydrol.2017.02.049
Records, R. M., Wohl, E., & Arabi, M. (2016). Phosphorus in the river corridor. *Earth-Science Reviews*, *158*, 65-88. https://doi.org/10.1016/j.earscirev.2016.04.010
Rodriguez-Iturbe, I., Cox, D. R., & Isham, V. (1987). Some models for rainfall based on stochastic point processes. *Proceedings of the Royal Society of London A: Mathematical, Physical and Engineering Sciences*, *410*(18392), 69-288. https://doi.org/10.1098/rspa.1987.0039
Ruiz-Villanueva, V., Bladé Castellet, E., Díez-Herrero, A., Bodoque, J. M., & Sánchez-Juny, M. (2014). Two-dimensional modelling of large wood transport during flash floods. *Earth Surface Processes and Landforms*, *39*(4), 438-449. https://doi.org/10.1002/esp.3456
Ruiz-Villanueva, V., Piégay, H., Gurnell, A. A., Marston, R. A., & Stoffel, M. (2016). Recent advances quantifying the large wood dynamics in river basins: New methods and remaining challenges. *Reviews of Geophysics*, *54*(3), 611-652. https://doi.org/10.1002/2015RG000514
Schmocker, L., & Weitbrecht, V. (2013). Driftwood: risk analysis and engineering measures. *Journal of Hydraulic Engineering*, *139*(7), 683-695. https://doi.org/10.1061/(ASCE)HY.1943-7900.0000728
Sear, D. A., Millington, C. E., Kitts, D. R., & Jeffries, R. (2010). Logjam controls on channel: floodplain interactions in wooded catchments and their role in the formation of multi-channel patterns. *Geomorphology*, *116*(3-4), 305-319. https://doi.org/10.1016/j.geomorph.2009.11.022
Scott, D. T., Keim, R. F., Edwards, B. L., Jones, C. N., & Kroes, D. E. (2014). Floodplain biogeochemical processing of floodwaters in the Atchafalaya River Basin during the

Mississippi River flood of 2011. *Journal of Geophysical Research: Biogeosciences*, *119*(4), 537-546. https://doi.org/10.1002/2013JG002477

Smith, M. J., Asal, F. F. F., & Priestnall, G. (2004). The use of photogrammetry and lidar for landscape roughness estimation in hydrodynamic studies. *International Archives of Photogrammetry, Remote Sensing and Spatial Information Sciences*, *35*(B3), 714-719.

Soulsby, C., Dick, J., Scheliga, B., & Tetzlaff, D. (2017). Taming the Flood–how far can we go with trees?. *Hydrological Processes*. https://doi.org/10.1002/hyp.11226

Straatsma, M. W., & Baptist, M. J. (2008). Floodplain roughness parameterization using airborne laser scanning and spectral remote sensing. *Remote Sensing of Environment*, *112*(3), 1062-1080. https://doi.org/10.1016/j.rse.2007.07.012

Vitousek, P. M., Aber, J. D., Howarth, R. W., Likens, G. E., Matson, P. A., Schindler, D. W., ... & Tilman, D. G. (1997). Human alteration of the global nitrogen cycle: sources and consequences. *Ecological Applications*, *7*(3), 737-750. https://doi.org/10.1890/1051-0761(1997)007[0737:HAOTGN]2.0.CO;2

Wegener, P., Covino, T., & Wohl, E. (2017). Beaver-mediated lateral hydrologic connectivity, fluvial carbon and nutrient flux, and aquatic ecosystem metabolism. *Water Resources Research*, *53*(6), 4606-4623. https://doi.org/10.1002/2016WR019790

Westbrook, C. J., Cooper, D. J., & Baker, B. W. (2006). Beaver dams and overbank floods influence groundwater–surface water interactions of a Rocky Mountain riparian area. *Water Resources Research*, *42*(6). https://doi.org/10.1029/2005WR004560

Wilford, D. J., Sakals, M. E., Innes, J. L., Sidle, R. C., & Bergerud, W. A. (2004). Recognition of debris flow, debris flood and flood hazard through watershed morphometrics. *Landslides*, *1*(1), 61-66. https://doi.org/10.1007/s10346-003-0002-0

Wohl, E. (2013). Floodplains and wood. *Earth-Science Reviews*, *123*, 194-212. https://doi.org/10.1016/j.earscirev.2013.04.009

Wohl, E., & Goode, J. R. (2008). Wood dynamics in headwater streams of the Colorado Rocky Mountains. *Water Resources Research*, *44*(9). https://doi.org/10.1029/2007WR006522

Wohl, E., Bledsoe, B. P., Fausch, K. D., Kramer, N., Bestgen, K. R., & Gooseff, M. N. (2016). Management of large wood in streams: an overview and proposed framework for hazard evaluation. *Journal of the American Water Resources Association*, *52*(2), 315-335. https://doi.org/10.1111/1752-1688.12388

Woltemade, C. J. (1994). Form and Process: Fluvial Geomorphology and Flood-Flow Interaction, Grant River, Wisconsin. *Annals of the Association of American Geographers*, *84*(3), 462-479. https://doi.org/10.1111/j.1467-8306.1994.tb01870.x

CHAPTER 5. STORM EFFECTS ON NITROGEN FLUX AND LONGITUDINAL VARIABILITY IN A RIVER-RESERVOIR SYSTEM

Tyler A. Keys, Madeline F. Ryan, and Durelle T. Scott

Submission: Planned April 2018
To: *River Research and Applications*
Status: In preparation

Abstract

Sustainable management of the nitrogen (N) and phosphorus (P) cycles remains a considerable global challenge that has major implications for aquatic ecosystems. Dams play a critical yet often neglected role in addressing this challenge as they increase hydraulic residence time and denitrification potential. However, during storm events when the majority of N and P loading occurs, dams have less potential to reduce N flux and can even increase the export of N. Here, we examined the flux of N species as well as phosphorus along a river-reservoir system at baseflow and across the falling limb of a multi-day storm hydrograph. Grab samples were taken at two U.S. Geological Survey stream gages as well as three additional locations along the river-reservoir-river transition. On three of the sampling days, we utilized high frequency sensors to obtain high spatial resolution longitudinal profiles of nitrate (NO_3^-) as well as other water quality variables across the river to reservoir hydraulic gradient to analyze N dynamics along an impounded portion of the river corridor. Results illustrated that the impoundment served as a net sink of N and P, retaining 3.4% of total N and 12.7% of total P loading from the storm event. Statistical analysis revealed that ammonium (NH_4^+) fluxes were significantly higher downstream of the dam in comparison to fluxes upstream of the dam, indicating that there was a net export of NH_4^+ from the reservoir. Along the river to reservoir transition, two primary clusters showed significant spatial autocorrelation for all variables, highlighting the sharp contrast between water quality within the river and reservoir.

5.1 Introduction

Managing the N cycle has been identified as one of the grand engineering challenges of the 21st century (Ellis, 2008). Anthropogenic disruption of the N cycle has led to an increase of N loading to aquatic ecosystems, primarily as NO_3^- (Vitousek et al., 1997; Galloway et al., 2008). Increased export of N from agricultural watersheds to rivers has led to large scale eutrophication in downstream or estuarine waters where N limits algal growth (Diaz, 2001; Conley et al., 2009), such as the Gulf of Mexico (e.g., McIsaac et al., 2001) and Chesapeake Bay (Rabalais et al., 2001). Due to the global importance of N, in-stream N processing and transport dynamics have been studied extensively (e.g., Mulholland et al., 2008), but primarily at base flow conditions. However, the majority of riverine N flux occurs during storm events, which may represent only 15% of the year but over 90% of the annual flux (Jawitz and Mitchell, 2011). Increased retention time from flooding can also alter biogeochemistry through contact with active surfaces at the sediment water

interface and development of redox gradients (Vidon et al., 2010). These processes can occur in various transient storage zones within river corridors including hyporheic zones, bank storage, and floodplains (Gomez-Velez et al., 2015; Harey and Gooseff, 2015; Covino, 2017).

Recent work has examined how different flow regimes and hydraulic properties affect riverine N dynamics, but in relatively unaltered systems (Hensley et al., 2015). Anthropogenic alterations of river networks such as dams or impoundments likely have a great impact on the fate and transport of N, particularly during storm events. While it is known that impoundments can impact hydrology (e.g., Graf, 2006), dissolved oxygen (e.g., Cushman, 1985), and fisheries (e.g., Ligon et al., 1985), little is known about how they affect the fate and transport of N. A key question that needs to be addressed is whether impoundments serve as a source or sink of N during storm events. During base flow, impoundments are more likely to serve as a sink of N due to increased residence time, denitrification, and assimilatory potential (Hensley et al., 2015), consistent with the findings of previous studies (e.g., David et al., 2006). Whereas during storm events, dams may serve as a source of N if the system is short-circuited, due to decreased residence time, denitrification, and assimilatory potential. In other words, reservoirs may transition from being transport limited systems to reaction limited systems during storm events (Covino, 2017). This notion is consistent with Gergel et al., 2005, who found that N loading increases during storm events but N removal rates decrease as recurrence interval increases. However, this study was entirely modeled and empirical data is needed to support this hypothesis and assess the uncertainty of simulations.

Another key challenge is understanding specifically how NO_3^-, the primary form of N from agricultural regions, is processed along river networks during storm events and how dams can affect various competing biogeochemical processes such as nitrification, mineralization, assimilation, and denitrification, often affected by stratification (Cottingham et al., 2015). This is challenging to address because monitoring NO_3^- across large systems is often very expensive and labor intensive. Traditionally, spatial sampling campaigns have been conducted by taking grab samples at various locations and analyzing results using statistical procedures (e.g., Singh et al., 2004; Juahir et al., 2011). However, this process is very labor intensive, time consuming, and still does not fully capture the spatial variability of a site (Van de Boger et al., 2012). An innovative technique for examining spatial water quality variability is by combining high frequency temporal sensors with a high speed sampling platform, such as a boat. Recent studies have employed variations of this technique to develop spatially contiguous estimates of water quality constituents (e.g., Crawford et al., 2014; Hensley et al., 2014; Kirchner et al., 2014). This approach provides an ideal platform for examining spatial variability of NO_3^- dynamics in rivers and studies have successfully utilized this technique to study riverine NO_3^- (Hensley et al., 2014; Kunz et al., 2017). Similar to N fluxes though, little research has evaluated spatial variability of NO_3^- dynamics along impounded portions of river corridors.

The overall goal of this research was to examine the spatial and temporal variability of N dynamics in a dam-impacted river across a storm hydrograph. Specific research objectives were to 1) determine whether a run-of-river dam served as a source or sink of N during a storm event and 2) quantitatively assess the longitudinal variability of surface water NO_3^- concentration across the river to reservoir gradients. Our first hypothesis was that the impoundment would serve as a source of N during the storm event due to increased N loading and decreased residence time. The second hypothesis was that surface water NO_3^- concentrations in the river and reservoir would be

statistically different at baseflow but statistically similar during the storm events. We tested these hypotheses through six sampling campaigns on a local run-of-river reservoir that is representative of those common throughout the U.S. Through these sampling campaigns, we were able to quantify the net export of N from the system as well as identify spatial and temporal patterns of biogeochemical processing of N.

5.2 Methods

5.2.1 Study Site

This study was conducted on the New River upstream and downstream of Claytor Dam, located in Pulaski County, Virginia (Figure 1). The New River is a sixth order river that flows northward 717 kilometers from Boone, North Carolina to Gauley Bridge, West Virginia, where it joins the Gauley River to form the Kanawha River (Spotila et al., 2015). Claytor Lake is located along the New River in the Valley and Ridge physiographic province and has an elevation of 563 meters above mean sea level (Boaze, 1972). The surrounding land cover types for the contributing area of the reach are primarily agricultural (29%) and forested (64%). The lake has a shoreline length of 161 km, surface area of 18.2 km^2, maximum volume of 0.28 km^3, an average depth of 15 m (Boaze, 1972; Palmer et al., 2005). Additionally, the lake has an average residence time of 33 days (Copeland, 1999) and is considered to be mildly eutrophic (Kohler et al., 1986).

Claytor Lake is impounded by Claytor Dam, a conventional run-of-river dam that is used primarily for hydroelectric energy production (Rosebery, 1951). The Appalachian Power Company operates the dam using conventional hydroelectric generation, releasing water from the bottom of the reservoir. An average daily discharge of 21.2 m^3/s is required, which the hydroelectric unit must operate at least 23 minutes every hour to meet. While there is no requirement for water levels, Appalachian Power Company generally maintains a reservoir surface elevation between 1845 ft (562.35 m) and 1846 ft (562.66 m) above sea level (Appalachian Power Company, 2011). Similar to other river-run dams, Claytor Dam has a spillway to release excess flows during periods of high flow. This means that during storm events, a combination of surface water and deep water is being released downstream from the dam.

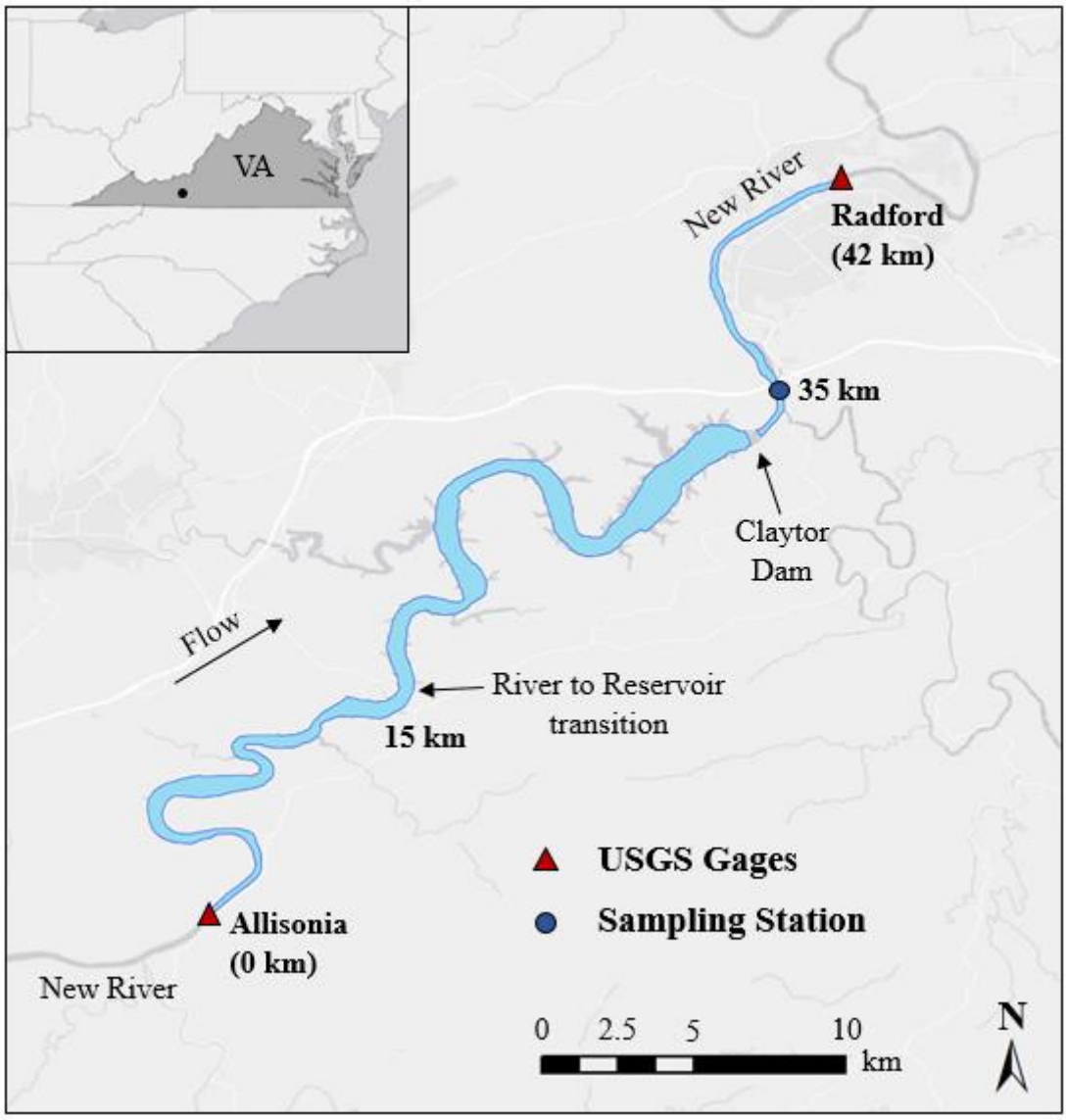

Figure 5-1. Site map of Claytor Lake. Red triangles indicate USGS stream gages and blue circles represent additional sampling locations.

5.2.2 Sampling campaigns and analysis

We conducted six sampling campaigns across a storm hydrograph to capture the spatiotemporal variability of N flux during a storm event. The first sampling campaign was conducted on September 25, 2017, prior to the storm event while the system was at base flow (Figure 5-2a). We then conducted five sampling campaigns across a storm event from October 24-October 28, 2017 (Figure 5-2b), at daily intervals along the receding limb of the storm hydrograph (Figure 2c-2d). For safety purposes, we did not conduct sampling during the rising limb of the storm hydrograph. We collected grab samples at a depth of 10 cm below the surface of the water at each of the three locations in Figure 5-1 to be analyzed for Total Dissolved Nitrogen (TDN), NO_3^-, NH_4^+, Dissolved Organic Carbon (DOC), and Phosphate (PO_4^{3-}). Samples for NO_3^-, NH_4^+, and PO_4^{3-} were collected

in 250 mL scintillation vials while TDN and DOC were collected in 250 mL glass amber vials with no head space. Grab samples were collected and filtered in situ through a 45 micron filter using a Geotech Peristaltic GeoPump. In addition to grab samples, field blanks were collected as a quality control measure. Following collection, samples were transported on ice to the Virginia Tech water quality laboratory and TDN and DOC samples were refrigerated while NO_3^-, NH_4^+, and PO_4^{3-} samples were frozen prior to analysis. Following each sampling campaign, TDN and DOC samples were immediately tested in the laboratory using a Shimadzu TOC-V CPH analyzer. Less than 28 days after sampling, NO_3^-, NH_4^+, and PO_4^{3-} were thawed and analyzed using a SEAL Analytical AA3 analyzer. Values of Nitrite (NO_2^-) were assumed to be zero and thus DON was calculated as the difference between TDN and the sum of NO_3^- and NH_4^+. Additionally, TDN and NO_3^- concentrations had nearly identical values ($R^2 = 0.94$) and thus NO_3^- was used as a proxy for TDN in subsequent analyses.

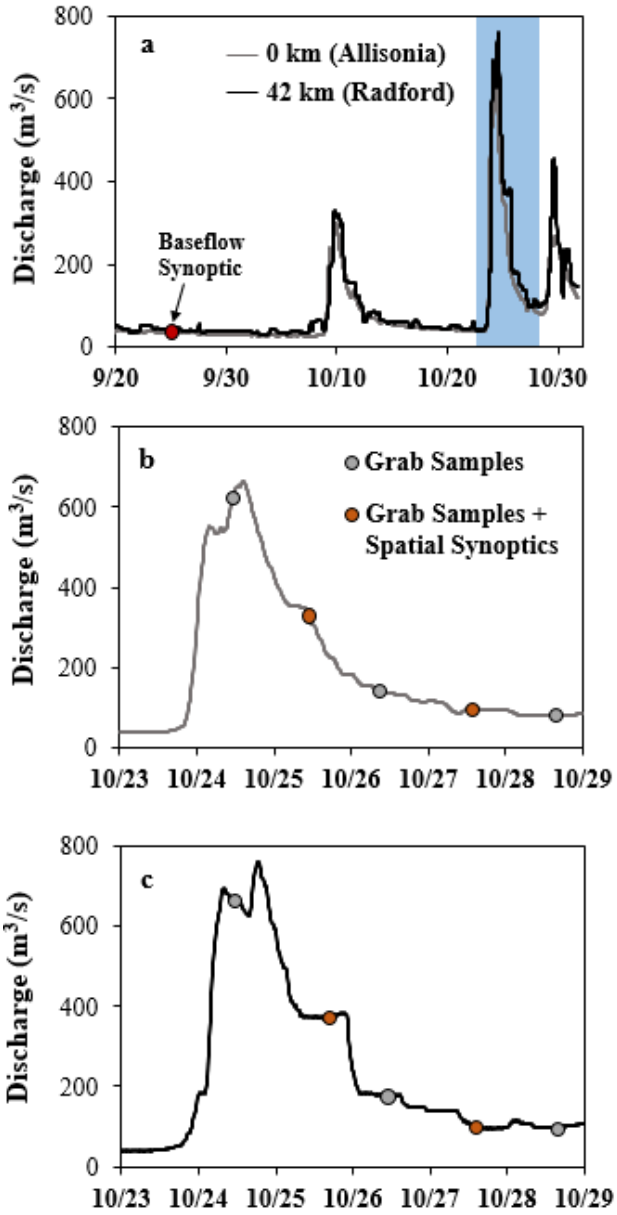

Figure 5-2. a) Long term hydrographs at the two USGS gages with the storm sampling period highlighted in light blue, b) storm hydrograph for the Allisonia USGS gage (0 km) with grab sample and spatial synoptic time points identified and d) storm hydrograph for the Radford USGS gage (42 km) with grab sample and spatial synoptic time points identified.

To quantify flux, discharge measurements were obtained at USGS gages 33 kilometers upstream of the dam (Allisonia, USGS 031688), 8 kilometers downstream of the dam (Radford, USGS 03171000), and continuous discharge estimates made at the dam (https://www.aep.com/environment/conservation/hydro). Grab samples were taken at each of the three sampling locations in Figure 5-1 and fluxes of each constituent were calculated for each cross section by multiplying discharge and solute concentrations. Flux values were then integrated across the falling limb of the storm hydrograph to determine the total mass (M) of each solute being transported at each location (Equation 1).

$$M = \int_0^{t=5} c(t) * Q(t)\, dt \quad (1)$$

where c(t) is the concentration at a given location as a function of time and Q(t) is the discharge at a given location as a function of time. Retention of each solute was then calculated as

$$R = \sum_{i=1}^{n} M_{u_i} - \sum_{i=1}^{n} M_{d_i} \quad (2)$$

where R is the retention mass, M_u is the mass at the Allisonia gage and M_d is the Mass at the outlet of Claytor Dam. We quantified fluxes of NO_3^-, NH_4+, DOC, and PO_4^{3-} at each site across the storm hydrograph to evaluate the effect of the impoundment on downstream transport of N. We then quantified total storm volume by integrating the storm hydrograph with respect to time (Equation 3).

$$V = \int_0^{t=5} Q(t)\, dt \quad (3)$$

Then, we divided this value by the maximum volume of the reservoir itself to calculate the percentage of storm volume compared to total volume within the system. Additionally, we utilized the USGS StreamStats application to determine the recurrence interval for the given flood event (https://streamstatsags.cr.usgs.gov/gagepages/html/03168000.htm). This information provided context as to how N dynamics in the system may differ for differing storm events.

5.2.3 Longitudinal Synoptics

To examine longitudinal variability along the reach, high-resolution longitudinal measurements of NO_3^-, DOC, temperature, dissolved oxygen (DO), conductivity, and turbidity were obtained using a high frequency sampling setup similar to that of Crawford et al. (2014). While moving downstream, water is pumped from 10 cm below the water surface through a S::CAN spectrometer and YSI data sonde while simultaneously geotagging data points with a Garmin Oregon 550T GPS unit. Data were collected at the highest frequency possible for each instrument: one-minute intervals for the S::CAN and 30-second intervals for the YSI. We chose to employ an Eularian

frame of reference so that we could feasibly measure the 33 km river-reservoir system and still spatially disaggregate NO_3^- estimates. The main caveat with this approach is that it cannot truly capture a snapshot of a given water body during time because water is continuously moving through the system. However, by moving the sampling platform at a velocity (~9 m/s) much greater than the streamflow velocity (~1 m/s), we were able to navigate the river from Allisonia to Claytor Dam in ~3 hours and get a reasonably accurate estimate of the spatial variability of NO_3^- and other water quality variables across the system. To validate field measurements, laboratory NO_3^- and DOC measurements were compared with in situ NO_3^- and DOC measurements.

5.2.4 Statistical analysis

To evaluate statistical differences between upstream and downstream solute fluxes, we examined flux data at 3 of our sites: the Allisonia USGS gage, outlet to Claytor Dam (35 km), and the Radford USGS gage. Normality of the data was evaluated using a Shapiro test and visual inspection of quantile-quantile plots. All of the datasets were found not to be normally distributed and thus non-parametric statistics were selected for further analyses. We examined statistical differences among the three flux datasets for each variable using a Kruskal-Wallis test and Wilcoxon Rank Sum tests for pairwise comparisons among groups (Hodges and Lehmann, 1963). P-values were then corrected for familywise error using a post hoc Bonferonni correction and statistical differences evaluated at an alpha value of 0.05. This portion of the statistical analysis was conducted using R statistical software (R core team, 2018).

We also examined the variability of the six longitudinal parameters using Anselin Local Moran's I statistical tests (Anselin, 1995). Moran's I is a measurement of spatial autocorrelation among samples, identifying spatial patterns and whether samples are clustered or randomly distributed. Moran's I can range from -1 to 1, with values close to 1 representing a high degree of clustering and values close to -1 a high degree of dispersion. The null hypothesis for Moran's test is that observations do not exhibit a spatial pattern. We selected this method to determine whether variables were random, dispersed, or clustered along the study reach, following a similar procedure as a previous study (Crawford et al., 2017). These analyses were conducted using the Spatial Statistics toolbox in ArcGIS 10.5.

5.3 Results

5.3.1 Temporal and spatial variability of fluxes

The storm event yielded a total volume of 1.05×10^8 m^3 of water over the course of the hydrograph, comprising 4.2% of the maximum volume of Claytor Lake. The storm event generated peak discharge values of 663 m^3/s and 762 m^3/s at the Allisonia and Radford USGS Gages, respectively (Figure 2b), representative of a 1-year storm event. Fluxes and concentrations of each solute increased during the storm event compared to baseflow and slowly receded back to baseline values over the course of the receding hydrograph limb (Figure 5-3). Total masses of N measured across the storm were 47.9 Mg at the Allisonia USGS gage, 46.3 Mg released from Claytor Dam, and 47.3 Mg measured at the Radford USGS gage. Thus, the impoundment served as a net sink of N as it retained 1.64 Mg of N, or 3.4% of the total mass of N moving through the system during the storm event. Similarly, the impoundment was a net sink of PO_4^{3-} and DOC, retaining 0.09 Mg

(12.7%) and 90.6 (25.6%) Mg, respectively. DON concentrations were found to be close to zero in all measurements and DON was therefore assumed to be negligible in this system. Among the three sites, average solute fluxes showed limited variation among sampling stations but solutes exhibited high temporal variability at each site due to flow weighted loading from the storm event (Table 5-1). Boxplots illustrate distributions and comparisons of each solute among the three sites (Figure 5-4). The only solute that exhibited statistical significant differences among sites was NH_4^+, with significantly greater fluxes occurring at both Claytor Dam and Radford compared to Allisonia.

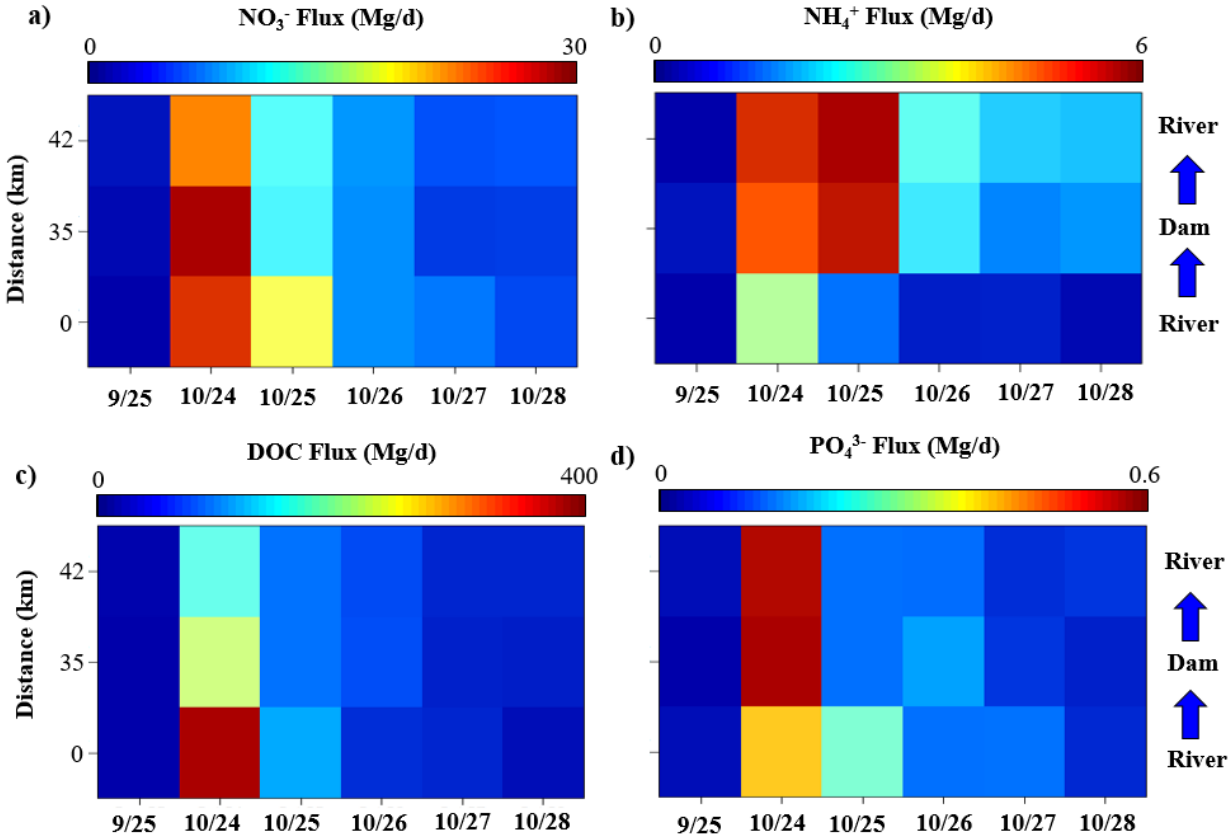

Figure 5-3. Color matrix plots illustrating spatiotemporal variability of fluxes of a) NO_3^- b) NH_4^+ c) DOC and d) PO_4^{3-}.

Table 5-1. Average solute fluxes (Mg/d) at the sampling locations across the storm event

Variable	Allisonia	Claytor	Radford
NO_3^-	9.86 ± 3.95	8.63 ± 4.08	8.22 ± 3.14
NH_4^+	0.56 ± 0.31	1.89 ± 0.67	2.09 ± 0.68
DOC	91.13 ± 59.36	62.28 ± 31.53	54.04 ± 22.08
PO_4^{3-}	0.15 ± 0.06	0.15 ± 0.08	0.14 ± 0.08

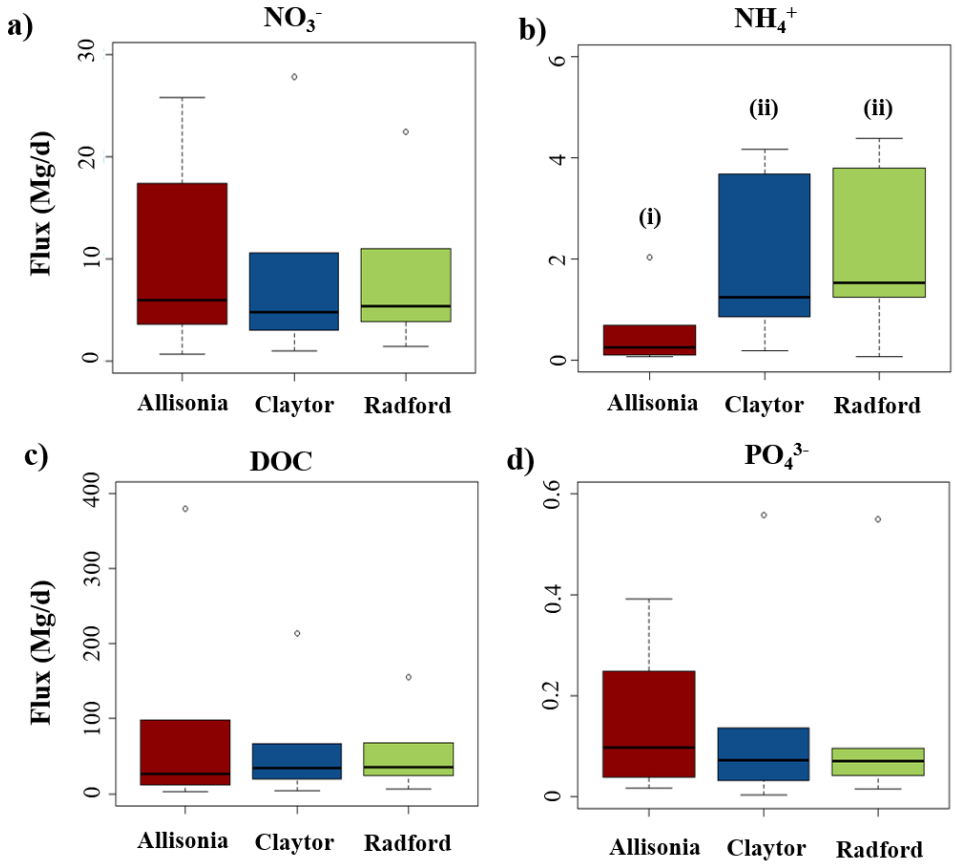

Figure 5-4. Boxplots of the distribution of fluxes of a) NO_3^- b) NH_4^+ c) DOC and d) PO_4^{3-}. Boxplots were created for samples taken at the Allisonia USGS gage, Claytor Dam, and the Radford USGS gage. Circle represent outliers and roman numerals signify statistical differences among groups.

5.3.2 Longitudinal variability of water quality

Longitudinal profiles taken above the dam for water quality variables showed significant differences in measurements along the transition from the New River to Claytor Lake (Figure 5-5). The first profile was conducted at baseflow on September 25, 2017 while the second and third profiles were conducted on the second and fourth day of storm sampling, October 25 and 27, 2017. We acquired 176, 170, and 157 measurements of Temperature, DO, Conductivity, and Turbidity at baseflow, on storm sampling day two, and on storm sampling day 4, respectively. Additionally, we acquired a total of 66, 67, and 67 measurements of NO_3^- and DOC at baseflow, on storm sampling day two, and on storm sampling day 4, respectively. Comparisons of NO_3^- produced an R^2 of 0.96 while comparisons of DOC yielded an R^2 of 0.98 and both regression lines fell close to the 1:1 line (Figure 5-6).

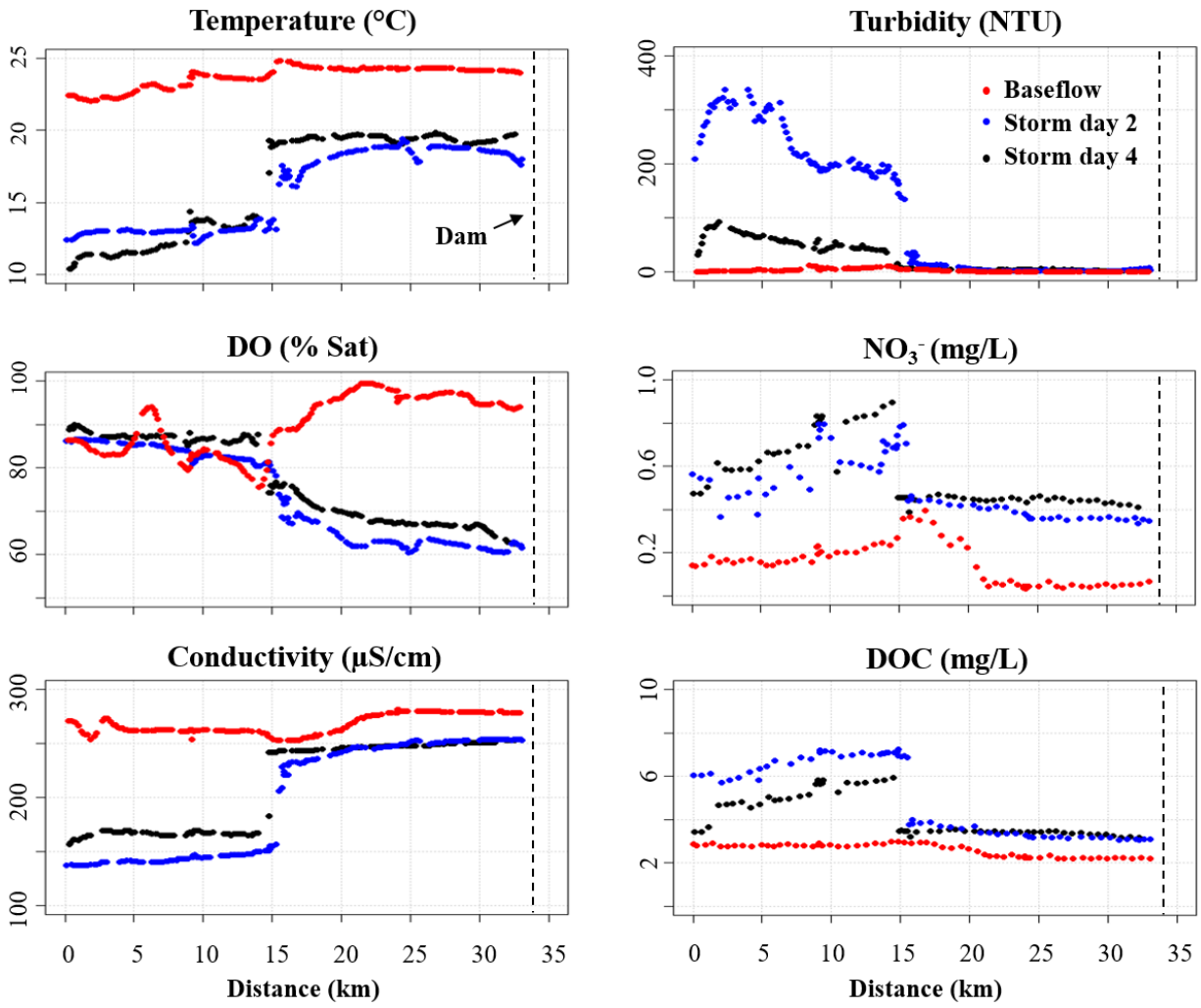

Figure 5-5. Longitudinal profiles of surface water Temperature, DO, Conductivity, Turbidity, NO_3^-, and DOC moving from the New River into Claytor Lake. Red points indicate baseflow measurements, blue points represent measurements on day 2 of storm sampling, and black points indicate measurements taken on day 4 of storm sampling. The river to lake transition occurs at a distance of 15 km downstream of the Allisonia USGS gage.

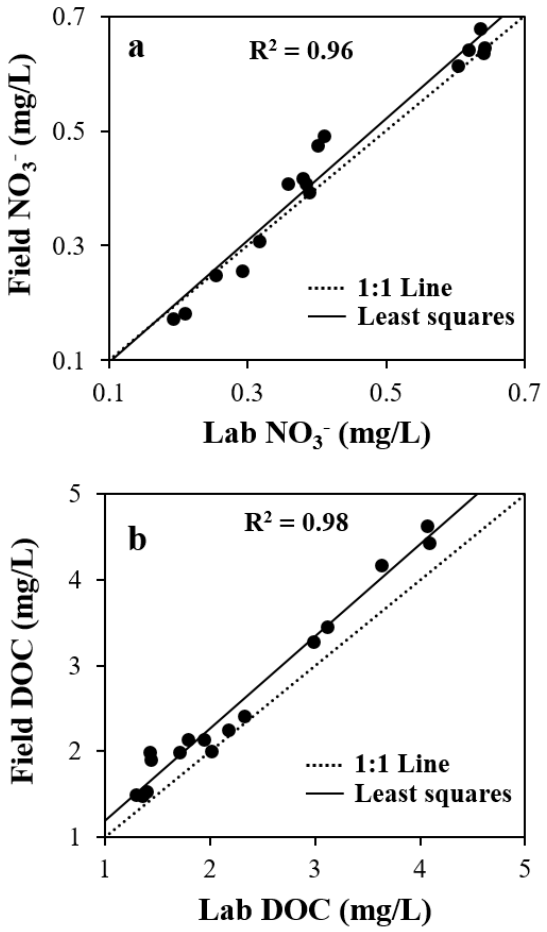

Figure 5-6. Validation plots of laboratory and in situ measurements of a) NO_3^- and b) DOC.

Moran's I tests showed significant autocorrelation among samples within the river and reservoir, with two primary clusters (Figure 5-7). All parameters showed statistically significant autocorrelation ($p < 0.05$) for all three sampling days. During baseflow, temperature and conductivity increased significantly moving downstream while turbidity, DOC, and NO_3^- all decreased significantly moving downstream. DO increased significantly moving downstream during baseflow but decreased significantly during both storm days. All of the variables had high Moran's index values for all three days (Table 5-2). The average Moran's Index was 0.95 among all of the measurements, indicating a high degree of clustering. Among the three sampling days, baseflow samples had an average Moran's index of 0.97, samples from day two of the storm event had an average Moran's index of 0.94, and samples from day four of the storm event an average Moran's index of 0.95. Across the three sampling synoptics, DO had the highest average Moran's index of 0.98 while NO_3^- had the lowest Moran's index of 0.91.

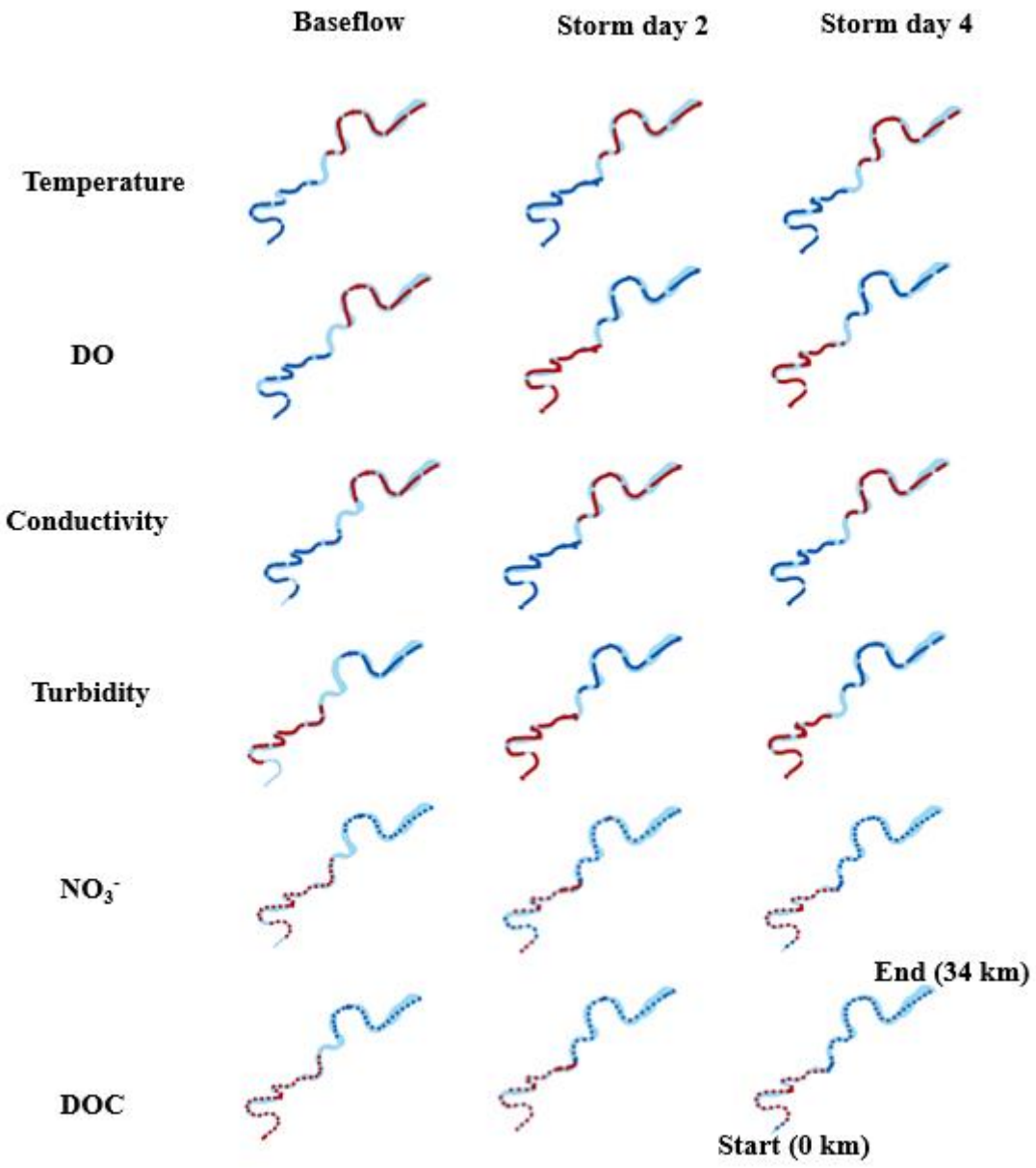

Figure 5-7. Results from Anselin Local Moran's I mapped clusters. Red points represent statistically significant clusters with high values, blue points represent statistically significant clusters with low values, and non significant points are omitted for clarity.

Table 5-2. Moran's Index for water quality variables across the river-reservoir reach for each sampling day

Variable	Baseflow	Storm day 2	Storm day 4
Temp	0.94	0.89	0.99
DO	0.97	0.99	0.99
Conductivity	0.98	0.99	0.95
Turbidity	0.96	0.91	0.99
NO_3^-	0.97	0.88	0.87
DOC	0.98	0.96	0.92

5.4 Discussion

5.4.1 Temporal and spatial variability of fluxes

As anticipated, fluxes of each solute were greater during the storm event than during baseflow. Stormflow only comprise 4.2% of the total volume in the reservoir, but solute fluxes all increased substantially during the storm event. In contrast to the original hypothesis, results illustrate that the impoundment served as a sink of net N flux during the storm event, retaining ~3.4% in comparison to the total flux of N loading from upstream. Additionally, N flux at the storm peak was greater downstream of the dam (27.9 Mg/d) than upstream (25.8 Mg/d), with the difference decreasing and eventually becoming greater upstream on the day following the hydrograph peak. This suggests that during a larger storm event (> 1-year recurrence interval), the impoundment may serve as a source instead of a sink. A key finding was that the impoundment served as a significant source of NH_4^+ during the storm event, with a ~200% increase in downstream NH_4^+ fluxes. Increased NH_4^+ fluxes suggest that N was either transformed from dissolved organic matter (DOM) to NH_4^+ through mineralization, from NO_3^- through dissimilatory nitrate reduction to ammonium (DNRA), or from a lack of nitrification.

5.4.2 Longitudinal variability of fluxes

Spatial synoptics identified the breakpoint where the New River transitions into Claytor Lake, approximately 15 km downstream of the Allisonia USGS gage and 18 km upstream of the dam. All of the variables measured in the top 10 cm of the water column changed significantly across this river to reservoir breakpoint. This was expected for temperature, conductivity, and DO, which are all a function of hydraulic residence time (Wetzel, 2001). Following the storm event, turbidity concentrations in the river increased from nearly zero to almost 350 NTU. However, within a km of crossing the river-reservoir breakpoint, turbidity dropped back to nearly zero due to increased residence time and settling as well as the plunge pool of water. While surface water NO_3^- concentrations decreased significantly across the river-reservoir transition during baseflow as expected, surface water NO_3^- concentrations also decreased significantly during the storm event as well. This NO_3^- removal could be explained by multiple processes such as biological assimilation, DNRA, and denitrification (Wall et. al., 2005; Barnes et al., 2012). However, longitudinal profiles of DO illustrate that surface water DO was significantly lower in the reservoir during the storm event. This suggests that deep, oxygen depleted water from the hypolimnion was being pushed up to the surface by the flood pulse. Because DO is necessary for nitrification to

occur (Stenstrom and Poduska, 1980), the low values of DO in the surface water likely limited the amount of nitrification that could occur. During storm events, this surface water is the primary source of water being transported downstream (over the dam's spillway). In contrast, water is primarily released from the bottom of the reservoir during baseflow. Because surface water that is This explains both increased downstream export of NH_4^+ and the decrease in NO_3^- in the reservoir during the storm event. However, additional data such as depth profiles and reservoir sediment samples would help to confirm these conclusions.

5.4.3. Future Recommendations

Several recommendations are suggested for future studies to improve upon this research. First, future research should examine the seasonal variability of N within dam-impacted systems. Seasonality likely plays a crucial role as denitrification rates are generally highest during spring and summer months (David et al., 2006). Additionally, studies should examine the diurnal variations of N in river-reservoir systems. This is particularly important as N species such as NO_3^- have the potential to exhibit diel variation similar to that of DO (Heffernan et al., 2010 ; Hensley and Cohen, 2016). Finally, depth profiles would help to quantify stratification of water quality parameters within the reservoir itself. In general, water within lakes and reservoirs are stratified with a division between warm, oxygen-rich epilimnion water, and cold, oxygen-depleted hypolimnion (Boehrer and Schultze, 2008). However, during storm events or in the winter, water within a reservoir can either mix with incoming water, can get pushed out of the reservoir by incoming water, or remain in place as incoming stormwater moves across the top. Understanding how this mixing occurs during storm events would be useful in further elucidating N dynamics within reservoirs.

5.5 Conclusions

The presented research provides a new perspective on the role that run-of-river dams play on the export of N in rivers. Findings from this research indicate that the studied dam slightly decreased the net export of N but significantly altered the composition of N constituents leaving the reservoir. Specifically, NO_3^- fluxes decreased slightly while NH_4^+ fluxes increased significantly. Ultimately, these fluxes of NH_4^+ only make up a small fraction of N export but could have implications for downstream ecosystems. Additionally, this research highlighted differences in denitrification between the river and reservoir, with a strong breakpoint occurring at the transition from river to reservoir. Overall, this study provides an improved understanding of N dynamics in dam-impacted rivers during storm events.

5.6 Acknowledgements

The authors would like to thank Dumitru Branisteanu, Allen Yoder, Laura Lehmann, and Asa Spiller for their assistance with instrumentation setup and troubleshooting. Additional thanks to Kelly Peeler and Lee Ellen Markley for their assistance with laboratory analyses.

5.7 References

Anselin, L. (1995). Local indicators of spatial association—LISA. *Geographical analysis*, *27*(2), 93-115.

Appalachian Power Company (2009). Claytor Project No. 739 Water Management Plan.

Barnes, R. T., Smith, R. L., and Aiken, G. R. (2012). Linkages between denitrification and dissolved organic matter quality, Boulder Creek watershed, Colorado. *Journal of Geophysical Research: Biogeosciences*, *117*(G1).

Boaze, J. L. (1972). Effects of landlocked alewife introduction on white bass and walleye populations, Claytor Lake, Virginia. Doctoral dissertation, Virginia Polytechnic Institute and State University.

Boehrer, B., and Schultze, M. (2008). Stratification of lakes. *Reviews of Geophysics*, *46*(2).

Cohen, M. J., Heffernan, J. B., Albertin, A., and Martin, J. B. (2012). Inference of riverine nitrogen processing from longitudinal and diel variation in dual nitrate isotopes. *Journal of Geophysical Research: Biogeosciences*, *117*(G1).

Conley, D. J., Paerl, H. W., Howarth, R. W., Boesch, D. F., Seitzinger, S. P., Karl, E., ... and Gene, E. (2009). Controlling eutrophication: nitrogen and phosphorus. *Science*, *123*, 1014-1015.

Copeland, J. R. (1999). Claytor Lake management report 1998. *F111R7, Final Report. Virginia Department of Game and Inland Fisheries, Richmond*.

Cottingham, K. L., Ewing, H. A., Greer, M. L., Carey, C. C., & Weathers, K. C. (2015). Cyanobacteria as biological drivers of lake nitrogen and phosphorus cycling. *Ecosphere*, *6*(1), 1-19.

Covino, T. (2017). Hydrologic connectivity as a framework for understanding biogeochemical flux through watersheds and along fluvial networks. *Geomorphology*, *277*, 133-144.

Crawford, J. T., Loken, L. C., Casson, N. J., Smith, C., Stone, A. G., and Winslow, L. A. (2014). High-speed limnology: Using advanced sensors to investigate spatial variability in biogeochemistry and hydrology. *Environmental Science & Technology*, *49*(1), 442-450.

Crawford, J. T., Loken, L. C., West, W. E., Crary, B., Spawn, S. A., Gubbins, N., ... & Stanley, E. H. (2017). Spatial heterogeneity of within-stream methane concentrations. *Journal of Geophysical Research: Biogeosciences*, *122*(5), 1036-1048.

Cushman, R. M. (1985). Review of ecological effects of rapidly varying flows downstream from hydroelectric facilities. *North American journal of fisheries Management*, *5*(3A), 330-339.

David, M. B., Wall, L. G., Royer, T. V., and Tank, J. L. (2006). Denitrification and the nitrogen budget of a reservoir in an agricultural landscape. *Ecological Applications*, *16*(6), 2177-2190.

Diaz, R. J. (2001). Overview of hypoxia around the world. *Journal of Environmental Quality*, *30*(2), 275-281.

Ellis, G. (2009). Grand challenges for engineering. *IEEE Engineering Management Review*, *1*(37), 3.

Galloway, J. N., Townsend, A. R., Erisman, J. W., Bekunda, M., Cai, Z., Freney, J. R., ... and Sutton, M. A. (2008). Transformation of the nitrogen cycle: recent trends, questions, and potential solutions. *Science*, *320*(5878), 889-892.

Gergel, S. E., Carpenter, S. R., and Stanley, E. H. (2005). Do dams and levees impact nitrogen cycling? Simulating the effects of flood alterations on floodplain denitrification. *Global Change Biology*, *11*(8), 1352-1367.

Gomez-Velez, J. D., Harvey, J. W., Cardenas, M. B., & Kiel, B. (2015). Denitrification in the Mississippi River network controlled by flow through river bedforms. *Nature Geoscience*, *8*(12), 941-945.

Graf, W. L. (1999). Dam nation: A geographic census of American dams and their large-scale hydrologic impacts. *Water resources research*, *35*(4), 1305-1311.

Graf, W. L. (2006). Downstream hydrologic and geomorphic effects of large dams on American rivers. *Geomorphology*, *79*(3), 336-360.

Harvey, J., and Gooseff, M. (2015). River corridor science: Hydrologic exchange and ecological consequences from bedforms to basins. *Water Resources Research*, *51*(9), 6893-6922.

Heffernan, J. B., Cohen, M. J., Frazer, T. K., Thomas, R. G., Rayfield, T. J., Gulley, J., ... and Graham, W. D. (2010). Hydrologic and biotic influences on nitrate removal in a subtropical spring-fed river. *Limnology and Oceanography*, *55*(1), 249-263.

Hensley, R. T., and Cohen, M. J. (2016). On the emergence of diel solute signals in flowing waters. *Water Resources Research*, *52*(2), 759-772.

Hensley, R. T., Cohen, M. J., and Korhnak, L. V. (2014). Inferring nitrogen removal in large rivers from high-resolution longitudinal profiling. *Limnology and Oceanography*, *59*(4), 1152-1170.

Hensley, R. T., Cohen, M. J., and Korhnak, L. V. (2015). Hydraulic effects on nitrogen removal in a tidal spring-fed river. *Water Resources Research*, *51*(3), 1443-1456.

Hodges Jr, J. L., and Lehmann, E. L. (1963). Estimates of location based on rank tests. *The Annals of Mathematical Statistics*, 598-611.

Jawitz, J. W., and Mitchell, J. (2011). Temporal inequality in catchment discharge and solute export. *Water Resources Research*, *47*(10).

Juahir, H., Zain, S. M., Yusoff, M. K., Hanidza, T. I. T., Armi, A. S. M., Toriman, M. E., and Mokhtar, M. (2011). Spatial water quality assessment of Langat River Basin (Malaysia) using environmetric techniques. *Environmental Monitoring and Assessment*, *173*(1), 625-641.

Kirchner, J. W., Feng, X., Neal, C., and Robson, A. J. (2004). The fine structure of water-quality dynamics: the (high-frequency) wave of the future. *Hydrological Processes*, *18*(7), 1353-1359.

Kohler, C. C., Ney, J. J., and Kelso, W. E. (1986). Filling the void: development of a pelagic fishery and its consequences to littoral fishes in a Virginia mainstream reservoir. *Reservoir fisheries management: strategies for the 80s*, 166-177.

Kunz, J. V., Hensley, R., Brase, L., Borchardt, D., and Rode, M. (2017). High frequency measurements of reach scale nitrogen uptake in a fourth order river with contrasting hydromorphology and variable water chemistry (Weiße Elster, Germany). *Water Resources Research*, *53*(1), 328-343.

Ligon, F. K., Dietrich, W. E., and Trush, W. J. (1995). Downstream ecological effects of dams. *BioScience*, *45*(3), 183-192.

McIsaac, G. F., David, M. B., Gertner, G. Z., and Goolsby, D. A. (2001). Eutrophication: Nitrate flux in the Mississippi river. *Nature*, *414*(6860), 166-167.

Mulholland, P. J., Helton, A. M., Poole, G. C., Hall, R. O., Hamilton, S. K., Peterson, B. J., ... and Dodds, W. K. (2008). Stream denitrification across biomes and its response to anthropogenic nitrate loading. *Nature*, *452*(7184), 202-205.

Palmer, G. C., Murphy, B. R., & Hallerman, E. M. (2005). Movements of walleyes in Claytor Lake and the upper New River, Virginia, indicate distinct lake and river populations. *North American Journal of Fisheries Management*, *25*(4), 1448-1455.

Rabalais, N. N., Turner, R. E., and Wiseman, W. J. (2001). Hypoxia in the Gulf of Mexico. *Journal of Environmental Quality*, *30*(2), 320-329.

R Core Team. (2013). R: A language and environment for statistical computing.

Rode, M., Wade, A. J., Cohen, M. J., Hensley, R. T., Bowes, M. J., Kirchner, J. W., ... and Skeffington, R. A. (2016). Sensors in the stream: the high-frequency wave of the present. *Environmental Science and Technology*,

Rosebery, D. A. (1951). Fishery management of Claytor Lake, an impoundment on the New River in Virginia. *Transactions of the American Fisheries Society*, *80*(1), 194-209.

Singh, K. P., Malik, A., Mohan, D., and Sinha, S. (2004). Multivariate statistical techniques for the evaluation of spatial and temporal variations in water quality of Gomti River (India)—a case study. *Water Research*, *38*(18), 3980-3992.

Smith, S. V., Renwick, W. H., Bartley, J. D., and Buddemeier, R. W. (2002). Distribution and significance of small, artificial water bodies across the United States landscape. *Science of the Total Environment*, *299*(1-3), 21-36.

Spotila, J. A., Moskey, K. A., and Prince, P. S. (2015). Geologic controls on bedrock channel width in large, slowly-eroding catchments: Case study of the New River in eastern North America. *Geomorphology*, *230*, 51-63.

Stenstrom, M. K., & Poduska, R. A. (1980). The effect of dissolved oxygen concentration on nitrification. *Water Research*, *14*(6), 643-649.

Tong, S. T., and Chen, W. (2002). Modeling the relationship between land use and surface water quality. *Journal of Environmental Management*, *66*(4), 377-393.

Turner, P. A., Griffis, T. J., Baker, J. M., Lee, X., Crawford, J. T., Loken, L. C., and Venterea, R. T. (2016). Regional-scale controls on dissolved nitrous oxide in the Upper Mississippi River. *Geophysical Research Letters*, *43*(9), 4400-4407.

Van de Bogert, M. C., Bade, D. L., Carpenter, S. R., Cole, J. J., Pace, M. L., Hanson, P. C., and Langman, O. C. (2012). Spatial heterogeneity strongly affects estimates of ecosystem metabolism in two north temperate lakes. *Limnology and Oceanography*, *57*(6), 1689.

Vidon, P., Allan, C., Burns, D., Duval, T. P., Gurwick, N., Inamdar, S., Lowrance, R., Okay, J., Scott, D., and Sebestyen, S. (2010). Hot spots and hot moments in riparian zones: potential for improved water quality management. *JAWRA Journal of the American Water Resources Association*, *46*(2), 278-298.

Vitousek, P. M., Aber, J. D., Howarth, R. W., Likens, G. E., Matson, P. A., Schindler, D. W., ... and Tilman, D. G. (1997). Human alteration of the global nitrogen cycle: sources and consequences. *Ecological applications*, *7*(3), 737-750.

Wall, L. G., Tank, J. L., Royer, T. V., and Bernot, M. J. (2005). Spatial and temporal variability in sediment denitrification within an agriculturally influenced reservoir. *Biogeochemistry*, *76*(1), 85-111.

Wetzel, R. G. (2001). *Limnology: lake and river ecosystems*. Saunders College Publishing, Philadelphia, Pennsylvania.

CHAPTER 6. MODELING THE CUMULATIVE EFFECTS OF SMALL IMPOUNDMENTS ON DOWNSTREAM FLOODPLAIN CONNECTIVITY

Tyler A. Keys, Connor O. Brogan, Robert W. Burgholzer, Joseph Kleiner, and Durelle T. Scott

Submission: Planned May 2018
To: *Journal of Hydrologic Engineering*
Status: Draft

Abstract

The implementation and management of impoundments plays an integral role in sustainable water resources management. Impoundments mitigate flooding, improve water quality, and reduce sediment loading to streams and rivers. While the effects of individual impoundments on downstream flooding has been well studied, the cumulative effects of impoundments on downstream flow alteration have been largely neglected. We examined this issue by modeling the impact of impoundments in a pilot watershed within the Commonwealth of Virginia. To do this, we utilized a web-based modeling framework for the state of Virginia that utilizes the Chesapeake Bay Watershed Model and allows users to add impoundments to the model along a given stream or river reach. Due to limited field data, impoundment bathymetry and outlet structure designs were estimated based on state design standards and remotely sensed data. The model was validated by comparing modeled discharge values at the outlet of the watershed to a US Geological Survey stream gage at the watershed outlet. We then conducted simulations of the watershed with and without impoundments from 1984-2005, and examined the results on downstream discharge. Then, we utilized impoundment outflow hydrographs in conjunction with a static inundation model to quantify floodplain connectivity. Results illustrate that incorporating impoundments to the river network decreased both downstream flood peaks and floodplain inundation area and volume. Findings from this study have implications for floodplain management and highlight the need for higher resolution watershed modeling.

6.1 Introduction

Water demand is projected to grow substantially over the coming decades to meet the needs of an increasing global population (Ercin and Hoekstra, 2014). In the midst of increasing water demand, sustainable management of river networks presents a major challenge, with a focus on the construction and management of impoundments. Impoundments are features that retain water for a variety of purposes including hydroelectric power generation, flood control, irrigation, consumption, and recreation (Brown et al., 2009). These benefits have been widely acknowledged, but impoundments can also cause serious environmental consequences, particularly in downstream portions of the river corridor (Graf, 2006; McCartney, 2009). Environmental impacts are taken into consideration when permitting and operating large impoundments, but small impoundments

are often undocumented and cumulative environmental impacts are neglected (Berg et al., 2016). Studies have examined the impacts of small impoundments along river networks on a variety of downstream organisms such as macroinvertebrates (e.g., Mackay and Waters, 1986; Adams, 2013; Mbaka and Mwaniki, 2015), amphibians (e.g., Kirchberg et al., 2016), and fisheries (e.g., Gabelhouse, 1984; Guy and Willis, 1991), as well as other in-stream metrics such as leaf litter composition (Mbaka and Schäfer, 2015) and thermal regime (Maheu et al., 2016). However, another important yet relatively unexplored question is how small impoundments cumulatively impact downstream peak flows and floodplain connectivity. It has been suggested that the total volume of these small impoundments may actually be greater than the total volume of large reservoirs (Sahagian, 2000). Furthermore, previous studies (e.g., Chaney et al., 2012) have suggested that the cumulative impacts of small impoundments on downstream hydrology may be quite substantial compared to those of large impoundments. In regions of increasing population and water demand, such as the Commonwealth of Virginia, impoundments play a crucial role in addressing the challenge of producing energy while providing food and water security.

There are currently over 73,000 impoundments across the Commonwealth of Virginia ranging from 0.25 to 100 acres in size (Scott et al., in prep). However, only 52 of the largest impoundments are currently permitted and incorporated into Virginia's online water use and withdrawal system, VAHydro. This existing framework provides a unique opportunity for studying the cumulative impacts of small impoundments across Virginia. The fundamental question is whether or not small impoundments, which are not yet incorporated into the VAHydro model, have a cumulative impact on downstream discharge and floodplain connectivity. Previous studies have suggested that impoundments alter the downstream flow regime in impounded rivers (e.g., Eyler et al., 2016). However, most of these studies neglect the fact that impacts along a river network are cumulative. Based on this concept, we hypothesize that reduction in peak flows will likely increase moving downstream as stream order increases. Another key question that has not been extensively studied is how small impoundments impact downstream floodplain inundation dynamics. This question is of great importance as floodplains provide a variety of critical ecosystem services such as habitat for wildlife (Harding et al., 1998), peak flood reduction (Sheaffer et al., 2002), and reactive solute processing (Scott et al., 2014). Previous studies (e.g., Kingsford, 2000; Hupp et al., 2015) suggest that impoundments have an impact on downstream ecosystem services, particularly pollutant and sediment transport processes. Due to the interconnectedness of floodplain connectivity and ecosystem services, quantifying alterations that impoundments have on floodplain connectivity can be a useful indicator of the degree to which ecosystem services are altered.

The overall goal of this research was to quantify the cumulative impacts that impoundments have on downstream peak flows and river-floodplain connectivity. Specific research objectives were to 1) determine whether or not small impoundments have a cumulative affect on downstream peak flow rates and 2) quantify the impacts of small impoundments on downstream inundation extent and volume. The main hypothesis was that incorporating impoundments into an existing modeling framework would result in decreased downstream discharge and floodplain inundation. We tested this hypothesis on a pilot watershed to gain a preliminary understanding of the cumulative effects of impoundments at the watershed scale.

6.2 Methods

6.2.1 Study Site

The commonwealth of Virginia provides a unique location for this study as it only contains two natural lakes but has over 73,000 impoundments. We chose to specifically examine the Difficult Run Watershed, located within the Piedmont physiographic province as well as the Chesapeake Bay and Potomac River Watersheds. This watershed was selected due to the number of impoundments located within its boundaries and because it contains a US Geological Survey (USGS) stream gage at the watershed outlet (Figure 6-1). The watershed has a total drainage area of 151 km^2 and a mean annual discharge of approximately 1.76 m^3/s at the watershed outlet (Hupp et al., 2013). Elevation within the watershed ranges from 20 to 157 m above sea mean sea level. Landcover for the watershed is 77% urban, 17% forested, and 6% agricultural. The watershed receives approximately 105 cm of rainfall and 56 cm of snowfall per year. Here, we have examined the cumulative effects of 13 impoundments within the Difficult Run Watershed located along the river network.

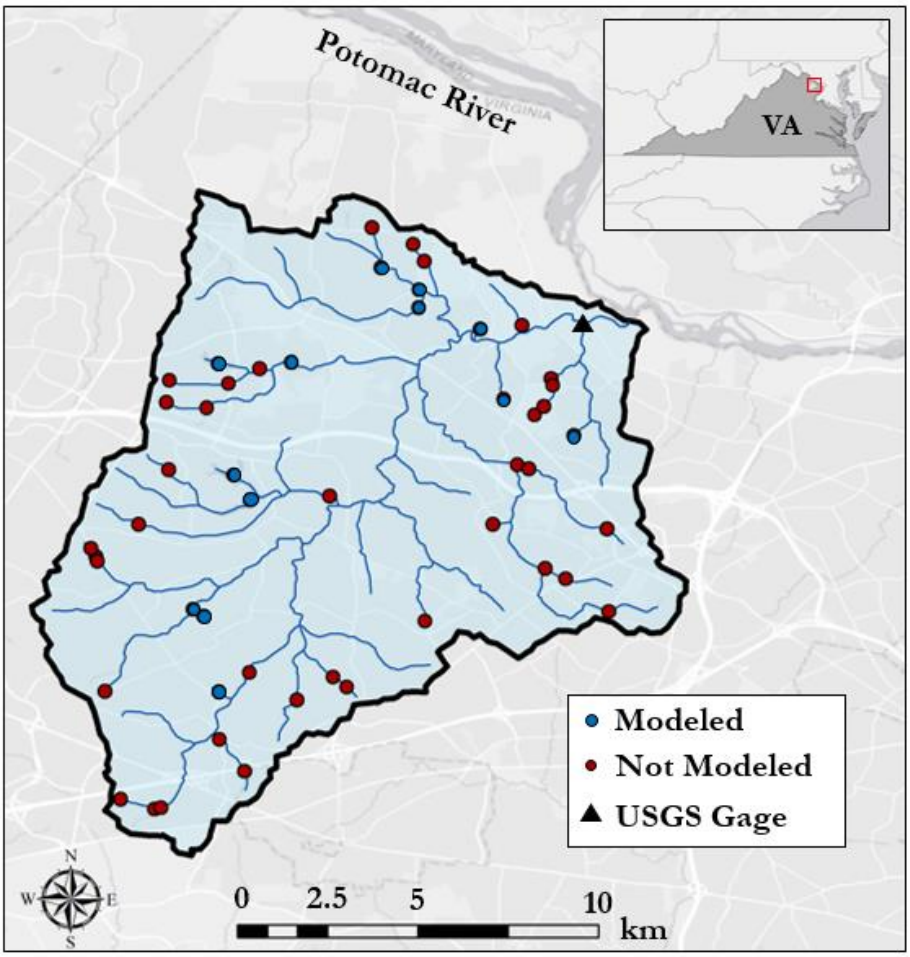

Figure 6-1. Map of the Difficult Run Watershed. Red circles indicate impoundments and the black triangle represents the USGS streamflow gage at the watershed outlet.

6.2.2 Modeling Approach

For hydrologic modeling, we utilized the VAHydro watershed modeling system to simulate the impacts that small impoundments have on downstream river discharge and floodplain connectivity. VAHydro is a web-based hydrologic modeling framework for the entire state of Virginia that is maintained by the Virginia Department of Environmental Quality. VAHydro utilizes the Chesapeake Bay Program (CBP) Phase 5 Watershed Model and is calibrated with United States Geological Survey (USGS) stream gage data. The model utilizes overland flow from the CBP watershed model which is routed through the selected river reaches using Muskingum hydrologic routing, a storage-based routing technique commonly used for river routing (Gill, 1978). Channel bathymetry for routing flow within VAHydro is assumed to be trapezoidal, a common assumption when channel bathymetry is unknown (Moglen, 2015).

The VAHydro interface allows users to add impoundments to specific geographic locations on the river network and edit the physical characteristics of the impoundments. Similar to other modeling frameworks, impoundments can be linked up as nodes within the VAHydro system. This allows for a unique opportunity to assess cumulative impacts within the selected watershed. Impoundments within the model use a simple water balance with runoff as the primary inflow and evapotranspiration, water withdrawals, and impoundment outflow as the primary outflows. The main user inputs for impoundment parameterization include outlet structure characteristics and pond bathymetry. Here, outlet structures were designed using National Resources Conservation Services (NRCS) guidelines (NRCS, 2011). Due to the variability of outlet structures in this watershed (Figure 6-2), we designed a generalized multi-stage riser outlet structure. An orifice was designed for the 10-year storm event and an emergency weir was designed for the 100-year storm event. Physical characteristics of each outlet structure were entered directly into the model and standard orifice and weir equations were used to calculate outflow. We then ran the entire 21-year model simulation to ensure that no overtopping occurred for each designed outlet structure. If overtopping occurred, we iteratively increased the outlet structure size to stop overtopping while also minimizing area. Impoundment bathymetry was estimated using a combination of approaches. First, data from the NID database was utilized to estimate stage-storage characteristics for regulated impoundments. For undocumented impoundments, surface area was obtained from the National Hydrography Dataset Plus (NHDPlus) and bathymetry was estimated by assuming 4:1 side slopes from the surface to the bottom of the impoundment, as suggested by the Virginia Stormwater design manual (Virginia D.C.R., 2010). Floodplain geometry was estimated based on a digital elevation model (DEM) of the surrounding landscape.

Figure 6-2. Examples of differing outlet structures for four of the impoundments within the watershed.

6.2.3 Hydrologic Analysis

Model simulations were run both with and without impoundments incorporated to quantify outflow hydrographs. Outflow hydrographs were simulated for the watershed outlet as well as each of the 13 impoundments. Model simulations were conducted using a 1 hour computational time step. The model was validated by comparing the long term hydrograph (1984-2005) at the watershed outlet aggregated to daily mean flow with the long term hydrograph at the USGS gage for Difficult Run near Great Falls, Virginia (USGS 01646000). The model fit was evaluated using the Nash-Sutcliffe Efficiency (NSE) metric (Equation 1):

$$NSE = 1 - \frac{\sum_{i=1}^{n}(Q_i^{obs} - Q_i^{sim})^2}{\sum_{i=1}^{n}(Q_i^{obs} - \overline{Q_{obs}})^2} \quad (1)$$

where Q_{obs} is the discharge observed at the USGS gage and Q_{sim} is the modeled discharge. The model was run both with and without impoundments incorporated to evaluate the overall model fit. Discharge values were then integrated across the entire 21 year record to determine the total volume of water moving leaving the watershed with and without impoundments incorporated. Hydrographs with and without impoundments incorporated were compared across the storm event and during annual peak flows. Additionally, low flow metrics were used to quantify the cumulative effects of impoundments on downstream low flows. Specifically, we calculated the median of minimum flows in the month of August, also known as August Low Flow (ALF), and the lowest 7-day average flow occurring once every 10 years (7Q10).

6.2.4 Floodplain Analysis

Floodplain dynamics were assessed using impoundment outflow hydrographs in conjunction with a static inundation model for the downstream portion of the river corridor. Floodplain geometry was acquired from the USGS Earth Explorer's freely available 3 meter resolution Light Detection and Ranging (LiDAR) derived DEM for the Difficult Run Watershed. Channel bathymetry was estimated by using inverse distance weighting (IDW) interpolation based on floodplain geometry and the stream's centerline, a procedure illustrated by previous work (Jones et al., 2015; Keys et al., 2016). For each downstream reach (1 kilometer downstream of each impoundment), a static inundation model was used to simulate floodplain inundation area and volume as a function of stage (Figure 6-3). This approach does not take fluid dynamics into consideration, making it much simpler than common process-based hydrodynamic models such as HEC-RAS. This approach was selected because it is easier to run at a large scale in comparison to a process-based model. Outflow hydrographs for each impoundment were converted to stage hydrographs using a composite Manning's equation approach. Stream channel bathymetry was estimated as described above and floodplain geometry was estimated using the DEM for the reach. An assumed Manning's n value of 0.03 was used for the channel while a value of 0.05 was used for the floodplain, based on general guidelines (Arcement and Schneider, 1989). A function solver was then used to calculate stage for each discharge value. Using the stage-area-volume relationships from the static inundation model, stage hydrographs were then converted to inundation area and volume hydrographs for the stream reach downstream of each impoundment. Similar to outflow hydrographs, floodplain inundation area and volume time series were computed with and without impoundments incorporated. These surface area and volume hydrographs were summed across the watershed with and without impoundments incorporated to determine cumulative effects as done with discharge hydrographs. All analyses were conducted using R statistical software (R Core team, 2017).

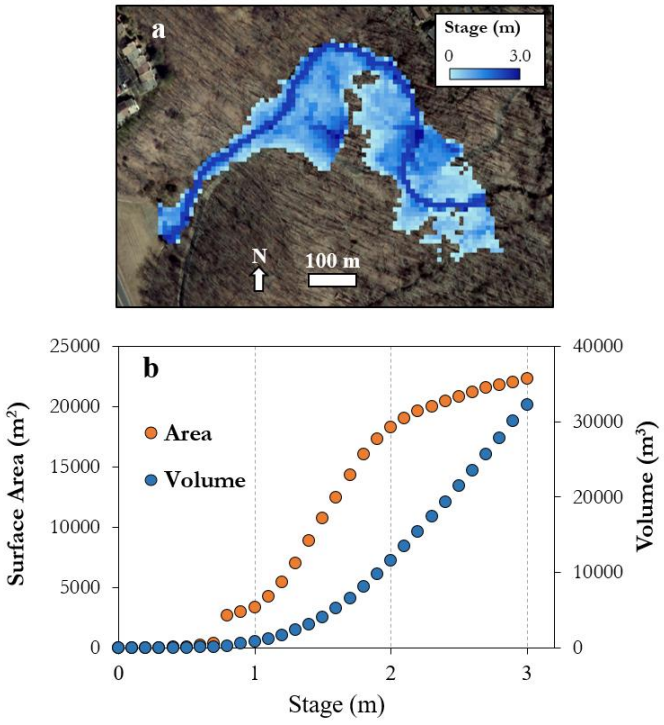

Figure 6-3. a) Aerial image of floodplain inundation for a 1 km stream reach downstream of the Lake Audubon impoundment and b) output from the static inundation model showing the stage-area-volume curves for Lake Audubon.

6.3 Results

6.3.1 Hydrologic Modeling

Model simulations showed a good fit when compared to observed data from the USGS gage at the watershed outlet (Figure 6-4), resulting in an R^2 of 0.77 NSE of 0.7. Yearly average mean daily flow and maximum daily flow ranged from year to year (Table 6-1). Cumulatively, incorporating impoundments into the model resulted in an overall reduction in average daily discharge and maximum discharge values for each of the 21 years in the simulation. Over the entire simulation, the average reduction in discharge was 3.1 L/s when incorporating impoundments. However, the average reduction in annual peak flow rates was 23.27 m^3/s when incorporating impoundments into the model. In contrast, adding impoundments to the model increased the value of low flows in the system. Values for ALF were 50.4 L/s and 65.7 L/s without and with impoundments, respectively, representing a 30% increase. Values for 7Q10 were 4.81 L/s and 4.25 L/s without and with impoundments, respectively, representing a 12% increase.

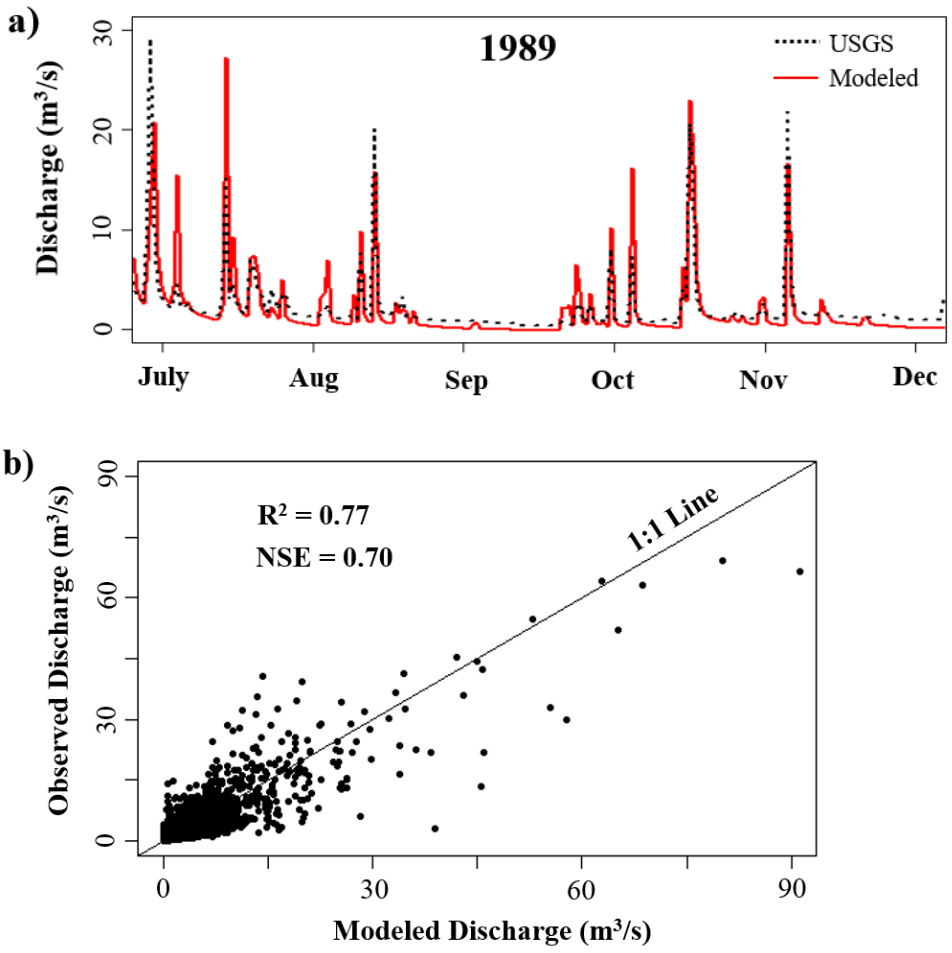

Figure 6-4. a) Model validation results illustrating the observed hydrograph from the USGS gage at the watershed outlet and modeled hydrographs with and without impoundments incorporated for a six month period in 1989 and b) 1:1 plot comparing modeled and observed discharge.

Table 6-1. Average mean daily discharge and maximum discharge values for each year modeled without and with impoundments incorporated.

Year	Average Discharge (L/s)		Maximum Discharge (m^3/s)	
	Without	With	Without	With
1984	1460	1460	46.02	37.94
1985	1120	1120	85.70	74.35
1986	1140	1140	85.96	77.14
1987	1490	1490	53.90	47.69
1988	1330	1320	61.73	51.69
1989	2000	1990	438.25	360.98
1990	2110	2110	83.86	79.17
1991	1260	1260	97.97	86.46
1992	1610	1600	105.37	87.19
1993	2500	2490	435.00	361.89
1994	2240	2240	94.70	84.94
1995	1350	1350	105.78	87.22
1996	3290	3300	333.54	278.76
1997	1560	1560	53.66	45.66
1998	2140	2140	166.06	142.58
1999	1580	1570	67.14	60.53
2000	1290	1290	40.07	33.77
2001	1380	1380	132.54	109.14
2002	1100	1100	35.63	30.84
2003	4050	4030	289.93	247.90
2004	1700	1700	54.84	46.23
2005	2290	2280	438.25	361.89
Average	1816	1813	150.27	127.00

6.3.2 Floodplain Modeling

Addition of impoundments to the model decreased floodplain inundation surface area and volume downstream of each impoundment. Overall, addition of impoundments to the model showed decreased floodplain connectivity over the course of the 21 year simulation (Figure 6-5). Across the watershed, the total cumulative change in flooded surface area downstream of the modeled impoundments was 2090 m^2/km/day and the total cumulative change in floodplain volume was

4500 m^3/km/day. The average difference between floodplain inundation area and volume with and without impoundments was 83 m^2 and 179 m^3, respectively.

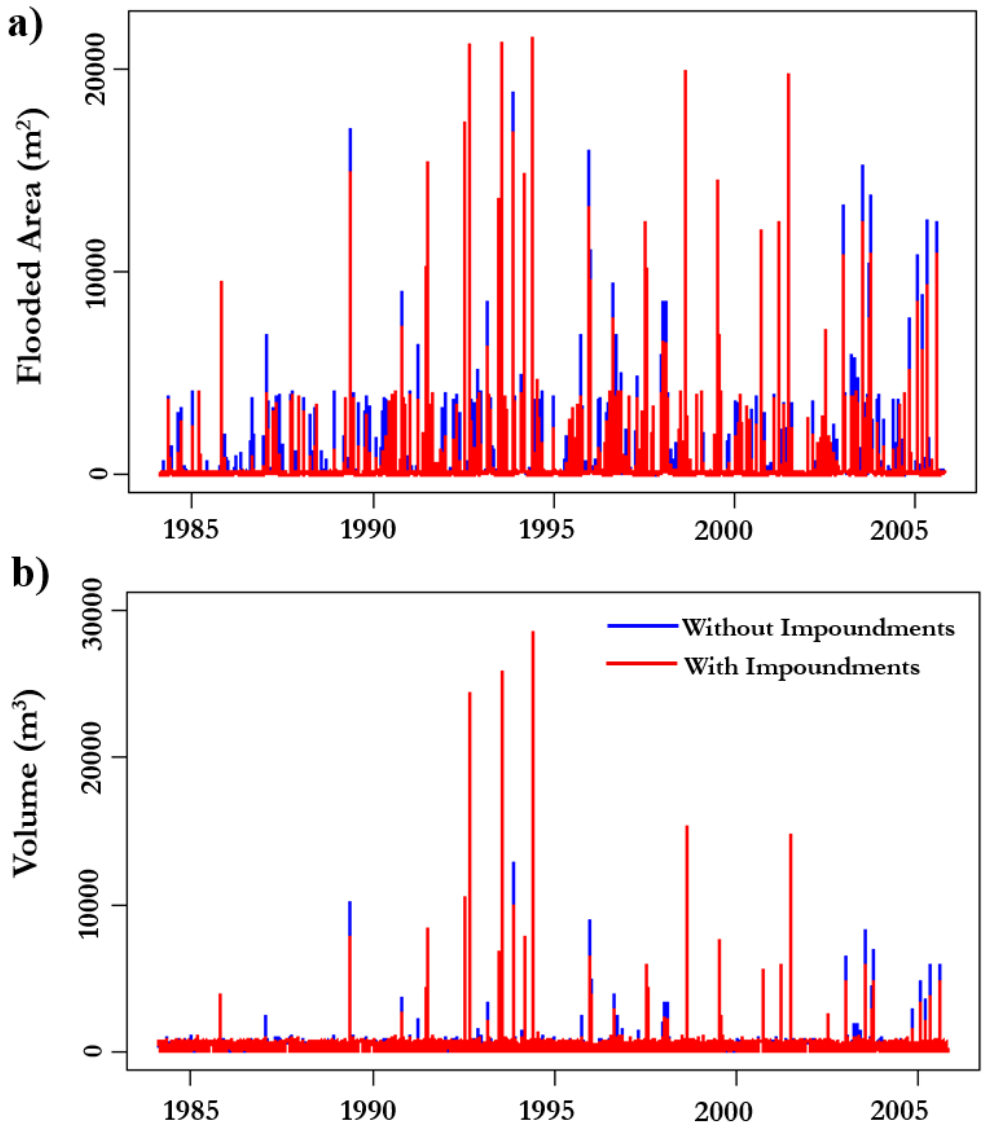

Figure 6-5. Plot of hydrographs for a) cumulative floodplain inundation area and b) cumulative floodplain volume

6.4 Discussion

Findings support the hypothesis that impoundments cumulatively affect downstream discharge and floodplain connectivity. Specifically, results illustrate that impoundments reduced downstream peak flows and increased downstream discharge during periods of low flow. This makes sense as many impoundments are designed specifically to retain water during periods of high flow and slowly release water following storm events. This increase in downstream discharge during periods of low flow can have positive ecological impacts, as drought flows can have negative

environmental impacts (Lake, 2011). However, impoundments also cumulatively decreased floodplain inundation surface area and volume. This reduction in floodplain connectivity also has a variety of ecological consequences. This is consistent with previous studies that impoundments can both positive and negative ecological effects (e.g., Tixier et al., 2011). Evaluating the tradeoff between these effects is crucial for sustainable management of river networks.

This work highlights the need for considering small impoundments in management decisions. In this study, impoundments had a substantial effect on both downstream discharge and floodplain connectivity for a relatively small (150 km^2, HUC10) watershed. At regional and national scales, these cumulative impacts are likely orders of magnitude higher. There are currently over 2.6 million impoundments across the conterminous United States (Smith et al., 2002), of which only 75,000 of these impoundments are documented in the United States Army Corps of Engineers' National Inventory of Dams (Graf, 1999). Understanding the cumulative effects of these impoundments on downstream hydrology is becoming increasingly more important as the total number of small impoundments will likely increase in response to increasing water demand in the coming decades.

6.5 Conclusions

While future work needs to be conducted to incorporate all of the impoundments within this watershed, the presented research illustrates that impoundments can have a cumulative effect on downstream discharge and floodplain connectivity. Future work should consider these cumulative impacts when making management decisions as these impacts can have substantial effects. Ultimately, higher resolution monitoring and modeling needs to be conducted to better understand these cumulative impacts and the potential tradeoffs between high and low flows. We suggest that researchers, planners, and managers should incorporate small impoundments into future work to manage river networks more effectively.

6.6 References

Adams, S. B. (2013). Effects of small impoundments on downstream crayfish assemblages. *Freshwater Science, 32*(4), 1318-1332.

Arcement, G. J., and Schneider, V. R. (1989). Guide for selecting Manning's roughness coefficients for natural channels and flood plains. Federal Highways Administration, US Department of Transportation, Report No. FHWA-TS-84-204, Washington.

Berg, M. D., Popescu, S. C., Wilcox, B. P., Angerer, J. P., Rhodes, E. C., McAlister, J., and Fox, W. E. (2016). Small farm ponds: overlooked features with important impacts on watershed sediment transport. *JAWRA Journal of the American Water Resources Association, 52*(1), 67-76.

Brown, P. H., Tullos, D., Tilt, B., Magee, D., and Wolf, A. T. (2009). Modeling the costs and benefits of dam construction from a multidisciplinary perspective. *Journal of Environmental Management, 90*, S303-S311.

Chaney, P. L., Boyd, C. E., and Polioudakis, E. (2012). Number, size, distribution, and hydrologic role of small impoundments in Alabama. *Journal of Soil and Water Conservation, 67*(2), 111-121.

Ercin, A. E., and Hoekstra, A. Y. (2014). Water footprint scenarios for 2050: A global analysis. *Environment international*, *64*, 71-82.

Eyler, S. M., Welsh, S. A., Smith, D. R., and Rockey, M. M. (2016). Downstream Passage and Impact of Turbine Shutdowns on Survival of Silver American Eels at Five Hydroelectric Dams on the Shenandoah River. *Transactions of the American Fisheries Society*, *145*(5), 964-976.

Gabelhouse, D. W. (1984). An assessment of crappie stocks in small midwestern private impoundments. *North American Journal of Fisheries Management*, *4*(4A), 371-384.

Gill, M. A. (1978). Flood routing by the Muskingum method. *Journal of hydrology*, *36*(3-4), 353-363.

Graf, W. L. (1999). Dam nation: A geographic census of American dams and their large-scale hydrologic impacts. *Water resources research*, *35*(4), 1305-1311.

Graf, W. L. (2006). Downstream hydrologic and geomorphic effects of large dams on American rivers. *Geomorphology*, *79*(3), 336-360.

Guy, C. S., and Willis, D. W. (1991). Evaluation of largemouth bass-yellow perch communities in small South Dakota impoundments. *North American Journal of Fisheries Management*, *11*(1), 43-49.

Harding, J. S., Benfield, E. F., Bolstad, P. V., Helfman, G. S., and Jones, E. B. D. (1998). Stream biodiversity: the ghost of land use past. *Proceedings of the National Academy of Sciences, U.S.A.* 95: 14843- 14847.

Hupp, C. R., Noe, G. B., Schenk, E. R., and Benthem, A. J. (2013). Recent and historic sediment dynamics along Difficult Run, a suburban Virginia Piedmont stream. *Geomorphology, 180*, 156-169.

Hupp, C. R., Schenk, E. R., Kroes, D. E., Willard, D. A., Townsend, P. A., and Peet, R. K. (2015). Patterns of floodplain sediment deposition along the regulated lower Roanoke River, North Carolina: annual, decadal, centennial scales. *Geomorphology*, *228*, 666-680.

Jones, C. N., Scott, D. T., Guth, C., Hester, E. T., and Hession, W. C. (2015). Seasonal variation in floodplain biogeochemical processing in a restored headwater stream. *Environmental Science and Technology*, *49*(22), 13190-13198.

Keys, T. A., Jones, C. N., Scott, D. T., and Chuquin, D. (2016). A cost-effective image processing approach for analyzing the ecohydrology of river corridors. *Limnology and Oceanography: Methods*, 14(6), 359-369.

Kingsford, R. T. (2000). Ecological impacts of dams, water diversions and river management on floodplain wetlands in Australia. *Austral Ecology*, *25*(2), 109-127.

Kirchberg, J., Price, S. J., White, E. M., and Haskell, D. G. (2016). Evaluating the impacts of small impoundments on stream salamanders. *Aquatic Conservation: Marine and Freshwater Ecosystems*, *26*(6), 1197-1206.

Lake, P. S. (2011). *Drought and aquatic ecosystems: effects and responses*. John Wiley & Sons. Hoboken, NJ.

Mackay, R. J., and Waters, T. F. (1986). Effects of small impoundments on hydropsychid caddisfly production in Valley Creek, Minnesota. *Ecology*, *67*(6), 1680-1686.

Maheu, A., St-Hilaire, A., Caissie, D., and El-Jabi, N. (2016). Understanding the Thermal Regime of Rivers Influenced by Small and Medium Size Dams in Eastern Canada. *River Research and Applications*, *32*(10), 2032-2044.

Mbaka, J. G., and Wanjiru Mwaniki, M. (2015). A global review of the downstream effects of small impoundments on stream habitat conditions and macroinvertebrates. *Environmental Reviews*, *23*(3), 257-262.

Mbaka, J. G., and Schäfer, R. B. (2015). Effect of small impoundments on leaf litter decomposition in streams. *River Research and Applications*.

Moglen, G. E. (2015). *Fundamentals of open channel flow*. CRC Press.

McCartney, M. (2009). Living with dams: managing the environmental impacts. *Water Policy*, *11*(S1), 121-139.

National Resources Conservation Service: Conservation Practice Standard (NRCS). (2011). Pond: code 378. District of Colombia, Washington D.C: NRCS.

R Development Core Team (2017). *R: A language and environment for statistical computing*. Vienna, Austria.

Sahagian, D. (2000). Global physical effects of anthropogenic hydrological alterations: sea level and water redistribution. *Global and Planetary Change*, *25*(1), 39-48.

Scott, D. T., Keim, R. F., Edwards, B. L., Jones, C. N., and Kroes, D. E. 2014. Floodplain biogeochemical processing of floodwaters in the Atchafalaya River Basin during the Mississippi River flood of 2011. *Journal of Geophysical Research: Biogeo*sciences, 119: 537-546.

Sheaffer, J. R., Mullan, J. D., and Hinch, N. B. (2002). Encouraging wise use of floodplains with market-based incentives. *Environmetnal Science, Policy, and Sustainable Development* 44: 32-43.

Smith, S. V., Renwick, W. H., Bartley, J. D., and Buddemeier, R. W. (2002). Distribution and significance of small, artificial water bodies across the United States landscape. *Science of the Total Environment*, *299*(1-3), 21-36.

Tixier, G., Lafont, M., Grapentine, L., Rochfort, Q., and Marsalek, J. (2011). Ecological risk assessment of urban stormwater ponds: literature review and proposal of a new conceptual approach providing ecological quality goals and the associated bioassessment tools. *Ecological Indicators*, *11*(6), 1497-1506.

Virginia, D. C. R. (2010). Stormwater Design Specification No. 8. *Infiltration Practices Version*, *1*.

CHAPTER 7. CONCLUDING REMARKS AND SUGGESTED FUTURE RESEARCH

7.1 Key findings

This research identified several key techniques and principals that can be useful for monitoring and management of river corridors. First, remote sensing approaches such as those presented in chapters 2 and 3 proved to be useful, cost-effective techniques for analyzing river corridors. Chapter 2 illustrated that simple image processing using supervised classification was an effective method of quantifying floodplain inundation dynamics for low order streams that are not easily recognizable from satellite imagery. Additionally, simplistic land cover indices can be effectively utilized to better understand seasonality of riparian vegetation and floodplain inundation dynamics. Chapter 3 demonstrated that freely available satellite remote sensing could be used to quantify storage variations in large lakes and reservoirs. Both of these chapters present cost-effective methods to capture the spatiotemporal variability of riverine ecosystems. Additionally, the techniques presented in these chapters can be easily applied to remote regions of the world or areas with limited hydrologic monitoring.

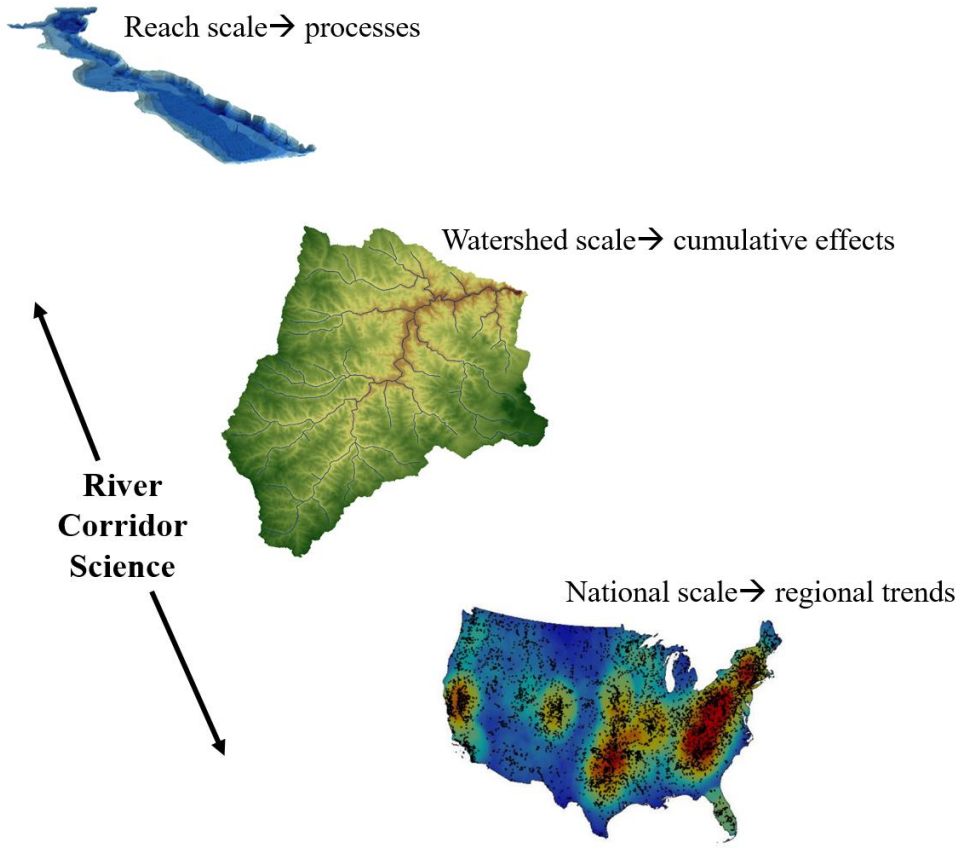

Figure 7-1. Diagram of river corridor processes across the spatial domain with increasing order of magnitude. This builds on the river corridor perspective presented by Harvey and Gooseff, 2015.

Second, the variety of scales used in Chapters 4-6 allowed for the identification of different river corridor processes across the spatial domain (Figure 7-1). Specifically, the presented research examined reach scale flooding dynamics, river-reservoir hydrology and biogeochemistry, and catchment scale floodplain connectivity. Each of these studies provides a new perspective for river corridor processes occurring across various scales. Chapter 4 demonstrated that reach scale floodplain connectivity can be increased using relatively simple techniques such as placing large wood in a stream channel. Chapter 5 illustrated the variability of nitrogen dynamics in a river-reservoir system during a storm event. Chapter 6 highlighted the cumulative effects that river alterations such as small impoundments can have on floodplain connectivity. Collectively, these studies take an important step towards understanding river corridor processes. Nonetheless, future work is needed to improve our overall understanding of river corridor science.

7.2 Suggestions for future research

The field of river corridor science is becoming increasingly more important as population and water demand increase. A great deal of progress has been made in recent decades to manage river networks in a sustainable manner, but much work is still needed to better analyze and fully understand river corridor science. The presented research provides several techniques and scientific findings that can be useful for better understanding river corridors. However, suggestions are provided to aid future studies in effectively monitoring and managing river corridors:

1) Simpler, cost-effective techniques should be developed to effectively monitor and manage floodplains. Floodplain management has always been challenging as it requires a balance between societal safety and ecological integrity (De Groote et al., 2010). Further, a lack of cost-effective monitoring techniques often inhibits floodplain managers from sustainably managing river corridors. Future studies should develop user-friendly, cost-effective, and open source techniques for managing riverine ecosystems using limited resources. Additionally, unique approaches such as citizen science can be useful for environmental monitoring in data-scarce regions and increasing public engagement (Conrad and Hilchey, 2011).

2) Future studies should seek to combine both spatial and temporal approaches to better understand river corridor processes. Due to the tradeoffs between spatial and temporal resolution, studies commonly focus specifically on either spatial or temporal variability for a given study. However, there is a great need to understand spatiotemporal dynamics of river corridors as hydrologic and biogeochemical processes can vary greatly with respect to space and time (Singh, 1997; McClain et al., 2003). Innovative approaches combining techniques such as remote sensing, modeling, and high frequency monitoring can capture this spatiotemporal variability and provide a new perspective on river corridor processes.

3) Scale is an important component of river corridor science that needs to be further investigated. Rivers are often analyzed at the reach scale without taking into consideration cumulative effects. While reach scale analyses can be useful for identifying specific processes, they are often site specific and don't capture cumulative effects or the spatial heterogeneity of large systems (Ward et al., 2001). Thus, a more integrated approach that examines river corridors across scales is necessary for future understanding of river corridor processes.

7.3 References

Conrad, C. C., and Hilchey, K. G. (2011). A review of citizen science and community-based environmental monitoring: issues and opportunities. *Environmental monitoring and assessment*, *176*(1-4), 273-291.

De Groot, R. S., Alkemade, R., Braat, L., Hein, L., and Willemen, L. (2010). Challenges in integrating the concept of ecosystem services and values in landscape planning, management and decision making. *Ecological complexity*, *7*(3), 260-272.

Harvey, J., and Gooseff, M. (2015). River corridor science: Hydrologic exchange and ecological consequences from bedforms to basins. *Water Resources Research*, *51*(9), 6893-6922.

McClain, M. E., Boyer, E. W., Dent, C. L., Gergel, S. E., Grimm, N. B., Groffman, P. M., ... & McDowell, W. H. (2003). Biogeochemical hot spots and hot moments at the interface of terrestrial and aquatic ecosystems. *Ecosystems*, *6*(4), 301-312.

Singh, V. P. (1997). Effect of spatial and temporal variability in rainfall and watershed characteristics on stream flow hydrograph. *Hydrological processes*, *11*(12), 1649-1669.

Ward, J. V., Tockner, K., Uehlinger, U., and Malard, F. (2001). Understanding natural patterns and processes in river corridors as the basis for effective river restoration. *River Research and Applications*, *17*(4-5), 311-323.

APPENDIX A. RAW DATA

Chapter 2 Data

Vegetation Analysis

Date	R/G Ratio	NDRGI
1-Jan-12	10.17	0.821
9-Jan-12	9.55	0.8104
16-Jan-12	10.78	0.8302
25-Jan-12	8.27	0.7842
31-Jan-12	9.65	0.8121
7-Feb-12	9.45	0.8086
14-Feb-12	8.59	0.7915
23-Feb-12	7.23	0.757
29-Feb-12	6.11	0.7185
6-Mar-12	5.17	0.676
13-Mar-12	4.48	0.6352
20-Mar-12	3.8	0.5835
27-Mar-12	4.49	0.6358
3-Apr-12	4.28	0.6136
10-Apr-12	3.44	0.5497
16-Apr-12	2.96	0.4947
24-Apr-12	2.53	0.4328
1-May-12	2.5	0.4287
8-May-12	2.15	0.3593
16-May-12	2.05	0.3449
2-Jun-12	2.32	0.3972
11-Jun-12	2.12	0.3589
18-Jun-12	2.68	0.4572
25-Jun-12	2.95	0.4939
2-Jul-12	2.68	0.4562
9-Jul-12	2.27	0.3884
16-Jul-12	2.79	0.4719
23-Jul-12	2.51	0.43
30-Jul-12	2.92	0.49
6-Aug-12	3.02	0.5022
13-Aug-12	3.34	0.5393
20-Aug-12	3.57	0.5624
27-Aug-12	4.7	0.649
4-Sep-12	4.96	0.6647
11-Sep-12	4.95	0.6636
19-Sep-12	7.68	0.7695
4-Oct-12	7.74	0.7765

11-Oct-12	9.66	0.8125
19-Oct-12	8.5	0.7894
25-Oct-12	9.05	0.8009
2-Nov-12	10.16	0.8208
9-Nov-12	11.93	0.8453
16-Nov-12	9.66	0.8124
24-Nov-12	12.05	0.8468
30-Nov-12	11.31	0.8375
5-Dec-12	10.38	0.8242

Chapter 3 Data

Tonle Sap Time Series

Estimate Number	L (m)		A (km^2)		ΔV (km^3)	
	Observed	Estimated	Observed	Estimated	Observed	Estimated
1	3.52	3.34	3595.58	2836.25	7062.63	9421.58
2	3.07	2.87	3298.11	2145.75	5055.22	7155.89
3	2.71	2.49	3075.64	2171.50	3662.36	5440.03
4	2.37	2.13	2876.65	2211.25	2520.79	3893.86
5	1.79	1.89	2558.37	2162.75	963.31	2902.09
6	1.79	1.70	2558.37	2271.25	963.31	2200.12
7	1.83	1.91	2579.57	2397.00	1054.94	2972.68
8	2.03	2.33	2687.15	2402.25	1548.16	4714.19
9	2.75	2.92	3099.73	4238.75	3807.77	7409.75
10	3.41	3.64	3520.73	3725.75	6544.60	10940.46
11	3.90	4.86	3865.64	4454.75	8988.24	17593.37
12	4.74	5.88	4533.44	4752.25	13993.67	24020.01
13	7.51	6.74	7648.87	11762.00	37806.46	30645.80
14	8.39	7.60	9012.30	10415.00	47718.54	38780.19
15	8.68	8.39	9508.53	8342.25	51232.95	48465.04
16	8.79	8.86	9703.15	10433.50	52598.15	55345.12
17	9.39	9.26	10829.06	12538.25	60355.99	62128.59
18	9.94	9.59	11961.08	14072.00	67929.51	68620.03
19	10.34	9.88	12847.69	14381.50	73715.19	74740.86
20	10.32	9.99	12802.05	16008.50	73420.35	77140.72
21	10.24	9.81	12620.89	12104.50	72246.85	73069.94
22	9.83	9.36	11726.75	8230.25	66379.44	64125.82
23	9.22	8.86	10498.79	7211.25	58104.52	55313.20

24	8.04	8.33	8445.03	4976.00	43640.69	47540.10
25	7.44	7.91	7549.15	4408.75	37066.59	42270.68
26	7.05	7.61	7015.81	3546.00	33075.55	38887.75
27	6.29	6.91	6078.85	3154.00	25936.76	32098.06
28	5.27	6.14	5012.05	2695.75	17682.42	25899.09
29	4.64	5.27	4448.37	2511.50	13343.72	20064.16
30	4.07	4.25	3992.57	2643.00	9918.02	14155.32
31	3.51	3.20	3588.72	2526.25	7014.81	8714.31
32	3.04	2.78	3279.07	2257.00	4931.91	6718.24
33	2.71	2.46	3075.64	2545.75	3662.36	5272.04
34	2.39	2.20	2888.08	2284.50	2583.27	4186.20
35	2.13	1.97	2741.98	2331.25	1816.69	3242.23
36	1.97	1.82	2654.59	2240.50	1394.06	2646.14
37	1.77	1.55	2547.81	2199.25	918.38	1648.93
38	1.61	1.40	2464.17	2159.00	579.92	1126.22
39	1.54	1.43	2428.05	2326.25	443.61	1233.77
40	1.74	1.84	2532.01	2512.25	852.06	2723.22
41	2.23	2.36	2797.55	2404.00	2099.84	4843.80
42	3.70	4.33	3721.23	4190.75	7948.46	14559.49
43	5.70	5.36	5437.04	3700.25	20976.82	20640.10
44	6.35	6.20	6148.16	3800.00	26469.66	26370.87
45	7.08	7.10	7055.53	6280.00	33374.66	33802.60
46	7.59	7.80	7764.36	11774.50	38660.80	41039.90
47	8.52	8.38	9231.75	13970.75	49278.77	48218.25
48	9.29	8.90	10633.69	12704.75	59026.48	56020.29
49	9.60	9.37	11249.68	12215.00	63195.53	64314.32
50	9.86	9.56	11790.25	12006.75	66800.43	67974.48
51	9.90	9.53	11875.40	11326.25	67363.80	67256.20
52	9.44	9.32	10927.93	9496.25	61026.22	63229.50
53	9.21	9.03	10479.65	8141.00	57973.40	58236.97
54	8.88	8.61	9865.06	6814.25	53728.29	51510.73
55	8.52	8.09	9231.75	5644.25	49278.77	44430.45
56	7.81	7.53	8090.46	5124.75	41058.44	38078.26
57	7.16	7.08	7162.49	4112.00	34178.72	33598.57
58	6.50	6.56	6324.83	3796.75	27824.93	29141.85
59	5.71	6.02	5447.34	3726.00	21056.64	25060.58
60	5.35	5.45	5088.53	2838.75	18274.87	21199.23
61	4.88	4.82	4655.26	2577.25	14928.16	17359.90
62	4.26	4.18	4139.19	2626.25	11007.16	13775.97
63	3.76	3.61	3764.01	2515.50	8254.25	10767.08
64	3.33	3.12	3467.18	2346.00	6178.96	8355.25

65	2.81	2.85	3136.15	2474.75	4030.27	7052.97
66	2.51	2.68	2957.37	2265.50	2970.39	6286.22
67	2.19	2.48	2775.23	2220.00	1984.83	5386.86
68	1.94	2.28	2638.40	2137.75	1318.98	4516.85
69	1.58	2.19	2448.66	1880.25	520.62	4135.79
70	1.43	2.11	2371.81	2172.00	243.87	3794.62
71	1.44	2.11	2376.90	2297.50	261.30	3778.13
72	1.62	2.31	2469.36	2274.75	599.97	4645.36
73	1.99	2.95	2665.41	2442.25	1444.84	7542.07
74	2.70	3.65	3069.64	2548.00	3626.38	10991.56
75	4.31	4.40	4178.63	3607.00	11302.55	14989.10
76	5.25	5.65	4993.10	3759.75	17535.77	22515.45
77	5.87	5.95	5614.77	4007.25	22353.78	24564.46
78	8.67	8.44	9491.01	7196.50	51109.72	49102.22
79	7.99	7.09	8366.74	5726.00	43072.76	33691.16
80	7.30	6.52	7353.40	4410.25	35608.34	28804.39
81	7.04	4.49	7002.62	3347.50	32976.14	15483.96
82	5.13	3.71	4880.94	2764.50	16668.14	11268.43
83	3.52	2.13	3595.58	2352.50	7062.63	3893.86
84	1.83	2.47	2579.57	2276.75	1054.94	5351.48
85	1.55	1.80	2433.19	2270.25	462.64	2561.84
86	1.40	2.21	2356.58	2788.50	192.47	4215.67
87	2.00	2.65	2670.84	2342.25	1470.45	6140.47
88	2.92	3.11	3203.84	4202.50	4451.85	8297.31
89	3.28	3.33	3434.09	4433.50	5955.18	9347.39
90	4.82	4.51	4602.66	3077.50	14524.16	15579.06
91	5.69	5.54	5426.76	3227.25	20897.13	21760.33
92	7.19	6.73	7202.99	8786.25	34482.66	30527.63
93	8.21	8.30	8716.32	7753.75	45599.00	47125.03
94	8.00	7.53	8382.35	5186.75	43186.05	38057.20
95	7.38	5.55	7464.66	3514.25	36438.12	21812.36
96	6.18	5.82	5953.77	3350.50	24973.45	23634.35
97	5.41	3.88	5146.66	2973.25	18725.35	12181.40
98	4.22	4.41	4107.89	2586.00	10773.48	15022.30
99	3.48	3.27	3568.20	2367.75	6872.21	9081.29
100	2.58	2.77	2998.35	2246.00	3205.93	6690.50
101	2.08	1.48	2714.47	2214.25	1680.60	1401.08
102	1.66	2.02	2490.15	2244.00	681.67	3427.13
103	1.58	2.26	2448.66	2122.00	520.62	4440.10
104	1.38	1.62	2346.46	2027.75	158.93	1892.14
105	1.28	1.83	2296.10	2019.00	0.00	2661.52

106	1.38	1.65	2346.46	2035.25	158.93	2001.19
107	1.38	2.32	2346.46	2130.50	158.93	4658.25
108	2.70	2.85	3069.64	2644.75	3626.38	7062.31
109	3.40	4.03	3514.00	2506.00	6498.39	12935.31
110	4.31	4.10	4178.63	2926.75	11302.55	13335.18
111	5.69	5.93	5426.76	6268.25	20897.13	24382.02
112	7.62	6.93	7808.09	9067.25	38983.58	32257.53
113	8.60	8.95	9369.21	11635.75	50251.19	56770.39
114	8.32	8.03	8896.11	6448.50	46888.65	43762.54
115	7.09	5.64	7068.81	4072.00	33474.66	22422.68
116	6.39	6.50	6194.79	3983.00	26827.85	28652.86
117	5.73	4.51	5467.99	3047.25	21216.74	15579.06
118	5.38	4.57	5117.51	2704.75	18499.45	15933.18
119	3.77	2.37	3771.18	2328.00	8305.73	4913.22
120	3.11	2.41	3323.64	2235.00	5221.67	5070.12
121	2.80	2.57	3130.06	2162.00	3992.82	5792.61
122	2.54	1.84	2974.88	2094.75	3070.46	2715.50
123	2.41	2.17	2899.55	2151.00	2646.33	4035.32
124	1.98	1.46	2660.00	2054.25	1419.38	1328.99
125	1.30	2.03	2306.14	2203.00	30.62	3479.75
126	1.29	1.63	2301.12	2040.25	15.23	1928.37
127	1.52	1.03	2417.78	2129.25	405.97	0.00
128	3.03	2.75	3272.74	3252.50	4891.10	6598.18
129	7.59	7.69	7764.36	8751.75	38660.80	39804.14
130	8.73	7.67	9596.55	11669.50	51851.31	39561.89
131	9.29	9.10	10633.69	10406.50	59026.48	59364.74
132	8.81	8.77	9738.92	8133.00	52848.27	53959.93
133	8.19	8.80	8683.99	6106.25	45366.42	54380.74
134	7.05	6.76	7015.81	4627.25	33075.55	30781.38
135	6.15	6.42	5920.10	3490.25	24713.79	28030.25
136	5.02	4.96	4780.33	3078.25	15891.30	18170.76
137	4.43	4.51	4274.80	2562.00	12026.38	15579.06
138	3.31	3.09	3453.91	2410.00	6089.01	8200.92
139	2.69	2.68	3063.65	2364.75	3590.54	6263.40
140	2.06	2.37	2703.52	2157.75	1627.19	4895.84
141	1.73	2.59	2526.75	2302.00	830.25	5860.06
142	1.52	1.64	2417.78	2390.00	405.97	1964.72
143	1.48	2.16	2397.30	2195.25	332.47	4006.12
144	1.77	2.02	2547.81	2234.25	918.38	3427.13
145	2.82	3.70	3142.26	2548.25	4067.86	11253.01
146	5.09	4.71	4844.12	5069.25	16383.61	16712.62

147	6.40	7.11	6206.50	8930.00	26917.77	33923.75
148	9.51	8.86	11067.68	8021.50	61970.69	55377.07
149	9.02	7.81	10121.74	5263.00	55509.81	41131.40
150	8.14	7.50	8603.65	3879.00	44787.53	37721.99
151	5.97	5.47	5721.99	3567.00	23183.49	21314.62
152	5.06	5.82	4816.68	2843.75	16171.74	23600.12
153	3.84	2.99	3821.77	2545.50	8670.17	7722.40
154	3.13	3.75	3336.47	2348.25	5305.78	11515.81
155	2.20	2.57	2780.80	2223.75	2013.36	5779.14
156	1.97	2.71	2654.59	2216.00	1394.06	6391.39
157	1.56	2.39	2438.34	2252.75	481.82	4982.83
158	1.46	2.35	2387.09	2146.25	296.59	4809.17
159	1.47	1.65	2392.19	3419.25	314.45	2001.19
160	1.84	2.45	2584.88	3317.00	1078.22	5228.01
161	1.88	2.22	2606.21	3255.25	1172.77	4253.61
162	2.02	2.97	2681.70	3760.00	1522.11	7622.64
163	3.49	4.39	3575.02	3791.25	6919.60	14911.71
164	3.84	4.46	3821.77	3451.75	8670.17	15283.18
165	5.77	5.96	5509.53	5909.50	21538.69	24606.71
166	6.88	7.14	6794.80	5013.00	31405.43	34186.18
167	7.71	7.43	7940.67	6300.25	39959.83	37020.06
168	8.16	7.57	8635.70	7597.25	45018.65	38491.37
169	8.72	8.66	9578.89	6718.25	51727.34	52282.98
170	8.18	8.68	8667.87	4879.25	45250.35	52598.54
171	7.17	6.39	7175.96	4756.50	34279.89	27781.37
172	6.48	6.70	6300.99	3230.75	27642.33	30250.75
173	4.96	5.19	4726.33	2518.00	15475.02	19557.89
174	4.20	4.39	4092.33	2477.75	10657.52	14933.81
175	2.97	3.19	3235.01	2456.25	4649.32	8685.09
176	2.46	3.11	2928.35	2256.00	2806.53	8302.13
177	1.62	2.47	2469.36	2189.50	599.97	5316.14
178	1.40	1.76	2356.58	2140.00	192.47	2409.89
179	1.40	2.23	2356.58	2110.25	192.47	4304.31
180	2.05	2.06	2698.06	2440.25	1600.70	3589.54
181	2.47	3.22	2934.14	2932.50	2839.01	8850.96
182	3.91	3.76	3873.00	2942.75	9041.76	11546.82
183	4.30	4.88	4170.71	3129.25	11243.18	17698.85
184	4.74	5.17	4533.44	3605.25	13993.67	19423.15
185	5.92	5.20	5668.13	2757.75	22766.81	19619.28
186	6.10	6.26	5864.40	6214.50	24283.96	26819.32
187	7.07	7.31	7042.27	6968.50	33274.81	35785.22

188	7.63	7.01	7822.71	6042.00	39091.47	32939.42
189	7.93	7.72	8273.69	5524.75	42396.06	40070.25
190	8.01	7.65	8397.98	6601.75	43299.49	39343.05
191	8.21	8.19	8716.32	8090.75	45599.00	45774.87
192	8.54	8.67	9265.94	8275.00	49521.00	52402.94
193	8.64	8.81	9438.64	7668.50	50740.90	54647.59
194	8.71	8.33	9561.25	6578.25	51603.53	47593.95
195	8.71	8.82	9561.25	5598.00	51603.53	54742.13
196	8.46	8.43	9129.86	5473.25	48555.60	48921.19
197	8.40	8.55	9029.01	6078.50	47837.69	50664.49
198	8.19	8.25	8683.99	4704.00	45366.42	46582.31
199	8.09	7.83	8524.00	4243.25	44212.28	41361.13
200	7.42	7.64	7520.89	3971.00	36856.52	39223.25
201	7.33	7.46	7394.94	4300.25	35918.41	37369.27
202	6.88	6.94	6794.80	3356.00	31405.43	32346.45
203	6.41	5.81	6218.24	2872.75	27007.82	23565.93

Lake Tana Time Series

Estimate Number	L (m)		A (km^2)		ΔV (km^3)	
	Observed	Estimated	Observed	Estimated	Observed	Estimated
1	1786.46	1785.90	2953.55	2937.50	6171.04	4453.84
2	1786.42	1786.47	2950.45	2951.75	6052.13	5989.85
3	1786.35	1786.35	2945.02	2970.00	5844.34	5650.80
4	1786.32	1786.35	2942.70	2967.25	5755.40	5650.80
5	1786.16	1786.16	2930.29	2933.00	5282.30	5113.97
6	1786.14	1786.10	2928.74	2960.25	5223.31	4944.45
7	1786.06	1786.05	2922.52	2933.25	4987.66	4803.18
8	1786.02	1785.97	2919.41	2926.75	4870.04	4577.15
9	1786.00	1786.09	2917.85	2914.00	4811.27	4916.20
10	1785.91	1785.93	2910.84	2933.50	4547.24	4464.13
11	1786.03	1786.03	2920.19	2947.75	4899.43	4746.67
12	1786.00	1786.07	2917.85	2929.25	4811.27	4859.69
13	1786.04	1786.08	2920.97	2906.50	4928.83	4887.94
14	1786.20	1786.22	2933.39	2936.00	5400.38	5283.50
15	1786.24	1786.28	2936.50	2911.00	5518.60	5453.02
16	1787.28	1786.57	3017.43	2968.50	8635.40	6272.39
17	1787.41	1787.40	3027.69	2979.00	9030.58	8617.47
18	1787.54	1787.55	3038.00	3015.25	9426.93	9041.28
19	1787.56	1787.39	3039.59	3011.00	9488.01	8589.22

20	1787.52	1787.48	3036.41	3012.25	9365.88	8843.50
21	1787.52	1787.51	3036.41	3027.75	9365.88	8928.26
22	1787.52	1787.51	3036.41	3019.75	9365.88	8928.26
23	1787.38	1787.47	3025.31	2997.00	8939.28	8815.25
24	1787.34	1787.29	3022.16	3006.50	8817.64	8306.68
25	1787.24	1787.13	3014.29	3013.75	8514.04	7854.61
26	1787.12	1786.86	3004.87	3034.25	8150.66	7091.75
27	1787.03	1786.66	2997.84	3008.00	7878.81	6526.67
28	1786.98	1786.71	2993.94	3001.50	7728.03	6667.94
29	1786.81	1786.85	2980.70	2956.00	7216.77	7063.50
30	1786.76	1786.89	2976.82	2957.25	7066.81	7176.52
31	1786.74	1786.72	2975.26	2956.25	7006.87	6696.20
32	1786.66	1786.71	2969.05	2945.25	6767.45	6667.94
33	1786.63	1786.55	2966.73	2962.00	6677.79	6215.88
34	1786.51	1785.84	2957.42	2935.00	6319.85	4209.85
35	1786.44	1786.39	2952.00	2954.00	6111.57	5763.82
36	1786.30	1786.27	2941.15	2936.75	5696.15	5424.77
37	1786.24	1786.27	2936.50	2975.75	5518.60	5424.77
38	1786.16	1785.91	2930.29	2938.00	5282.30	4407.62
39	1786.11	1786.05	2926.41	2930.25	5134.88	4803.18
40	1785.89	1785.59	2909.28	2977.25	4488.66	3503.50
41	1785.81	1785.59	2903.04	2927.75	4254.67	3503.50
42	1785.78	1785.46	2900.69	2888.25	4167.06	3136.19
43	1785.73	1785.76	2896.78	2922.50	4021.21	3983.81
44	1785.71	1785.73	2895.21	2897.25	3962.93	3899.05
45	1785.76	1785.35	2899.13	2894.00	4108.69	2825.40
46	1785.71	1785.84	2895.21	2912.50	3962.93	4209.85
47	1785.76	1785.88	2899.13	2902.25	4108.69	4322.86
48	1786.00	1785.98	2917.85	2996.50	4811.27	4605.40
49	1786.40	1786.41	2948.90	2940.50	5992.72	5820.32
50	1786.80	1786.79	2979.92	2958.00	7186.76	6893.98
51	1787.00	1787.18	2995.50	2976.75	7788.32	7995.88
52	1787.30	1787.28	3019.01	3043.25	8696.12	8278.42
53	1787.40	1787.45	3026.90	3000.50	9000.14	8758.74
54	1787.47	1787.50	3032.44	3024.50	9213.37	8900.01
55	1787.34	1787.11	3022.16	3033.50	8817.64	7798.10
56	1787.28	1787.30	3017.43	3000.75	8635.40	8334.93
57	1787.28	1787.10	3017.43	3021.00	8635.40	7769.85
58	1787.10	1787.04	3003.31	2991.00	8090.20	7600.33
59	1787.06	1786.99	3000.18	2996.25	7969.36	7459.06
60	1786.99	1786.87	2994.72	2991.75	7758.17	7120.01

61	1786.86	1786.88	2984.59	2987.75	7366.92	7148.26
62	1786.74	1786.73	2975.26	2965.00	7006.87	6724.45
63	1786.71	1786.71	2972.93	2957.00	6917.03	6667.94
64	1786.65	1786.70	2968.28	2960.50	6737.56	6639.69
65	1786.57	1786.70	2962.07	2962.75	6498.68	6639.69
66	1786.48	1786.59	2955.10	2956.00	6230.54	6328.90
67	1786.44	1786.54	2952.00	2967.00	6111.57	6187.63
68	1786.32	1786.27	2942.70	2956.00	5755.40	5424.77
69	1786.18	1786.36	2931.84	2938.75	5341.33	5679.05
70	1786.13	1786.09	2927.96	2947.00	5193.82	4916.20
71	1786.02	1786.03	2919.41	2924.50	4870.04	4746.67
72	1786.00	1786.01	2917.85	2945.75	4811.27	4690.16
73	1785.77	1785.71	2899.91	2925.00	4137.87	3842.54
74	1785.68	1785.73	2892.86	2912.00	3875.58	3899.05
75	1785.60	1785.40	2886.57	2913.25	3643.01	2966.67
76	1785.57	1785.53	2884.21	2901.00	3555.93	3333.97
77	1785.50	1785.20	2878.69	2912.25	3353.07	2401.59
78	1785.26	1785.18	2859.64	2919.50	2660.79	2345.08
79	1785.17	1785.14	2852.44	2900.50	2402.50	2232.07
80	1785.20	1785.11	2854.84	2882.00	2488.52	2147.30
81	1785.10	1785.19	2846.81	2833.50	2202.12	2373.34
82	1785.17	1785.19	2852.44	2843.00	2402.50	2373.34
83	1785.52	1785.52	2880.27	2890.00	3410.99	3305.72
84	1785.96	1785.96	2914.74	2922.50	4693.84	4548.89
85	1786.24	1786.32	2936.50	2927.50	5518.60	5566.04
86	1786.37	1786.37	2946.57	2942.50	5903.67	5707.31
87	1786.41	1786.42	2949.67	2941.50	6022.42	5848.58
88	1786.26	1786.36	2938.05	2931.75	5577.75	5679.05
89	1786.27	1786.23	2938.82	2934.75	5607.34	5311.75
90	1786.21	1786.14	2934.17	2942.00	5429.93	5057.47
91	1786.12	1786.15	2927.18	2923.25	5164.35	5085.72
92	1785.99	1785.97	2917.08	2915.75	4781.90	4577.15
93	1785.93	1786.00	2912.40	2917.25	4605.86	4661.91
94	1785.86	1785.90	2906.94	2915.75	4400.85	4379.37
95	1785.81	1785.74	2903.04	2919.00	4254.67	3927.31
96	1785.70	1785.71	2894.43	2916.75	3933.80	3842.54
97	1785.68	1785.71	2892.86	2918.00	3875.58	3842.54
98	1785.60	1785.71	2886.57	2911.75	3643.01	3842.54
99	1785.56	1785.57	2883.42	2898.75	3526.93	3446.99
100	1785.44	1785.47	2873.95	2902.00	3179.52	3164.45
101	1785.35	1785.44	2866.81	2903.25	2919.80	3079.69

102	1785.31	1785.29	2863.63	2894.25	2804.59	2655.88
103	1785.12	1785.17	2848.42	2873.00	2259.32	2316.83
104	1785.03	1785.10	2841.17	2879.00	2002.17	2119.05
105	1785.02	1785.01	2840.36	2859.00	1973.65	1864.76
106	1784.90	1784.84	2830.62	2866.25	1632.04	1384.45
107	1784.72	1784.79	2815.86	2846.00	1122.14	1243.18
108	1784.75	1784.72	2818.34	2836.00	1206.92	1045.40
109	1784.60	1784.59	2805.93	2836.75	783.90	678.10
110	1784.56	1784.53	2802.59	2830.25	671.46	508.57
111	1784.48	1784.41	2795.90	2810.75	447.03	169.52
112	1784.32	1784.35	2782.38	2826.50	0.04	0.00
113	1784.44	1784.44	2792.54	2809.25	335.05	254.29
114	1784.50	1784.43	2797.58	2786.00	503.08	226.03
115	1784.91	1784.87	2831.43	2826.25	1660.46	1469.21
116	1785.07	1785.02	2844.40	2850.25	2116.37	1893.02
117	1785.54	1785.68	2881.85	2914.00	3468.94	3757.78
118	1786.26	1786.12	2938.05	2937.00	5577.75	5000.96
119	1786.44	1786.48	2952.00	2891.25	6111.57	6018.10
120	1786.67	1786.59	2969.83	2971.75	6797.35	6328.90
121	1786.63	1786.59	2966.73	2960.25	6677.79	6328.90
122	1786.64	1786.62	2967.50	2960.25	6707.67	6413.66
123	1786.46	1786.48	2953.55	2954.25	6171.04	6018.10
124	1786.35	1786.40	2945.02	2947.25	5844.34	5792.07
125	1786.28	1786.32	2939.60	2931.00	5636.94	5566.04
126	1786.16	1786.18	2930.29	2935.50	5282.30	5170.48

Balbina Reservoir Time Series

Estimate Number	L (m)		A (km^2)		ΔV (km^3)	
	Observed	Estimated	Observed	Estimated	Observed	Estimated
1	47.77	48.22	1620.87	717.00	1925.67	1029.37
2	48.59	48.81	1821.22	747.50	2351.92	1396.36
3	48.11	48.44	1700.01	698.50	2076.51	1181.54
4	47.93	47.68	1657.43	652.75	1545.65	1100.98
5	47.47	47.55	1555.54	711.75	1463.65	895.11
6	48.18	48.48	1716.99	747.75	2106.14	1212.87
7	47.03	46.64	1467.11	692.75	876.99	698.18
8	45.97	46.13	1287.58	624.50	572.31	223.78
9	47.81	47.32	1629.89	612.75	1306.89	1047.27
10	45.67	45.50	1244.53	540.20	218.82	89.51

11	45.64	45.55	1240.39	541.75	245.65	76.08
12	45.91	45.89	1278.72	603.75	435.16	196.92
13	46.16	46.11	1316.52	648.00	558.91	308.81
14	47.39	47.51	1538.81	684.25	1434.29	859.30
15	47.13	47.25	1486.46	695.75	1265.14	742.94
16	46.19	46.04	1321.21	606.75	518.31	322.24
17	46.43	46.31	1359.98	616.00	680.07	429.65
18	45.47	45.09	1217.51	511.00	0.00	0.00
19	45.88	46.05	1274.33	558.25	528.14	183.50
20	47.51	47.98	1564.01	702.00	1754.55	913.01
21	46.60	47.09	1388.83	633.50	1160.54	505.73
22	46.89	46.78	1440.77	631.25	964.14	635.52
23	46.74	46.65	1413.46	596.75	882.52	568.39
24	46.64	46.17	1395.78	596.00	596.86	523.64
25	47.36	47.30	1532.62	639.00	1296.43	845.87
26	47.56	47.43	1574.70	611.25	1380.55	935.39
27	47.79	47.88	1625.37	633.25	1683.38	1038.32
28	48.72	48.65	1855.99	698.00	2234.43	1454.55
29	47.94	48.26	1659.75	686.75	1949.80	1105.46
30	47.63	47.96	1589.86	625.00	1737.22	966.71
31	47.51	48.01	1564.01	629.00	1774.00	913.01
32	47.64	47.50	1592.05	605.00	1426.97	971.19
33	47.44	47.18	1549.23	587.25	1217.17	881.68
34	47.54	47.32	1570.41	619.75	1306.24	926.43
35	48.26	47.79	1736.69	648.50	1623.08	1248.67
36	48.32	47.97	1751.67	650.00	1745.53	1275.53
37	48.50	48.20	1797.64	656.00	1906.56	1356.08
38	47.88	48.20	1645.87	628.00	1909.39	1078.60
39	48.14	48.39	1707.26	712.50	2046.28	1194.97
40	48.10	48.37	1697.61	698.00	2031.20	1177.06
41	47.74	48.19	1614.15	651.50	1900.90	1015.94
42	46.94	47.22	1450.08	615.75	1245.65	657.90
43	46.00	45.71	1292.06	505.50	330.33	237.20
44	46.02	45.54	1295.07	495.00	239.06	246.15
45	46.46	46.86	1364.99	548.25	1013.48	443.08
46	46.84	47.01	1431.56	555.75	1110.10	613.15
47	47.00	47.29	1461.40	589.25	1291.21	684.76
48	47.00	47.11	1461.40	580.50	1172.73	684.76
49	47.04	46.88	1469.03	545.00	1025.40	702.66
50	47.08	46.61	1476.73	476.75	857.38	720.56
51	46.96	46.61	1453.83	494.50	858.00	666.85

52	47.24	47.13	1508.24	494.75	1184.29	792.17
53	47.74	47.63	1614.15	533.00	1511.94	1015.94
54	47.92	47.84	1655.11	583.25	1660.03	1096.50
55	47.46	47.95	1553.43	625.75	1735.83	890.63
56	47.04	47.42	1469.03	566.50	1373.29	702.66
57	47.26	47.13	1512.26	534.25	1183.65	801.12
58	46.74	46.91	1413.46	485.50	1046.16	568.39
59	47.24	47.11	1508.24	508.75	1173.37	792.17
60	46.74	46.97	1413.46	487.50	1082.81	568.39

Chapter 4 Data

Flood Hydrographs

Time (min)	Upstream (L/s)		Downstream (L/s)	
	Flood 1	Flood 2	Flood 1	Flood 2
0	0.08	0.00	0.00	0.00
1	0.10	0.00	0.00	0.00
2	0.13	0.00	0.00	0.27
3	0.13	0.00	0.00	0.87
4	40.46	27.96	0.00	1.90
5	54.07	47.47	24.96	4.93
6	55.76	54.76	38.40	15.33
7	53.01	51.51	47.06	35.80
8	48.80	46.28	51.03	44.07
9	43.52	41.04	53.06	47.77
10	38.51	35.19	50.07	48.69
11	33.57	29.57	45.26	46.76
12	28.58	24.36	40.65	43.90
13	24.17	19.85	36.23	39.34
14	20.64	16.33	31.81	35.21
15	17.51	13.06	28.44	31.66
16	14.67	10.35	24.49	26.58
17	12.23	8.00	20.62	22.68
18	10.28	6.16	17.51	19.54
19	8.73	4.73	14.18	16.35
20	7.32	3.64	10.64	12.53
21	6.32	2.78	7.82	9.56
22	5.51	2.16	5.48	7.07
23	4.80	1.66	3.22	5.21

24	4.29	1.30	2.02	3.35
25	3.86	1.01	1.43	2.02
26	3.54	0.81	1.07	1.60
27	3.29	0.63	0.84	1.15
28	3.09	0.52	0.61	0.97
29	2.91	0.44	0.90	0.70
30	2.78	0.35	0.72	0.68
31	2.68	0.32	0.68	0.54
32	2.58	0.26	0.87	0.48
33	2.49	0.24	0.69	0.32
34	2.45	0.20	0.65	0.26
35	2.38	0.18	0.35	0.16
36	2.34	0.15	0.37	0.07
37	2.27	0.14	0.19	0.03

Floodplain Hydrographs

	XS1 Stage (cm)		XS2 Stage (cm)		XS3 Stage (cm)	
Time (min)	Without LW	With LW	Without LW	With LW	Without LW	With LW
0	0.00	0.00	0.00	0.00	0.00	0.00
1	0.00	0.00	0.00	0.00	0.00	0.00
2	0.32	0.50	0.00	0.00	0.00	0.00
3	4.15	3.81	0.00	0.00	0.00	0.08
4	4.50	5.81	0.98	0.25	0.00	0.09
5	4.12	5.33	3.58	4.80	0.77	0.19
6	3.67	4.67	6.39	7.98	5.28	0.36
7	2.73	3.42	7.34	9.37	8.48	0.46
8	1.75	2.48	7.48	9.79	10.59	1.93
9	0.77	1.95	7.46	10.01	11.49	7.39
10	0.00	1.64	6.55	9.57	11.86	10.76
11	0.00	0.91	5.76	8.87	11.97	13.66
12	0.00	0.95	4.62	7.40	11.75	15.31
13	0.00	0.39	3.29	6.00	11.30	16.25
14	0.00	0.22	2.02	4.46	10.48	16.40
15	0.00	0.09	0.75	2.63	9.59	16.21
16	0.00	0.00	0.03	1.21	8.74	16.01
17	0.00	0.00	0.09	0.00	7.68	15.51
18	0.00	0.00	0.00	0.00	6.71	14.57
19	0.00	0.00	0.00	0.00	5.41	13.76

20	0.00	0.00	0.00	0.00	4.14	12.76
21	0.00	0.00	0.00	0.00	2.87	11.85
22	0.00	0.00	0.00	0.00	1.48	10.87
23	0.00	0.00	0.00	0.00	0.17	9.66
24	0.00	0.00	0.00	0.00	0.00	8.51
25	0.00	0.00	0.00	0.00	0.00	7.48
26	0.00	0.00	0.00	0.00	0.00	6.23
27	0.00	0.00	0.00	0.00	0.00	5.06
28	0.00	0.00	0.00	0.00	0.00	3.96
29	0.00	0.00	0.00	0.00	0.00	3.07
30	0.00	0.00	0.00	0.00	0.00	2.03
31	0.00	0.00	0.00	0.00	0.00	1.43
32	0.00	0.00	0.00	0.00	0.00	0.63
33	0.00	0.00	0.00	0.00	0.00	0.00
34	0.00	0.00	0.00	0.00	0.00	0.00
35	0.00	0.00	0.00	0.00	0.00	0.00
36	0.00	0.00	0.00	0.00	0.00	0.00
37	0.00	0.00	0.00	0.00	0.00	0.00
38	0.00	0.00	0.00	0.00	0.00	0.00
39	0.00	0.00	0.00	0.00	0.00	0.00
40	0.00	0.00	0.00	0.00	0.00	0.00

Large Wood Placement

XS ID	No LW Q_{FP}/Q_{tot} (%)	With LW Q_{FP}/Q_{tot} (%)	Difference (%)
1	18.52	40.86	22.34
2	26.09	30.00	3.91
3	18.99	23.94	4.94
4	13.37	37.50	24.13
5	23.81	18.18	-5.63
6	29.20	30.00	0.80
7	12.45	21.43	8.98
8	12.76	32.50	19.74
9	7.86	36.13	28.27
10	16.38	40.21	23.83
11	8.25	37.50	29.25
12	15.68	37.78	22.10
13	15.81	23.65	7.83
14	17.88	31.51	13.63

15	9.89	25.58	15.69
16	6.27	18.88	12.61
17	18.16	32.02	13.87
18	9.28	50.00	40.72
19	9.52	17.99	8.46
20	22.22	26.19	3.97
21	26.06	38.46	12.40
22	22.31	30.00	7.69
23	18.13	44.44	26.31
24	18.87	44.44	25.58
25	40.63	75.00	34.38
26	37.50	68.57	31.07
27	29.08	40.91	11.83
28	50.00	59.44	9.44
29	37.50	33.87	-3.63
30	18.41	37.50	19.09
31	17.68	24.54	6.86
32	7.65	14.00	6.35
33	11.70	20.00	8.30
34	7.02	21.76	14.74
35	8.78	33.33	24.55
36	20.15	33.33	13.19
37	10.43	18.18	7.75
38	7.66	25.00	17.34
39	15.87	34.27	18.40
40	17.56	25.00	7.44
41	8.94	40.91	31.97
42	12.13	22.22	10.09
43	4.40	23.53	19.13
44	11.19	37.50	26.31
45	6.33	33.33	27.00
46	6.45	23.93	17.48
47	8.74	23.30	14.56
48	14.04	15.45	1.42
49	15.16	34.38	19.21
50	8.15	24.87	16.73

Synthetic Storm Events

Recurrence Interval	Without LW Q_{FP}/Q_{tot} (%)	With LW Q_{FP}/Q_{tot} (%)
1	14.84	42.68
2	29.56	45.98
3	41.81	50.26
5	55.62	58.63
10	64.36	65.86
15	68.54	68.97
25	72.89	72.89
50	76.22	76.38
100	80.19	80.18
200	82.69	82.78
500	87.86	87.86
1000	88.31	88.31

Chapter 5 Data

Grab Sample Solute Concentrations

Site	NH_4^+ (mg/L)	NO_3^- (mg/L)	DOC (mg/L)	PO_4^{3-} (mg/L)	C:N	N:P
Al1	0.02	0.25	1.43	0.007	5.96	36.32
Al2	0.04	0.48	7.09	0.007	11.82	82.08
Al3	0.03	0.64	3.63	0.009	7.12	55.75
Al4	0.02	0.53	2.34	0.008	5.44	54.74
Al5	0.03	0.64	2.98	0.012	5.52	46.67
Al6	0.01	0.49	1.63	0.005	4.08	76.72
GS1	0.02	0.39	1.71	0.002	5.34	149.46
GS2	0.05	0.40	3.56	0.011	8.28	40.82
GS3	0.07	0.62	4.09	0.008	7.30	70.40
GS4	0.03	0.41	2.09	0.003	5.65	117.41
GS5	0.01	0.41	2.33	0.003	6.66	109.25
GS6	0.01	0.41	2.33	0.003	6.13	123.18
UP1	0.02	0.21	1.35	0.001	6.14	219.32
UP2	0.07	0.33	1.94	0.010	5.88	31.53
UP3	0.04	0.36	1.79	0.004	5.42	85.70
UP4	0.05	0.39	1.83	0.004	5.08	92.90
UP5	0.03	0.38	2.01	0.004	5.58	94.74

UP6	0.03	0.40	2.06	0.003	5.57	112.72
DWN1	0.05	0.29	1.29	0.001	4.78	283.49
DWN2	0.09	0.65	4.98	0.013	9.22	41.43
DWN3	0.14	0.35	2.21	0.003	5.67	124.66
DWN4	0.11	0.48	3.47	0.010	7.08	48.70
DWN5	0.12	0.42	3.1	0.007	6.33	73.25
DWN6	0.14	0.43	2.82	0.004	6.00	107.82
RAD1	0.01	0.32	1.43	0.004	5.11	79.58
RAD2	0.07	0.39	2.71	0.010	7.13	39.77
RAD3	0.14	0.34	2.11	0.003	5.55	128.57
RAD4	0.11	0.43	2.87	0.006	6.52	73.44
RAD5	0.16	0.46	2.96	0.005	6.17	96.97
RAD6	0.15	0.48	2.94	0.005	6.00	90.20

Grab Sample Water Quality Concentrations

Site	DO (% Sat)	Turb (NTU)	Cond (mS/cm)	Temp (°C)	pH
Al1	83.7	0.4	0.25	21.93	7.46
Al2	N/A	N/A	N/A	N/A	N/A
Al3	84.2	234.9	0.137	11.51	6.62
Al4	87.9	138.7	0.142	9.91	6.98
Al5	87.4	98.7	0.172	11.5	6.62
Al6	86	30.9	0.151	9.63	7.35
GS1	87.7	4.6	0.254	24.15	7.26
GS2	N/A	N/A	N/A	N/A	N/A
GS3	81.6	186.2	0.149	13.25	6.49
GS4	76	11.2	0.253	17.6	6.5
GS5	75.1	7.1	0.39	18.66	6.62
GS6	68.5	8.4	0.241	17.53	6.83
UP1	94.2	-0.8	0.278	23.9	7.77
UP2	N/A	N/A	N/A	N/A	N/A
UP3	62.2	5.4	0.254	17.81	6.81
UP4	81.9	2.1	0.253	18.35	6.55
UP5	66.7	0.7	0.256	19.89	6.73
UP6	68	3.5	0.254	17.76	6.75
DWN1	50.8	0.5	0.279	21.95	6.66
DWN2	N/A	N/A	N/A	N/A	N/A
DWN3	63.5	18.1	0.258	17.32	6.92
DWN4	72.2	29.5	0.262	14.3	6.78

DWN5	62.7	44	0.246	16.49	7
DWN6	60.6	21.3	0.218	15.19	6.73
RAD1	93.7	0	0.292	22.58	7.49
RAD2	N/A	N/A	N/A	N/A	N/A
RAD3	88	15.9	0.28	17.58	6.7
RAD4	78.7	22.7	0.273	14.92	6.7
RAD5	73.6	42.9	0.344	15.9	7.13
RAD6	71	18.7	0.331	14.72	6.66

APPENDIX B. STATISTICAL AND PROCESSING CODE

Chapter 2 Code

Image Processing Script (MATLAB)

```
function [Output] = auto_segment_v4(sig,thres)
% sig is the sigma for the Gaussian function;
% thres is the pixel value threshold (range);
% Set as (2.5,42) for summer photos;

FileIn = uigetfile({'*.jpg;*.tif;*.png;*.gif','All Image Files';
'*.*','All Files' },'Select files..','MultiSelect','on');
% uigetfile > displays dialog box of directory for user to select files;

FileName = cell(1);             % Constructs cell aray;
if class(FileIn) == 'char'      % Sets as character array;
FileName{1} = FileIn;
else
FileName = FileIn;
end
NrOfFiles = size(FileName,2);               % Creates variable for array dimensions;
IMGtemp = cell(1,1);
IMGtemp = imread(FileName{1});              % Reads 1st input image from selection;
imshow(IMGtemp,[]), impixelinfo;

Pimg1 = [       % Creates a dataset of ground control points in pixel distance
 350, 245;      % Bottom left
 405, 250;      % Bottom rights
 45, 365;       % Upper left
 245, 400;      % Upper right
];

for i=1:size(Pimg1, 1)
 rectangle('Position', [Pimg1(i,1)-10 Pimg1(i,2)-10 20 20], 'FaceColor', 'r');
end

Pworld1 = [     % Creates a dataset of actual values corresponding to pixel values above
 0, 0;          % Bottom left
 100, 0;        % Bottom right
 0, 1000;       % Upper left
 100, 1000;     % Upper right
];

Tform1 = fitgeotrans(Pimg1,Pworld1,'projective');
Iout1 = imwarp(IMGtemp,Tform1);
% Orthorectifies image based on the above ground control points
```

```
figure;                 % Creates graphic object;
imshow(Iout1);          % Displays image;
impixelinfo;            % Creates tool that displays info of pixel bellow cursor;
h = imrect;             % Creates dragable rectangle;
wait(h);                                % Waits for user;
IMGroi = getPosition(h);                % Returns extent of region of interest (ROI);
delete(h);                              % Removes dragable rectangle;
imshow(imcrop(Iout1,IMGroi));           % Displays cropped image by ROI;
[Xi, Yi, Vals] = impixel;               % Gets pixel values;
IMGcoords = [Xi Yi];                    % Creates pixel coordinate variable;
close(gcf);                             % Deletes current figure;

for n=1:NrOfFiles
%IMGtemp1 = imread(FileName{n}); % Reads image from folder;

ADJ = imadjust(Iout1,[.2 .3 0; .6 .7 1],[],1.5);
% Adjusts image intensity values (contrast/sharpness);

Iout2 = ADJ;
IMGin{n} = imcrop(Iout2,IMGroi);  % Crops all selected images;
end

%-----------------------------


% Begin Image Processing;

R = IMGin{n}(:,:,1);                    % Stores red channel values for each pixel
G = IMGin{n}(:,:,2);                    % Stores green channel values for each pixel
B = IMGin{n}(:,:,3);                    % Stores blue channel values for each pixel
RowMeanR = mean(R);                     % Mean of red values in each row of pixel array
MeanR = mean(RowMeanR);                 % Mean of the mean red values for each row
RowMeanG = mean(G);                     % Mean of green values in each row of pixel array
MeanG = mean(RowMeanG);                 % Mean of the mean green values for each row
RowMeanB = mean(B);                     % Mean of blue values in each row of pixel array
MeanB = mean(RowMeanB);                 % Mean of the mean blue values for each row
r = MeanR/(MeanR+MeanG+MeanB);          % Percent red values in ROI
g = MeanG/(MeanR+MeanG+MeanB);          % Percent green values in ROI
b = MeanB/(MeanR+MeanG+MeanB);          % Percent blue values in ROI
NDRGI = (r-g)/(r+g);
% Calculates the normalized difference red green vegetation index

display(NDRGI);

for p=1:NrOfFiles
MaskTemp = zeros(size(IMGin{1},1),size(IMGin{1},2));
```

```
%creates array of zeros matching image parameters;
for m=1:size(IMGcoords,1)
[CutMap, CutImg] = segmento(IMGin{p},IMGcoords(m,:),2.5,42);
%calls segmento func described below;
MaskTemp = MaskTemp + CutMap;          % segmento output for each run;
end

disp(p);                                                    %step of images run;
MaskFlat = logical(MaskTemp);                               %creates binary mask;
MaskFlatFilled = imfill(MaskFlat,'holes');                  %fills holes;
IMGcut{p}(:,:,1) = uint8(MaskFlatFilled) .* IMGin{p}(:,:,1);
IMGcut{p}(:,:,2) = uint8(MaskFlatFilled) .* IMGin{p}(:,:,2);
IMGcut{p}(:,:,3) = uint8(MaskFlatFilled) .* IMGin{p}(:,:,3);

% generates image of original pixels within mask.
figure;

subplot(3,1,1); imagesc(MaskTemp); axis image;    %displays image clusters;
subplot(3,1,2); imshow(IMGin{p}); axis image;     %displays image;
subplot(3,1,3); imshow(IMGcut{p}); axis image;    %displays image & mask;
pixarea = bwarea(MaskFlatFilled);                 % calculates pixel area;
FileName = FileName{p};
Output{1,p} = FileName;
Output{2,p} = pixarea;          % outputs variable linking pixel area and file name;


% Creates an output text file with masked pixel area
fid= fopen('pixarea.txt','w');
fprintf(fid,'Pixel Area  ');
fprintf(fid, ' %6.2f     %6.2f', pixarea);
fclose(fid);

type pixarea.txt          % Displays what .txt file will look like below
end
%----------------------

function [stream_select,stream_cut_original] = segmento(Img,Coords,Sig,Thres)
% analysis function;

RGB = double(Img(Coords(2),Coords(1),:));          %convert values to double;
gaussH = zeros(256,3);                             % Returns a 256 by 3 matrix of zeros;
gaussH(:,1) = gaussFunc(0:255,Sig,RGB(1));         % runs gaussian function on R;
gaussH(:,2) = gaussFunc(0:255,Sig,RGB(1));         % runs gaussian function on G;
gaussH(:,3) = gaussFunc(0:255,Sig,RGB(1));         % runs gaussian function on B;
% calls on gaussFunc, a gaussian function described below this function;
```

```
pic_histeq(:,:,1) = histeq(Img(:,:,1),1-gaussH(:,1));
pic_histeq(:,:,2) = histeq(Img(:,:,2),1-gaussH(:,2));
pic_histeq(:,:,3) = histeq(Img(:,:,3),1-gaussH(:,3));
% uses histogram equalization per color scheme;

stream_mask(:,:,1) = pic_histeq(:,:,1) >= (255-Thres);
stream_mask(:,:,2) = pic_histeq(:,:,2) >= (255-Thres);
stream_mask(:,:,3) = pic_histeq(:,:,3) >= (255-Thres);
% populate stream_mask variable using histogram result above threshold;

stream_mask_consolidated = stream_mask(:,:,1) | stream_mask(:,:,2) | stream_mask(:,:,3);
% load all RGBs into mask;

stream_labels = bwlabel(stream_mask_consolidated,4);       %creates analysis clusters;
stream_select = bwselect(stream_labels,Coords(1),Coords(2),4);
% selects clusters containing analysis pixel coordinates;

stream_cut_original(:,:,1) = uint8(stream_select) .* Img(:,:,1);
stream_cut_original(:,:,2) = uint8(stream_select) .* Img(:,:,2);
stream_cut_original(:,:,3) = uint8(stream_select) .* Img(:,:,3);
% multiplies arrays to output original image within mask;

%%------------------------------

function [gaussOut] = gaussFunc(X,Sig,C)
gaussOut = exp(-(X-C).^2./(2*Sig.^2));
% gaussian function used above;

%-------------------------------
```

Static Inundation Model (R statistical software)

```
################################################################################
#Name: Static Inundation Model
#Developed by: C. Nathan Jones
#Modified by: Tyler A. Keys
#Date: 3/4/2016
#Purpose: Method to estimate inundation area and volume assuming static inundation
################################################################################
#Notes
  #Make sure to create a directory with the following structure
     #DEM_Inundate
        #SpatialData
           #InputData
           #OutputDat
  #Make sure to define the parent dirctory (wd)
```

```
  #Include FloodplainDEM and Centerline in DEM_Inundate/Spatial Data/InputData
  #define max stage increase and the step in step 3

################################################################################
#Step 1: Setup Workspace
################################################################################

#Clear Memory
rm(list=ls(all=TRUE))

#Define parent directory
wd<-"C:\\Users/grad/Google Drive/FP_Image_Processing"

#Set Working Directory
setwd(paste0(wd,"Spatial Data/"))


setwd("C:\\Users\\Grad\\Google Drive\\FP_Image_Processing\\Spatial Data")


#Download packages
library(raster)
library(sp)
library(gstat)
library(rgdal)
library(maptools)
library(foreign)
library(rgeos)

#download data
dem<-raster("dem")
cnt<-readOGR(".","streamline")

################################################################################
#Step 2: Process DEM
################################################################################

#Create Clip
fp_clip<-dem*0

#Clip centerline
cnt<-crop(cnt, fp_clip)

#Create raster
cnt<-rasterize(cnt, fp_clip)
```

```
#Extract Elevation
cnt<-cnt*0+dem

#create points
cnt<-rasterToPoints(cnt, spatial=F)
cnt<-data.frame(cnt)
  colnames(cnt)<-c("x","y", "ele")

#Create IDW Raster
IDW<-gstat(id="layer", formula=ele~1, locations=~x+y, data=cnt, nmax=7, set=list(idp=4.2))
IDW<-interpolate(fp_clip, IDW)
IDW<-mask(IDW, fp_clip)

#Correct dem for valley slope
dem_norm<-dem-IDW

#Create Minimum Raster
dem_min<-dem*0+minValue(dem_norm)

#############################################################################
#Step 3: Estimate static inundation area
#############################################################################

setwd(paste0(wd,"FP_Image_Processing/OutputData/"))

#Define max increase and step increase heights
zmax<-3
dz<-0.1

#Create function to return conditional raster
Con<-function(condition, trueValue, falseValue){
  return(condition * trueValue + (!condition)*falseValue)
}

#Create Dataframe to house information
df<-data.frame(matrix(0, ncol=3, nrow=zmax/dz))
  colnames(df)<-c("relative_ele", "area", "volume")
df$relative_ele<-seq(dz,zmax, dz)

#Loop through inundation sims
for(i in 1:(zmax/dz)){
  #define satge increase
  z<-dz*i

  #calculate area and volume rasters
  area<-Con(dem_norm>(dem_min+z),0,1)
```

```
  volume<-(((z+dem_min)-dem_norm)*area)*res(dem)[1]*res(dem)[2]

  #add to df
  df$area[i]<-cellStats(area, 'sum')*res(area)[1]*res(area)[2]
  df$volume[i]<-cellStats(volume, 'sum')

  #Export volume raster
  fun <- function(x) { x[x<0.001] <- NA; return(x) }
  volume<-calc(volume, fun)
  writeRaster(volume,paste0("Inundate",i), format="GTiff", overwrite=T)
}

#Export df
write.csv(df, paste0(wd,"output.csv"))
```

Chapter 3 Code

MODIS Download and Processing Script (R statistical software)

```
#################################################################################
#Name: Lake and Reservoir Delineation Code
#Developed by: Tyler A. Keys
#Date: 6/1/2017
#Purpose: Fully automated lake and reservoir delineation code
#################################################################################


#################################################################################
#Step 1: Setup Workspace
#################################################################################

#Sets the directory
setwd("C:\\Users\\tkeys\\Documents\\Projects\\Lakes")

#Reads in the file with the coordinates of the analysis region
x<-read.csv("Location.csv")

#Attaches dataframe
attach(x)

#Loads packages to be used in analysis
library(MODISTools)
library(data.table)

#Make sure that directory does not already contain .asc files
```

```
################################################################################
#Step 2:  Specifications
################################################################################

#Converts a set of coordiates from degrees minutes seconds to decimal degrees format
#XY is the name of the input dataset containing coordinate information
#FileSep is used to delimit characters of a file
#LatColName is the name of the column within the XY file corresponding to latitude input data
#LongColName is the name of the column within the XY file corresponding to longitude input
data
modis.subset <- ConvertToDD(XY = x, FileSep = NULL, LatColName = "lat", LongColName =
"long")

#Creates a new data frame with the latitiude and longitude values in decimal degrees format
modis.subset <- data.frame(lat = modis.subset[ ,1], long = modis.subset[ ,2])

#Sets the start date for the analysis
modis.subset$start.date <- rep(2000, nrow(modis.subset))

#Sets the end date for the analysis
modis.subset$end.date <- rep(2016, nrow(modis.subset))

#Displays the different available datasets or "products" that can be downloaded
GetProducts()

#Displays the avaiable bands for a given product
GetBands(Product = "MOD09A1")

#Displays dates for the selected dataset
GetDates(Product = "MOD09A1", Lat = modis.subset$lat[1], Long = modis.subset$long[1])

################################################################################
#Step 3: Download Data
################################################################################

#Downloads reflectance values within a given size subset of a MODIS tile
#Size corresponds to the specified subset size in kilometers in the x and y directions
MODISSubsets(LoadDat = modis.subset, Products = "MOD09A1", StartDate = TRUE,
Bands = c("sur_refl_b04", "sur_refl_b07"),
Size = c(10,10))

#Output is an .asc file that is placed within the working directory

################################################################################
#Step 4: Data Analysis
```

```
################################################################################

#Reads in the created .asc file
data <- read.csv(list.files(pattern = ".asc")[1],
header = FALSE, as.is = TRUE)

#Removes unnecessary information
data[1:7] <- list(NULL)
data[2:3] <- list(NULL)

#Transposes the data
data_transposed <- t(data)

#Creates new data frame from transposed data
data.new <- data.table(data_transposed)

#Removes column names from the data fram
data.new <- data.new[-1,]

#Converts data to numeric format and creates a new data frame
dataNum <- matrix(data = NA, nrow = dim(data.new)[1], ncol = dim(data.new)[2])
for (i in 1:dim(data.new)[2]) {
   dataNum[,i] <- c(as.numeric(data.new[[i]]))
}

#MNDWI calculation
MNDWI <- (dataNum[,1:(ncol(dataNum)/2)]-
dataNum[,((ncol(dataNum)/2)+1):ncol(dataNum)])/
(dataNum[,1:(ncol(dataNum)/2)]+dataNum[,((ncol(dataNum)/2)+1):ncol(dataNum)])

#Conditional statement for binary classification of water pixels
Water_pix <- ifelse(MNDWI > 0, 1, 0)

#Sums water pixels for give column(date)
Water_total <- colSums(Water_pix, na.rm = TRUE)

#Surface area calculation based on spatial resolution
Surface_area <- Water_total*500*500/1000000
Surface_area

write.csv(Surface_area, file = "Surface_Area.csv")
```

Chapter 4 Code

Synthetic Rainfall-Runoff Model (R statistical software)

```
##############################################################################
#Name: Precipitation Time Series Modeling
#Developed by: C. Nathan Jones
#Modified by: Tyler A. Keys
#Date: 11/20/2016
#Purpose: Simulate subdaily rainfall timeseries as input into SCS curve number
#See http://www.itia.ntua.gr/en/softinfo/3/ for more details
##############################################################################

##############################################################################
#Step 1:  Setup Workspace
##############################################################################

#Clear Memory
rm(list=ls(all=TRUE))

#Set Working Directory
setwd("C:/Users/tkeys/Desktop/LWD Flood")

#add appropriate libarary
library("HyetosMinute")
library(reshape)

##############################################################################
#Step 2:  Format Historic Data
##############################################################################

#Download historic data
df<-read.csv("C:\\users\\tkeys \\LWD Flood\\Modeling\\Precip
Modeling\\Precip_Observed.csv")
df$date_time<-strptime(df$date_time, "%m/%d/%Y %H:%M")

#Create time series to populate
ts<-seq(strptime("10/1/2011 1",  "%m/%d/%Y %H"),
      strptime("9/30/2016 24", "%m/%d/%Y %H"),
      by="hour"
)
ts<-data.frame(ts)
  colnames(ts)<-"date_time"
ts$date_time<-strptime(ts$date_time,"%Y-%m-%d %H")
ts<-data.frame(ts[format(ts$date_time,"%m-%d")!="02-29",])
  colnames(ts)<-"date_time"
```

```
#Aggregate df by hour
df$date_time<-format(df$date_time,"%m/%d/%Y %H")
df<-aggregate(df$precip_mm, list(df$date_time), sum)
colnames(df)<-c("date_time","precip_mm")
df$date_time<-strptime(df$date_time, "%m/%d/%Y %H")

#Populate timeseries df
df<-merge(ts, df, by='date_time', all.x=T)
df[is.na(df)]<-0
remove(ts)

#define time collumns
df$day<-as.POSIXlt(df$date_time)$yday
  df$day<-ifelse(df$day>=273, df$day-272, df$day+93)
df$month<-1
df$year<-rep(seq(1,5),each=(365*24))
df$hour<-seq(1,24)

#Remove dat_time collumn
df$date_time<-NULL

#Reshape dataframe
df<-reshape(df,timevar="hour", direction="wide", idvar=c("day","month","year"))

#export
write.table(df,"HistHourlyData.txt", sep="\t", row.names=F,col.names=F, quote=F)

##############################################################################
#Step 3:  Develop Synthetic Flow Record
##############################################################################

# Run simulation
n.years<-10
SequentialSimul(Length=(365*n.years),
            BLpar=list(lambda=0.324,
                  phi=0.0318,
                  kappa=0.0751,
                  alpha=99,
                  v=2.32,
                  mx=99,
                  sx=NA),
            CellIntensityProp=list(Weibull=FALSE,iota=NA),
            TimeScale=1,
            ExportSynthData=list(exp=TRUE,
                        FileContent=c("AllDays"),
```

```
                    DaysPerSeason=365,
                    file="SynthRPBLM.txt"),
          ImportHistData=list(imp=TRUE,
                    file="HistHourlyData.txt",
                    ImpDataTimeScale=1,
                    na.values="NA",
                    FileContent=c("AllDays"),
                    DaysPerSeason=365,
                    DailyValues=TRUE),
          PlotTs=FALSE,
          Statistics=list(print=TRUE,plot=FALSE),
          RandSeed=5)

##############################################################################
#Step 4:  Organize Data
##############################################################################

#Read exported data
df<-read.csv("SynthRPBLM.txt",sep="\t")
  colnames(df)<-c("day","month","year",seq(1,25))
  df[,28]<-NULL
  df$month<-NULL

#Reorganize to longitudinal
df<-melt(df,id.vars=c('year','day'))
df<-df[order(df$year, df$day, df$variable),]
  colnames(df)<-c("year","day","hour", "precip")

#Export
write.csv(df, "Precip_Modeled_1000yrs.csv")


##############################################################################
#Step 5: Model Inputs
##############################################################################

#Precipataion Data
precip<-read.csv("Precip_Modeled_1000yrs.csv")
  precip$day<-paste(format(as.Date(precip$day, origin=as.Date(paste0(1000+precip$year,"-01-
01"))), "%Y%m%d"))
  precip$precip<-precip$precip/25.4
  precip<-precip[,c("day","hour","precip")]

precip<-precip[1:(365*24*10),]

#Blank Runoff Data
```

```
runoff<-data.frame(matrix(0, ncol=4,nrow=length(precip$day)*60))
colnames(runoff)<-c("day", "hour","minute", "Q_cfs")
runoff$day<-rep(precip$day,each=60)
runoff$hour<-rep(seq(1,24), each=60)
runoff$minute<-seq(1,60)
runoff[length(runoff[,1]):(length(runoff[,1])+1000),]<-0


##############################################################################
#Step 6: Hydrology Model
##############################################################################

#Function to estimate runoff from SCS triangular unit hydrograph
unit_hydrograph.fun<-function(n) {
  #Precip variables
  P<-precip$precip[n]
  day<-precip$day[n]
  hour<-precip$hour[n]

  if(P>0){
    #Watershed Characteristics
    A<-0.3833     #Watershed Area (mi^2)
    CN<-65        #Taken from SSURGO and LULC
    tlag<-3       #0.4144  #Lag Time from CN in hours

    #Time variables (Units in Hours)
    D<-1          #Duration of rain (1 hour timestep)
    tp<-D/2+tlag  #Time to peak
    tb<-2.67*tp   #Time to base
    tr<-tb-tp     #Time of recession

    #Calculate runoff depth (NRCS Method)
    S<-1000/CN-10
    Q<-(((P-0.05*S)^2)/(P+0.95*S))

    #Calculate height of unit hydrograph (NRCS Unit hydrograph)
    Qp<-484*A*Q/(D/2+tlag) #CFS

    #Cacluate flow from unit hydrograph
    Qn<-c(sapply(seq(1,tp*60,1),function(x){Qp/(tp*60)*x}),
        sapply(seq(1,tr*60),function(x){Qp-(Qp/(tr*60)*x)}))

    #Create (Output hydrograph)
    start<-which(runoff$day==day & runoff$hour==hour)[1]+1
    end<-start+tb*60-2
    runoff$Q_cfs[start:end]<-runoff$Q_cfs[start:end]+Qn
```

```
   assign('runoff',runoff,.GlobalEnv)
  }
  n
}

#Run model
t0<-Sys.time()
lapply(seq(1,87600),unit_hydrograph.fun)
tf<-Sys.time()
tf-t0

#plot
runoff$date<-strptime(paste(runoff$day,runoff$hour), format="%Y%m%d %H")
plot(runoff$date, runoff$Q_cfs, type="l")

#Write Output
write.csv(runoff$Q_cfs, "runoff_output.csv")
```

Chapter 5 Code

Data Matching Script (R statistical software)

```
#############################################################################
#Name: Data Matching Code
#Developed by: Tyler A. Keys
#Date: 8/22/2016
#Purpose: Match geographic locations with measurements based on time stamp
#############################################################################

#Before you begin:
#Make sure that times are adjusted to proper timezone such that all instruments match up
#Make sure times are in proper format (i.e. hh:mm:ss)
#Make sure that all .csv files have a column titled "Time"

#############################################################################
#Step 1: Setup Workspace
#############################################################################


setwd("C:\\Users\\tkeys\\Documents\\Projects\\Boat Sampling\\Claytor_10_27_17")

#Download data.table package...btw, this package is pretty sweet
#load package
library(data.table)
```

```
################################################################################
#Step 2: Read in data and change timestamps from characters to numeric values
################################################################################


GPS <- read.csv(file="GPS_Up.csv",head=TRUE,sep=",")
GPS$Time <- as.POSIXct(GPS$Time,format="%H:%M:%S")
GPS2 <- data.table(GPS)
GPS2

Scan <- read.csv(file="Scan_Up.csv",head=TRUE,sep=",")
Scan$Time <- as.POSIXct(Scan$Time,format="%H:%M:%S")
Scan2 <- data.table(Scan)
Scan2

YSI <- read.csv(file="YSI_Up.csv",head=TRUE,sep=",")
YSI$Time <- as.POSIXct(YSI$Time,format="%H:%M:%S")
YSI2 <- data.table(YSI)
YSI2


################################################################################
#Step 3: Data matching
################################################################################

#Merge data based on closest GPS time data point
#Note: If two points are equidistant, the code will select the first time point.

setkey(GPS2,Time)
Combined_Scan <-GPS2[Scan2,roll="nearest"]
Combined_YSI <-GPS2[YSI2,roll="nearest"]

#Check to make sure that data looks correct

Combined_Scan
Combined_YSI

################################################################################
#Step 4: Exporting Data
################################################################################

#Create new .csv files with merged data

write.csv(Combined_Scan, file = "Scan _GIS_Input.csv")
write.csv(Combined_YSI, file = "YSI_GIS_Input.csv")
```

Flux Statistical Script (R statistical software)

```
################################################################################
#Name: Flux Boxplot Code
#Developed by: Tyler A. Keys
#Date: 2/25/2018
#Purpose: Creating boxplots for each of the flux datasets
################################################################################


################################################################################
#Step 1: Setup workspace
################################################################################

library(ggplot2)

setwd("C:\\Users\\tkeys\\Documents\\Projects\\Boat Sampling")


################################################################################
#Step 2: Read in data and check for normality
################################################################################

Flux<-read.csv("Flux_Wilcoxon.csv",header=TRUE)
AlNO3 <-Flux$AlNO3
DamNO3 <-Flux$DamNO3
RadNO3 <-Flux$RadNO3
AlNH3 <-Flux$AlNH3
DamNH3 <-Flux$DamNH3
RadNH3 <-Flux$RadNH3
AlPO4 <-Flux$AlPO4
DamPO4 <-Flux$DamPO4
RadPO4 <-Flux$RadPO4
AlDOC <-Flux$AlDOC
DamDOC <-Flux$DamDOC
RadDOC <-Flux$RadDOC


# Function to test data for normality

check.norm <- function(x, ...)
{
  par(mfrow=c(2,2))
  if(sum(is.na(x)) > 0)
```

```
   warning("NA's were removed before plotting")
  x <- x[!is.na(x)]
  hist(x, main = "Histogram and non-\nparametric density estimate", prob = T)
  iqd <- summary(x)[5] - summary(x)[2]
  lines(density(x, width = 2 * iqd))
  boxplot(x, main = "Boxplot", ...)
  qqnorm(x)
  qqline(x)
  plot.ecdf(x, main="Empirical and normal cdf")
  LIM <- par("usr")
  y <- seq(LIM[1],LIM[2],length=100)
  lines(y, pnorm(y, mean(x), sqrt(var(x))))
  shapiro.test(x)
}

check.norm(AlNO3)
check.norm(DamNO3)
check.norm(RadNO3)
check.norm(AlNH3)
check.norm(DamNH3)
check.norm(RadNH3)
check.norm(AlPO4)
check.norm(DamPO4)
check.norm(RadPO4)
check.norm(AlDOC)
check.norm(DamDOC)
check.norm(RadDOC)

#############################################################################
#Step 3: Pairwise Wilcoxon Rank sum tests
#############################################################################

#NO3 Wilcoxon Rank Sum Tests

wilcox.test(Flux$AlNO3,Flux$RadNO3,paired=TRUE)
wilcox.test(Flux$AlNO3,Flux$DamNO3,paired=TRUE)
wilcox.test(Flux$DamNO3,Flux$RadNO3,paired=TRUE)

#NH3 Wilcoxon Rank Sum Tests

wilcox.test(Flux$AlNH3,Flux$RadNH3,paired=TRUE)
wilcox.test(Flux$AlNH3,Flux$DamNH3,paired=TRUE)
wilcox.test(Flux$DamNH3,Flux$RadNH3,paired=TRUE)


#PO4 Wilcoxon Rank Sum Tests
```

```
wilcox.test(Flux$AlPO4,Flux$RadPO4,paired=TRUE)
wilcox.test(Flux$AlPO4,Flux$DamPO4,paired=TRUE)
wilcox.test(Flux$DamPO4,Flux$RadPO4,paired=TRUE)

#DOC Wilcoxon Rank Sum Tests

wilcox.test(Flux$AlDOC,Flux$RadDOC,paired=TRUE)
wilcox.test(Flux$AlDOC,Flux$DamDOC,paired=TRUE)
wilcox.test(Flux$DamDOC,Flux$RadDOC,paired=TRUE)

#################################################################################
#Step 4: Create boxplots
#################################################################################

#Create boxplots
boxplot(Flux~Site,data=Flux,ylim = c(0,400),main="",ylab="Flux (g/s)",
      col=c("darkred","dodgerblue4","darkolivegreen3"),yaxt='n')

#Adjuct tick mark intervals
yticks <- seq(0,400,100)

axis(side=2, at=yticks)
```

Color Matrix Script (R statistical software)

```
#################################################################################
#Name: Color Matrix Code
#Developed by: Tyler A. Keys
#Date: 2/25/2018
#Purpose: Creating spatiotemporal color matrices for each of the flux datasets
#################################################################################


#################################################################################
#Step 1: Setup workspace and read in data
#################################################################################

#Download packages
library(colorRamps)
library(fields)

setwd("C:\\Users\\tkeys\\Documents\\Projects\\Boat Sampling")

NO3<-read.csv("NO3.csv",header=FALSE)
```

```
NH3<-read.csv("NH3.csv",header=FALSE)
PO4<-read.csv("PO4.csv",header=FALSE)
Cl<-read.csv("Cl.csv",header=FALSE)
CtoN<-read.csv("CtoN.csv",header=FALSE)
NtoP<-read.csv("NtoP.csv",header=FALSE)
DOC<-read.csv("DOCx.csv",header=FALSE)
DO<-read.csv("DO.csv",header=FALSE)
Temp<-read.csv("Temp.csv",header=FALSE)
Cond<-read.csv("Cond.csv",header=FALSE)
Turb<-read.csv("Turb.csv",header=FALSE)
pH<-read.csv("pH.csv",header=FALSE)

#############################################################################
#Step 2: Setup dataframe and plotting parameters
#############################################################################


#Attaches dataframe
attach(NO3)

#Create a dataframe with a data
df<-data.frame(NO3)
cols<-matlab.like(256)

#Define plotting parameters
par(ps=14)
par(cex.lab=14/12)
par(cex.axis=10/12)
par(mar=c(4.2,4,1,5.5))
par(mgp=c(1.7,0.5,0))
par(yaxt="s")

#Add blank plot
plot(df[,1:2], type="n",
    #Axes Limits
    xlim=c(-0.058,1.056), ylim=c(-0.194,1.2),
    #Axes Options
    xaxt="n", yaxt="n",
    #Axes Labels
    ylab="Distance (km)", xlab="Sampling Day")

#############################################################################
#Step 3: Create color matrix within created plot area
#############################################################################

#Add Raster plot
```

```
image(t(as.matrix(df)), col=cols, add=T, xaxs="n")

#6 x 3 matrix - Add Axis
axis(1, rev(c("Oct-28", "Oct-27", "Oct-26", "Oct-25", "Oct-24","Sep-25")),at=seq(0,1, length.out
= 6))
axis(2, rev(c("42 (riv)", "31 (riv)","0 (riv)")),
   at=seq(0,1, length.out = 3))

#6 x 5 matrix -Add Axis
axis(1, rev(c("Oct-28", "Oct-27", "Oct-26", "Oct-25", "Oct-24","Sep-25")),at=seq(0,1, length.out
= 6))
axis(2, rev(c("42 (riv)", "31 (riv)","28 (res)","7 (riv-res)","0 (riv)")),
    at=seq(0,1, length.out = 5))


#5 x 5 matrix -Add Axis
axis(1, rev(c("Oct-28", "Oct-27", "Oct-26", "Oct-25", "Sep-25")),at=seq(0,1, length.out = 5))
axis(2, rev(c("42 (riv)", "31 (riv)","28 (res)","7 (riv-res)","0 (riv)")),
    at=seq(0,1, length.out = 5))

#Add bounding box
box()

#Add legend
image.plot(add=TRUE,zlim=c(6.5,7.75), legend.only=TRUE,legend.lab="NO3",
         legend.line = 2.75)
         #smallplot = c(.85,.9,0.1,.9)
```

Longitudinal Profile Script (R statistical software)

```
################################################################################
#Name: Longitudinal Profile Code
#Developed by: Tyler A. Keys
#Date: 2/25/2018
#Purpose: Plotting longitudinal profiles of water quality measurements
################################################################################


################################################################################
#Step 1: Setup workspace
################################################################################

rm(list = ls())
library(dplyr)
library(tidyr)
```

```
library(readxl)
library(lubridate)


setwd("C:\\Users\\tkeys\\Documents\\Projects\\Boat Sampling\\Claytor_10_27_17")

################################################################################
#Step 2: Read in data
################################################################################

YSI <- read_excel("YSI_Down_Long_Combined.xlsx", sheet="YSI_Down_Long")
distance <- YSI$`Dist (km)`
DO <- YSI$ODOsat
distance2 <- YSI$`Dist (km)2`
DO2 <- YSI$ODOsat2
distance3 <- YSI$`Dist (km)3`
DO3 <- YSI$ODOsat3
Temp <- YSI$Temp
Temp2 <- YSI$Temp2
Temp3 <- YSI$Temp3
Cond <- YSI$SpCond
Cond2 <- YSI$SpCond2
Cond3 <- YSI$SpCond3
pH <- YSI$pH
pH2 <- YSI$pH2
pH3 <- YSI$pH3
Turb <- YSI$Turbid
Turb2 <- YSI$Turbid2
Turb3 <- YSI$Turbid3
dist <- YSI$Dist
dist[dist==0] <-NA
dist2 <- YSI$Dist2
dist2[dist2==0] <-NA
dist3 <- YSI$Dist3
dist3[dist3==0] <-NA

Scan <- read_excel("Scan_Down_Long_Combined.xlsx", sheet="Scan_Down_Long")
distance2 <- Scan$`Dist (km)`
NO3 <- Scan$NO3
NO32 <- Scan$NO32
NO33 <- Scan$NO33
DOC <- Scan$DOC
DOC2 <- Scan$DOC2
DOC3 <- Scan$DOC3
dist4 <- Scan$Dist
dist4[dist4==0] <-NA
```

```
dist5 <- Scan$Dist2
dist5[dist5==0] <-NA
dist6 <- Scan$Dist3
dist6[dist6==0] <-NA


################################################################################
#Step 3: Plot multiple longitudinal profiles for each water quality parameter
################################################################################

###DO

plot(dist, DO, xlim = c(0,35), ylim = c(50,100),pch=19, type="p", main="DO",
    xlab="Distance (Km)", ylab="DO (% Sat)", col="black",panel.first=grid())

points(dist2, DO2, xlim = c(0,35), pch=19, type="p", main="DO",
    xlab="Distance (Km)", ylab="DO (% Sat)", col="blue")

points(dist3, DO3, xlim = c(0,35), pch=19, type="p", main="DO",
      xlab="Distance (Km)", ylab="DO (% Sat)", col="red")

abline(v=33.5,lty=2)

###Temp

plot(dist, Temp, xlim = c(0,35),ylim = c(10,25),pch=19, type="p", main="Temperature",
    xlab="Distance (Km)", ylab="Temp (C)", col="black",panel.first=grid())

points(dist2, Temp2, xlim = c(0,35), pch=19, type="p", main="DO",
      xlab="Distance (Km)", ylab="DO (% Sat)", col="blue")

points(dist3, Temp3, xlim = c(0,35), pch=19, type="p", main="DO",
      xlab="Distance (Km)", ylab="DO (% Sat)", col="red")

abline(v=33.5,lty=2)

###Cond

plot(dist, Cond, xlim = c(0,35), ylim = c(0.1,0.3),pch=19, type="p", main="Conductivity",
    xlab="Distance (Km)", ylab="Cond. (mS/cm)", col="black",panel.first=grid())

points(dist2, Cond2, xlim = c(0,35), pch=19, type="p", main="DO",
      xlab="Distance (Km)", ylab="DO (% Sat)", col="blue")

points(dist3, Cond3, xlim = c(0,35), pch=19, type="p", main="DO",
      xlab="Distance (Km)", ylab="DO (% Sat)", col="red")
```

```
abline(v=33.5,lty=2)

###pH

plot(dist, pH, xlim = c(0,35),ylim = c(6,8.5), pch=19, type="p", main="pH",
    xlab="Distance (Km)", ylab="pH", col="black",panel.first=grid())

points(dist2, pH2, xlim = c(0,35), pch=19, type="p", main="DO",
      xlab="Distance (Km)", ylab="DO (% Sat)", col="blue")

points(dist3, pH3, xlim = c(0,35), pch=19, type="p", main="DO",
      xlab="Distance (Km)", ylab="DO (% Sat)", col="red")

abline(v=33.5,lty=2)

###Turb

plot(dist, Turb, xlim = c(0,35), ylim = c(0,400),pch=19, type="p", main="Turbidity",
    xlab="Distance (Km)", ylab="Turb (ntu)", col="black",panel.first=grid())

points(dist2, Turb2, xlim = c(0,35), pch=19, type="p", main="DO",
      xlab="Distance (Km)", ylab="DO (% Sat)", col="blue")

points(dist3, Turb3, xlim = c(0,35), pch=19, type="p", main="DO",
      xlab="Distance (Km)", ylab="DO (% Sat)", col="red")

abline(v=33.5,lty=2)

###NO3

plot(dist4, NO3, xlim = c(0,35), ylim=c(0,1),pch=19, type="p", main="NO3",
    xlab="Distance (Km)", ylab="NO3 (mg/L)", col="black",panel.first=grid())

points(dist5, NO32, xlim = c(0,35), pch=19, type="p", main="NO3",
    xlab="Distance (Km)", ylab="NO3 (mg/L)", col="blue")

points(dist6, NO33, xlim = c(0,35), pch=19, type="p", main="NO3",
      xlab="Distance (Km)", ylab="NO3 (mg/L)", col="red")

abline(v=33.5,lty=2)

###DOC

plot(dist4, DOC, xlim = c(0,35), ylim=c(2,8),pch=19, type="p", main="DOC",
    xlab="Distance (Km)", ylab="DOC (mg/L)", col="black",panel.first=grid())
```

```
points(dist5, DOC2, xlim = c(0,35), pch=19, type="p", main="DOC",
    xlab="Distance (Km)", ylab="DOC (mg/L)", col="blue")

points(dist6, DOC3, xlim = c(0,35), pch=19, type="p", main="DOC",
      xlab="Distance (Km)", ylab="DOC (mg/L)", col="red")

abline(v=33.5,lty=2)
```

Chapter 6 Code

Data Aggregation and Hydrograph Plotting Script (R statistical software)

```
#################################################################################
#Name: Data aggregation and Plotting Code
#Developed by: Tyler A. Keys
#Date: 2/25/2018
#Purpose: Aggregate hourly discharge data to daily means and plot hydrographs
#################################################################################


#################################################################################
#Step 1: Setup workspace and read in data
#################################################################################

library(dplyr)
library(lubridate)

setwd("C:\\Users\\tkeys\\Documents\\Projects\\Impoundments\\Hydrographs")

USGS<-
read.delim("C:/Users/tkeys/Documents/Projects/Impoundments/Hydrographs/USGS.txt");
names(USGS)<-c("Agency","StationID","Date","AvgFlow","ID");USGS$Date<-
as.Date(USGS$Date)

Outlet<-read.csv("Outlet.csv",header=TRUE)

#################################################################################
#Step 2: Aggregate data
#################################################################################

DF2<-data.frame(Outlet,Day = as.Date(Outlet$thisdate,"%m/%d/%Y"))
calib <-aggregate(cbind(impoundment_Qout) ~ Day, DF2, mean)
calib2 <-aggregate(cbind(impoundment_Qout2) ~ Day, DF2, mean)
```

```
################################################################################
#Step 3: Plot data
################################################################################

#1:1 Plot
plot(calib$impoundment_Qout,USGS$AvgFlow, xlim=c(0,3000),ylim=c(0,3000),pch=20)
x<-c(-200,3300)
y<-c(-200,3300)
lines(x,y)

plot(calib2$impoundment_Qout2,USGS$AvgFlow, xlim=c(0,3000),ylim=c(0,3000),pch=20)
x<-c(-200,3300)
y<-c(-200,3300)
lines(x,y)

length(calib$impoundment_Qout)

#Hydrograph Plot for July-December 1989
plot(1958:2192,calib$impoundment_Qout[1958:2192],col="red",type='l',lwd=2,xlim=c(1958,21
92),ylim=c(0,750),
    axes=FALSE, xaxp  = c(1960, 2180, 5))
axis(side=1, at=seq(1960, 2180, by=50))
axis(side=2, at=seq(0, 750, by=150))
box()

lines(1958:2192,USGS$AvgFlow[1958:2192],col="black",lty=3,lwd=2)
lines(2000:2192,calib2$impoundment_Qout2[2000:2192],col="blue",type='l',lwd=2)

################################################################################
#Step 4: Summary statistics for data
################################################################################

calibration.lm = lm(calib$impoundment_Qout ~ USGS$AvgFlow)
summary(calibration.lm)

calibration.lm2 = lm(calib2$impoundment_Qout2 ~ USGS$AvgFlow)
summary(calibration.lm2)

num<-sum((USGS$AvgFlow-calib$impoundment_Qout)^2)
den<-sum((USGS$AvgFlow-mean(USGS$AvgFlow))^2)
RSR<-sqrt(num)/sqrt(den)
NSE<-1-(num/den)
rm(num,den)
RSR;NSE
```